



TAMPEREEN TEKNILLINEN YLIOPISTO  
TAMPERE UNIVERSITY OF TECHNOLOGY

Sreekanth Perumbilavil

## **Soliton-assisted Random Lasing in Nematic Liquid Crystals**



Julkaisu 1602 • Publication 1602

Tampere 2018

Tampereen teknillinen yliopisto. Julkaisu 1602  
Tampere University of Technology. Publication 1602

Sreekanth Perumbilavil

## **Soliton-assisted Random Lasing in Nematic Liquid Crystals**

Thesis for the degree of Doctor of Philosophy to be presented with due permission for public examination and criticism in Sähköotalo Building, Auditorium SJ204, at Tampere University of Technology, on the 27<sup>th</sup> of November 2018, at 12 noon.

Doctoral candidate: Sreekanth Perumbilavil  
Laboratory of Photonics  
Faculty of Natural Sciences  
Tampere University of Technology  
Finland

Supervisor: Professor Martti Kauranen  
Laboratory of Photonics  
Faculty of Natural Sciences  
Tampere University of Technology  
Finland

Instructor(s) Professor Gaetano Assanto  
Laboratory of Photonics  
Faculty of Natural Sciences  
Tampere University of Technology  
Finland

Pre-examiners: Professor Hui Cao  
Department of Physics  
Yale University  
USA

Professor Iam Choon Khoo  
Liquid Crystals and Nonlinear Optics Laboratory  
The Pennsylvania State University  
USA

Opponent: Professor Francesco Simoni  
Department of Materials, Environmental Science and  
Urban Planning  
Università Politecnica delle Marche  
Italy

ISBN 978-952-15-4268-8 (printed)  
ISBN 978-952-15-4275-6 (PDF)  
ISSN 1459-2045

## Abstract

Random lasers are resonator-less light sources where the optical feedback for lasing arises from recurrent multiple scattering events in a disordered gain medium. During the past 20 years, random lasers have been the subject of intense theoretical and experimental investigations due to their novelty, simplicity and ruggedness as well as their great potential for applications ranging from imaging to biomedical diagnostics. Common random lasers, however, tend to emit light in a wide range of directions with poor beam quality. The lack of pre-determined directionality and its control along with poor spatial characteristics hinder the applications of random lasers in many fields.

It has been shown that dye-doped nematic liquid crystals can random lase when optically pumped within the absorption region of the dye molecules. Moreover, through molecular reorientation they support the propagation of self-guided optical beams, known as nematicons, which act as real-time graded-index optical waveguides.

In order to address the problems of conventional random lasers, this Thesis focuses on the demonstration of a configuration where an efficient random laser with directional output is realized in dye-doped nematic liquid crystals by combining optical gain, random scattering, and nematicons. A planar cell filled with a mixture of commercial E7 nematic liquid crystals (host) and PM 597 (guest) is used as the material. A near infrared continuous-wave beam is used to launch a nematicon, while a 6 ns pulsed beam at 532 nm is used to optically pump the material. The synergy of random lasing and nematicons in this geometry provides several breakthrough results.

By adopting a pumping geometry collinear with the nematicon, we demonstrate random laser emission from the initial region of the nematicon. The nematicon waveguide provides transverse confinement to the emitted photons, resulting in directionality, high photon collection, and high slope efficiency. The nematicon also modulates the emission, allowing the realization of a random transistor laser, where a low-power continuous-wave input is able to lower the threshold for lasing.

By taking advantage of the response of nematicons to external stimuli, we also demonstrate a random laser emitting in a voltage-controlled direction. Finally, we demonstrate in-plane random laser steering by external magnetic field. The latter approach allows us to steer the random laser beam over  $14^\circ$ .



## Preface

This Thesis was prepared in the Laboratory of Photonics of Tampere University of Technology (TUT) during the years 2015-2018. I gratefully acknowledge Academy of Finland for financial support for the work.

First and foremost, I am deeply grateful to my advisors, Prof. Gaetano Assanto and Prof. Martti Kauranen for their scientific guidance, valuable advice, support and encouragement in the journey towards my Ph.D. I also thank them for providing theoretical as well as technical guidance needed to be a good researcher and for having a keen interest in my research progress throughout my Ph.D. Working at the laboratory of Photonics has been a great learning experience for me.

I have been extremely fortunate to have some very helpful lab mates and it was a great pleasure working with them. I would like to express my sincere thanks to Dr. Raouf Barboza, Dr. Armando Piccardi, and Dr. Alessandro Alberucci for providing me all the basic knowledge on the topic, answering my queries and helping me with building the experimental setup and writing analysis codes.

I would like to thank our collaborators Prof. Giuseppe Strangi and Dr. Oleksandr Buchnev for providing us the random laser materials and cells, enlightening discussions and critical suggestions. Special thanks to our collaborator Prof. Arri Priimagi for allowing us to utilize his laboratory and equipments for the sample preparation and characterization. I want to thank Nazanin Karimi for being a wonderful friend and lab mate. I extend my thanks to Antti Kiviniemi for his valuable technical support particularly for laser synchronization.

I would like to thank Godo, Piotr, Mikko N., Mikko H., Matti Virki and Kalle for all the discussions about random lasers and experimental techniques. I have benefitted much from these discussions. My sincere thanks to Caroline for being a good friend and being there for me whenever I needed any help. My deepest thanks to all the members of the laboratory who made my journey very happy especially Zahra, Abba, and Shanti. In addition, I am grateful to Prof. Goery Genty, Prof. Juha Toivonen and other members of the laboratory for the pleasant and highly motivating working atmosphere. A special thanks to my friends outside the university who made me happier. I thank my former supervisors Prof. Nandakumar Kalarikkal and Prof. Reji Philip for helping me to grow and be successful in all my ventures.

Last but not least, my deepest and most sincere gratitude to my mother, grandmother, brother and all my relatives for their unconditional love and constant support over the years.

Tampere 24.09. 2018

Sreekanth Perumbilavil

# Contents

ABSTRACT .....	III
PREFACE.....	V
CONTENTS.....	VII
LIST OF SYMBOLS AND ABBREVIATIONS .....	IX
LIST OF PUBLICATIONS .....	XI
AUTHOR'S CONTRIBUTION .....	XIII
1 INTRODUCTION .....	1
1.1 Aims and scope of the work .....	2
1.2 Structure of the Thesis .....	3
2 LASING IN RANDOM MEDIA.....	5
2.1 Coherent backscattering .....	5
2.2 Amplified spontaneous emission.....	6
2.3 Random lasers.....	7
2.4 Random lasing in nematic liquid crystals.....	11
2.5 Applications of random lasers .....	13
3 NONLINEAR OPTICS IN NEMATIC LIQUID CRYSTALS.....	15
3.1 Nematic liquid crystals.....	15
3.2 Optical properties of nematic liquid crystals.....	16
3.3 Continuum theory and reorientational nonlinearity.....	17
3.4 Soliton formation in nematic liquid crystals.....	18



4	NEMATICON-ASSISTED RANDOM LASING .....	21
4.1	Sample.....	21
4.2	Experimental setup .....	23
4.3	Interaction geometry .....	24
4.4	Input versus output characteristics .....	25
4.5	Statistical analysis of emitted spectra.....	28
4.6	Transistor-like operation of nematicon random laser .....	30
4.7	Beaming the random laser emission .....	32
4.8	Efficiency of the random laser .....	33
5	RANDOM LASER STEERING WITH NEMATICON.....	35
5.1	Voltage-controlled angular steering .....	35
5.2	In-plane angular steering using external magnetic field.....	38
5.3	Comparison of RL steering methods .....	43
6	SUMMARY AND OUTLOOK .....	45
	REFERENCES .....	47
	ORIGINAL PAPERS .....	59

## List of Symbols and Abbreviations

ASE	Amplified spontaneous emission
CW	Continuous-wave
$E_p$	Pump energy
FWHM	Full-width at half maximum
ITO	Indium Tin Oxide
NIR	Near infrared
NLC	Nematic liquid crystal
OBJ	Objective
PM	Pyromethene
RL	Random laser
SM	Spectrometer
UV	Ultraviolet
$A$	Electric field amplitude
$N$	Number of spectra
$V$	Voltage
$L_c$	Cavity length
$\lambda$	Wavelength
$\mathbf{n}(r, t), \mathbf{n}$	Molecular director
$\Delta\varepsilon$	Dielectric anisotropy
$\Delta n$	Optical anisotropy
$n$	Refractive index

$n_e$	Extraordinary refractive index
$\mathbf{k}$	Wavevector
$\mathbf{S}$	Poynting vector
$\Delta\lambda$	Spectrometer resolution
$w_0$	Beam waist
$\xi$	Elevation angle
$\delta, \alpha$	Walk-off angle
$\theta_m$	Magnetic field orientation angle
$\theta$	Angle between wavevector and molecular director
$\eta$	Efficiency
$\mathbf{E}$	Electric field
$K_1, K_2, K_3$	Frank constants
$l^*$	Average path length
$\theta_{max}$	Critical coherence angle
$\bar{I}_{Max}$	Average intensity
$\sigma_I^2$	Variance

## List of Publications

- I. Sreekanth Perumbilavil, Armando Piccardi, Oleksandr Buchnev, Martti Kauranen, Giuseppe Strangi, Gaetano Assanto, "Soliton-assisted random lasing in optically-pumped liquid crystals," *Applied Physics Letters*, vol. 109, p. 16105, 2016.
- II. Sreekanth Perumbilavil, Armando Piccardi, Oleksandr Buchnev, Martti Kauranen, Giuseppe Strangi, Gaetano Assanto, "All-optical guided-wave random laser in nematic liquid crystals," *Optics Express*, vol. 25, p. 4572, 2017.
- III. Sreekanth Perumbilavil, Armando Piccardi, Raouf Barboza, Oleksandr Buchnev, Martti Kauranen, Giuseppe Strangi, Gaetano Assanto, "Beaming random lasers with soliton control," *Nature Communications*, vol. 9, no. 3863, pp. 1-6, 2018.
- IV. Sreekanth Perumbilavil, Martti Kauranen, Gaetano Assanto, "Magnetic steering of beam-confined random laser in liquid crystals," *Applied Physics Letters*, vol. 113, p. 121107, 2018.



## Author's Contribution

This Thesis consists of four publications. **Publications I** and **II** deal with the basic features of soliton-assisted random lasing. In **Publications III** and **IV**, fully controllable random lasers in soft matter are reported with several new results. A short description of the publications and the author's contribution is given below.

**Publication I** This paper reports on the design and demonstration of a novel soliton-assisted random laser configuration in dye-doped nematic liquid crystals. The synergy of nematicons and scattering mediated lasing yields a random laser with tunable efficiency and emission features. The author and A. Piccardi built the experimental setup. O. Buchnev and G. Strangi prepared the samples. The author performed all the measurements, data analysis and prepared all the figures for the publication. G. Assanto wrote the first draft of the paper and the author also contributed to writing. M. Kauranen and G. Assanto supervised the activity.

**Publication II** This paper reports additional features of nematicon-assisted random lasers such as tuning slope efficiencies and global spectral narrowing. The evidence of directionality and beaming the random laser emission is also reported in this paper. The author modified the basic experimental setup together with A. Piccardi and performed all the experiments and data analysis. The author also contributed to manuscript preparation and prepared all the figures for the paper. O. Buchnev and G. Strangi prepared the samples. M. Kauranen and G. Assanto supervised the activity.

**Publication III** This paper represents several advanced features of nematicon-assisted random lasers and contains the core results of this Thesis. The paper demonstrates a random laser with well-defined beam features and the soliton control provides all-optical switching and enhanced conversion efficiency. This paper also presents the first random laser emitting in a voltage-controlled direction. Overall, this paper solves certain random laser issues. The author and R. Barboza upgraded the experimental setup by incorporating additional elements in order to completely characterize the random laser emission. The author performed all the experiments and data analysis. R. Barboza performed the statistical analysis. The author also contributed to manuscript preparation and prepared all the figures for the paper. O. Buchnev and G. Strangi prepared the samples. M. Kauranen and G. Assanto supervised the activity.

**Publication IV** This paper demonstrate magneto-optic in-plane angular steering of a random laser. Using an external magnetic field acting on the active medium itself, the random laser beam steered over an angle as large as  $14^\circ$  without hampering the key

properties of the emission. The author designed and built the experimental setup for the magnetic steering and performed all the experiments and data analysis. The author wrote the manuscript. M. Kauranen and G. Assanto finalized the manuscript and supervised the activity.

# 1 Introduction

Lasers have found extensive use in scientific research, industry, military, biomedicine and many other areas of modern life.<sup>1</sup> A conventional laser consists of a gain medium and a resonant cavity. A Fabry-Perot resonator made of two mirrors is the most common configuration for a laser cavity.<sup>2</sup> Any inhomogeneities causing scattering within this cavity produce additional loss in the lasing action and hence are considered unfavorable for laser action.

Multiple scattering is a well-known phenomenon that occurs mostly in opaque materials. Therefore, it is quite common in nature, e.g., in clouds, powders, and even in biological tissues.<sup>3</sup> Multiple scattering due to randomness is also inherently present in photonic materials such as photonic crystals, where it is considered as a drawback arising from structural defects. However, disorder-induced multiple scattering opened a completely new direction in scientific research. Recent developments in the field of photonics show the possibilities of making effective optical structures by taking advantage of disorder in photonic materials.<sup>3</sup> A beautiful example of this is a random laser (RL), where the laser action arises from the disorder-induced multiple scattering. Surprisingly, disordered gain media have repeatedly demonstrated to be excellent candidates for obtaining laser-like emission, thus eliminating the need for an external cavity needed for conventional lasers.

RLs are attracting much attention because of their applications in various fields. Lasing in random media have been studied using materials including highly-ordered periodic materials, such as photonic crystals, completely disordered materials such as powders or strongly scattering materials, and partially-ordered materials such as liquid crystals.<sup>4</sup>

Liquid crystals are mesophases, that is, they share the structural features and properties of liquids as well as crystalline phases. They are characterized by certain level of order in the molecular arrangements. The most common liquid crystalline phases are the nematic, cholesteric, smectic, and blue phases.<sup>5, 6</sup> Liquid crystals are very attractive from the viewpoint of optics due to their high birefringence, optical transparency over a wide



range of wavelengths, as well as high and nonlocal response to externally applied electric and magnetic fields.<sup>7</sup> This last property is particularly useful for the exploration of nonlinear optical phenomena. Nematic liquid crystals (NLC) are the most widely used liquid crystals for practical applications, such as liquid-crystal displays, light modulators, optical signal processing, and RLs.

In recent years, a great deal of attention has been dedicated to spatial optical solitons in NLC so-called nematicons.<sup>8</sup> Nematicons are diffractionless self-confined light beams where the diffraction is balanced out by self-focusing through the nonlinearity. Moreover, owing to the highly nonlocal character of the response, nematicons are stable in two transverse dimensions and robust against external perturbations. Nematicons are self-induced graded-index channel waveguides and they can guide other optical signals at arbitrary wavelengths. Therefore, they provide an avenue for all-optical signal processing.

## 1.1 Aims and scope of the work

Unlike conventional lasers, RLs usually emit in many directions like a common light bulb. An important challenge that most RLs face is to not only make their output directional but also to produce highly collimated beam, which offers a wide range of applications ranging from imaging to security scanning. Other important goals in the research on RLs are to make their emission spectrum, directionality and transverse output profile externally tunable. A tunable RL could be used as a multi-purpose light source with a customized functionality determined by its design and external control. RLs based on liquid crystals offer distinctive features, which can be directly exploited to tune the emission properties.

The ultimate aim of this research work was not only to demonstrate the interaction between two nonlinear effects occurring in dye-doped NLC, namely beam self-confinement and random lasing, but also to realize an efficient random laser configuration that would solve the above-mentioned vexing issues of RLs.

The first goal of the work was to design and demonstrate a soliton-assisted random laser configuration in a dye-doped NLC cell. Upon collinear pumping, the co-existence of random lasing and soliton gives rise to beaming of the emission along the soliton. Such a configuration could also features directionality, and enhanced conversion efficiency.

The second goal of this work was to take advantage of NLC's high sensitivity towards external stimuli such as voltage and magnetic field. The soliton trajectory in NLC can be easily deviated by using such external stimuli, which act on the director distribution of the liquid crystal molecules. This approach allows steering "at will" the RL emission and

beaming it to various output directions without hampering the key properties of the RL. Each part of this thesis serves one common goal: completely overcoming the uncontrollable nature of RLs rather than just suggesting some solutions to certain problems of RLs.

The scope of this work is rather broad and is not limited to a few potential applications such as imaging, sensing and labelling. This work can be helpful to understand fundamental issues of soliton-assisted random lasing. These results can also open a new route towards light controlled RLs. RL beaming and routing could also be achieved by means of other strategies such as inter-digitated electrodes on the planar interfaces, and extra light beams. I believe that these experimental realizations would not only be interesting from the physics point of view, but would also enlarge the scope of fully controllable RLs and their applications.

## **1.2 Structure of the Thesis**

This Thesis summarizes the work presented in four original articles published in peer-reviewed journals. The Thesis is divided into six chapters. Chapter 1 introduces the main topics to the reader, gives the overall idea about the work and highlights the main results obtained. Chapter 2 introduces the basic concepts of lasing in random media and other related phenomena. This chapter also gives a background on the state-of-the-art research on RLs, random lasing in NLC and applications of RLs. Chapter 3 introduces spatial optical solitons in nematic liquid crystals. Optical properties of NLC, insight into the formation of nematicons and the governing equations are also described in this chapter.

Chapters 4 and 5 are the most important part of this Thesis. The details of the materials used, sample preparation and the experimental setup are described in Chapter 4. The experimental results on soliton-assisted random lasing and its key properties, such as enhanced slope efficiency, beaming the emission direction and all-optical switching, are also described in this chapter. Chapter 5 presents the key results on random laser beaming and routing “at will” using external stimuli acting on the NLC director distribution. Altogether, these two chapters describe an efficient strategy for controlling RLs in soft-matter and for tuning their key properties. Further, a summary of the results and perspectives for future work are presented in Chapter 6. The thesis is supplemented by four original peer-reviewed publications supplied as appendices.



## 2 Lasing in random media

Active random scattering media have been demonstrated to be excellent candidates for the realization of RLs. This is because of the ability of such materials to provide the feedback mechanisms through multiple recurrent scattering events, which eliminate the need for a regular laser cavity. Since its prediction, several efforts were devoted to understand and demonstrate random lasing in a plethora of disordered systems. Because of the miniature size, easy fabrication procedure, low price and the emission properties that, to a certain extent resemble normal lasers, RLs have become one of the hot topics in photonics research. In this Chapter, the fundamentals and current developments in the field of RLs and random lasing in NLC will be discussed.

### 2.1 Coherent backscattering

When a light wave is incident on a highly disordered medium, it undergoes multiple scattering inside the medium. Due to such multiple scattering, the photons can change their direction of propagation at every scattering point before they escape from the medium.<sup>1</sup> When the scattered light follows completely random paths and never returns to the initial position, the phase relations between all the paths are random and the feedback will be incoherent in nature. Conversely, the scattered light returning to its initial position through random trajectories will be in phase and then leaves the medium in the direction opposite to the incident light.

Scattering in random media can be classified into different cases.<sup>1,2</sup> (i) When the spatial distance between two scattering points, i.e., the scattering mean free path is much greater than the incident wavelength, the light is in the weak-scattering regime and eventually loses its coherence. (ii) When the scattering mean free path is of the order of the incident wavelength, the light transport will be diffusive in nature. (iii) When the scattering mean free path is equal or less than the incident wavelength, the scattered light forms

closed loops and its transport is eventually terminated. This regime is known as the localization regime and the process is known as Anderson Localization.<sup>9</sup> Even when the scattering mean free path is larger than the wavelength, light localization can be realized in a two-dimensional random medium if the medium size exceeds localization length.<sup>2, 9</sup>

When light waves propagate through a strongly scattering medium, interference effects play an important role because of multiple scattering. The coherent backscattering phenomenon is one of such interference phenomena. In a strongly scattering media, there exist scattering paths that are time reversed invariants of each other.<sup>10</sup> In the backscattering direction, each trajectory interferes constructively with its time-reversed counterpart and gives rise to enhanced back scattering intensity.<sup>3, 11,12</sup> The phase difference between two waves increases when their scattering paths deviates from the backscattering direction, giving rise to a conical shape in the backscattering profile.<sup>13</sup> The width of the coherent backscattering cone is an important parameter, since it depends on the transport mean free path length. The smallest average path length ( $l^*$ ) is related to the maximum angular cone width (critical coherence angle) as

$$\theta_{max} \approx \frac{\lambda}{\sqrt{2}l^*} \quad (2.1)$$

The coherent backscattering enhancement was first observed by Y. Kuga et al. in a dense distribution of latex microspheres,<sup>13</sup> but its connection to time reversed path and photon localization was made clear only after the observations of M. Van Albada<sup>14</sup> and G. Maret.<sup>15</sup> Later, R. Sapienza et al. demonstrated that coherent backscattering experiments manifested weak localization of light even in anisotropic systems, such as NLC.

<sup>16</sup>

## 2.2 Amplified spontaneous emission

Amplified spontaneous emission (ASE) occurs in gain media that are excited over a long and narrow volume. If the amplification factor is large, for example, in high gain systems or long amplifiers, the photons along the long axis of the excited volume experience more amplification than those emitted in other directions (see Fig. 2.1), producing a beam of ASE with a divergence depending on the aspect ratio  $L/a$  of the amplifier. The spectrum of ASE is also narrower than the spontaneous emission spectrum, because the gain curve has a maximum at the wavelength where the amplification is strongest. This process is called gain narrowing. Therefore, ASE may share some properties with laser light such as threshold, directionality, and partial coherence even though there is no feedback.<sup>17-19</sup> However, the threshold for ASE is softer than laser threshold produced by feedback in a cavity, but for long and thin amplifiers the difference is hard to tell. ASE

has been widely studied in many systems,<sup>20, 21</sup> including even X-ray lasers<sup>6</sup> due to the lack of good mirrors at that wavelength range.<sup>22</sup>

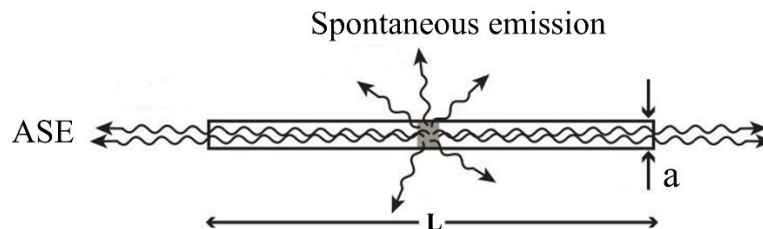


**Figure 2.1.** ASE in an amplifier of length  $L$  and width  $a$ . Spontaneous emission along the length is amplified and produces a narrow ASE beam.

## 2.3 Random lasers

A laser is an optical device that emits light amplified by stimulated emission. A conventional laser consists of an amplifying medium enclosed within a resonant cavity formed by two mirrors (Fig. 2.2 (a)). When the amplifying medium is pumped, the spontaneously emitted photons are amplified as they travel multiple times through the gain medium while they are reflected back and forth between the two mirrors. One of the mirrors is made partially transparent so that some of the light can act as an output of the laser. Due to stimulated emission, intensity starts building up within the amplifying medium. The emitted photons will be in phase with and travelling in the same direction as the stimulating photon. Thus, the light will be well collimated and highly coherent. The light in the cavity undergoes constructive interference after travelling a round trip between the two mirrors and returning to its original position. This implies that the phase delay of a round trip must be equal to an integer multiple of  $2\pi$ . This results in the requirement that only certain wavelengths  $\lambda$  that satisfy the relation  $\lambda = 2L/n$ , where  $L$  is the length of the cavity and  $n$  is an integer, can be supported by the cavity. At such cavity resonance wavelengths, light experiences minimum loss and remains in the cavity for a long time. When the optical amplification of light overcomes the total cavity losses (mirror leakage and material absorption loss) lasing occurs at the resonant wavelengths.<sup>1, 23, 24</sup> In a conventional laser, one can tune the laser emission wavelengths. It is obvious that the mirrors and the amplifying medium should be free from defects. Scattering due to defects is detrimental to the laser action as it increases the losses that reduce the net amplification.

In a conventional laser, disorder and scattering thus play a negative role. However, in a highly disordered medium with gain, multiple light scattering plays a positive role in laser action. The photons bounce back and forth due to random multiple scattering and this

increases the path length and dwell time of light in the gain medium, which in turn enhances laser amplification. These kinds of lasers are called random lasers.

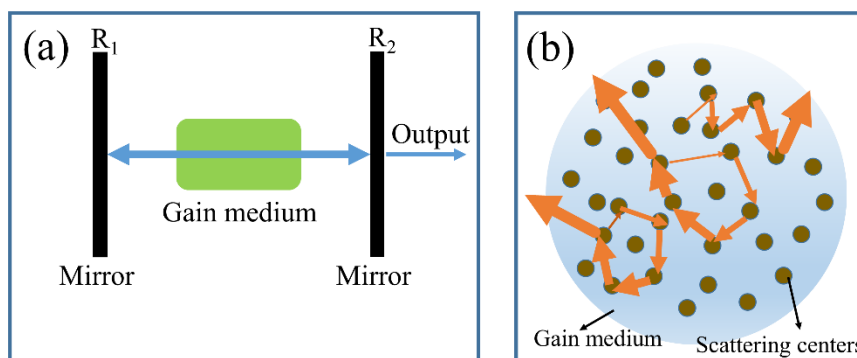


**Figure 2.2.** (a) Schematic of a Fabry-Perot laser cavity. The light bounces back and forth between the two mirrors that form the cavity. (b) Schematic of random laser action. Multiple scattering of light between the particles in a disordered gain medium provides the feedback for lasing.

In 1960s, Letokhov et al. theoretically predicted that one could obtain laser like emission from amplifying disordered media using nonresonant feedback via multiple scattering of light (Fig. 2.2.(b)).<sup>25, 26</sup> He introduced this theory followed by the experimental work with a new type of laser cavity having one scattering surface.<sup>27</sup> When the reflecting surface is rough, the reflection from that surface will not be specular, but diffuse. This assumption was used in the first implementation of RLs. In such a case, the feedback in the gain medium is nonresonant and incoherent. In 1986, Markushev et al.<sup>28</sup> experimentally observed the phenomenon of light amplification from neodymium in sodium lanthanum molybdate powders. When pumping the sample above threshold, they observed that the emission spectrum from neodymium was narrowed to a single line and the duration of the emitted pulse was shortened by nearly four orders of magnitude. Followed by this, laser-like emission from a wide range of powder samples has been investigated.<sup>29</sup>

In 1994, Lawandy et al.<sup>30</sup> reported laser-like emission from a laser dye solution containing strongly scattering particles (titanium dioxide). In this case, the scatterers and the gain medium were independent. A lasing threshold in the input-output characteristics of the peak intensity was observed and, at the same value, the emission collapsed into a very narrow spectrum. The smooth emission spectrum above threshold indicated that the feedback for lasing was nonresonant. In such scattering media, there are no discrete equispaced resonant modes formed due to the absence of a definite reflecting boundary. The interaction of various modes and the high losses experienced by each mode resulted in a smooth spectrum. In addition, the authors also noticed that the threshold energy for lasing was surprisingly low. Later on, this laser-like phenomenon observed in random media was assigned the term random lasers.<sup>31</sup> Nonresonant random lasing has been observed in many other disordered materials.<sup>32-35</sup>

In 1998, Cao et al. demonstrated a different kind of lasing mechanism in disordered semiconductor powders and polycrystalline films.<sup>36, 37</sup> When the pump intensity exceeded the threshold value, discrete narrow peaks emerged in the emission spectra and more sharp peaks appeared upon increasing the pump level. The frequencies of the sharp peaks depended on the sample position and they exhibited large intensity fluctuations. The emission spectrum exhibited characteristics of a multimode laser oscillator, even though in the absence of an external cavity. The authors suggested that the feedback for lasing is resonant. In such scattering medium, light returns to a scatterer from which it was initially scattered. Therefore, the light forms closed loops after multiple scattering events. In such a case, constructive interference of the returning light occurs only at certain frequencies and this defines the resonant frequencies. Similar lasing phenomena have also been observed in luminescent  $\pi$ -conjugated polymer films, organic dye-doped gel films, opal crystals saturated with polymer and laser dye solutions.<sup>38-43</sup>

In the early 2000's Cao et al. classified RLs into two categories based on the feedback mechanism<sup>23, 24, 44</sup> (i) RLs with incoherent and nonresonant feedback (ii) RLs with coherent and resonant feedback. In the former case, the feedback mechanism is intensity or energy feedback, which is phase insensitive (i.e., incoherent) and frequency independent (i.e., nonresonant). In the latter case, it is field or amplitude feedback, which is phase sensitive (i.e., coherent) and therefore frequency dependent (i.e., resonant). Surprisingly, there exist another class of RLs where coherent lasing occurs through nonresonant feedback in a disordered medium, wherein extended modes undergo large amplification to generate ultranarrow peaks.<sup>45-47</sup>

So far, RLs have been realized in various material system such as semiconductor nanoparticles,<sup>36,37,44,48-50</sup> ceramic powders,<sup>51, 52</sup> organic materials,<sup>38,42,53</sup> polymers,<sup>40,41,54</sup> and biological tissues.<sup>55-58</sup> After preliminary experimental studies, laser action in disordered media has been the subject of intense experimental and theoretical studies. It was proposed by Florescu et al. and experimentally verified by Cao et al. that the RL emission spectra above the threshold show poissonian statistics, which characterizes the coherent emission of a laser source.<sup>59, 60</sup> Later on, Jiang et al. proposed a time-dependent theory for RLs.<sup>61</sup> Using a finite-difference time-domain method, they constructed a random lasing system and studied the interplay between scattering and localization. Their formulations allowed them to calculate the field evolution beyond the threshold amplification and also the field pattern and the localized modes inside the system. Vanneste et al. proposed rate equations in two-dimensional (2D) random media by coupling Maxwell's equations in disordered medium with rate equations for a four-level atomic system.<sup>62</sup> The results were in good agreement with the experimental results reported by Cao et al.<sup>37</sup>

Modes in a conventional laser are determined by the laser cavity. They usually consist of a standing wave pattern.<sup>3</sup> The characteristics of the lasing modes in a RL system have been studied both theoretically and numerically by Andreasen et al.<sup>63</sup> Noginov et al. and Lui et al. studied third-order nonlinear effects in RLs and discussed the variations of



frequency and structure of lasing modes.<sup>64, 65</sup> In most RLs the interference in multiple scattering leads to a granular distribution of the intensity called speckle. Therefore, in such RL systems the spatial profile of the modes is dominated by the speckle pattern. Also, in most RL system the intensity is distributed throughout the sample and the modes are extended rather than localized. The localization can occur only in extremely strongly scattering materials. The average spatial extent of these localized modes is called the localization length. Later on, Fallert et al. experimentally revealed the co-existence of both extended and localized modes.<sup>47</sup> In 2011, Lopez et al. discovered that laser mode locking can spontaneously arise in RLs and realized the smallest ever mode-locked device.<sup>66</sup> Furthermore, they engineered a mode selective pumping scheme and showed that one can continuously change the system from a configuration in which the various excited electromagnetic modes interact weakly to a collective strongly interacting regime.

It was believed that only strong scattering can support the field feedback for lasing. However, it has been shown that the field feedback mechanism is also possible in weakly scattering regimes.<sup>39-42</sup> In some random systems in the weakly scattering regime, the laser emission spectra exhibit narrow and equally spaced sharp peaks over the fluorescence/ASE background. In this context, Polson and Vardeny proposed the power Fourier transform technique to understand the periodic nature of the emission peaks. They found that the ensemble-averaged power Fourier transform of the emission spectra contains sharp, well-resolved Fourier components and their harmonics. These are the characteristics of a well-defined laser resonator.<sup>42</sup> Followed by these discoveries, Cao et al. performed a detailed experimental and numerical investigation on RL action in weakly scattering systems.<sup>44</sup> They used TiO<sub>2</sub>, ZnO and SiO<sub>2</sub> nanoparticles in different dye solutions for the experiments. They found that the lasing spectra exhibit certain periodicity and the periodicity changes with parameters such as dye concentration, nanoparticle density. Based on experimental and numerical findings, Cao proposed two regimes of operation: under-coupling and over-coupling regimes, based on the coupled-wave theory of distributed feedback lasers. In the former regime, the quasi-modes are formed mainly by the feedback from the scatterers near the system boundary, while in the latter case, the feedback is mainly from the scatterers inside the system. Therefore, the quasi-modes of an under-coupled system with high quality factor have almost regular frequency spacing. Based on these observations and findings, Cao proposed the existence of an effective cavity in such systems.

RLs emit light in an uncontrolled way, over a wide range of output directions, hindering their application in various fields. In this context, several efforts have been devoted to obtain directional random lasing by adopting different geometries. K. C. Jorge et al.<sup>67</sup> used a hollow-core antiresonant reflecting optical waveguide containing the gain medium, while Bachelard et al.<sup>68, 69</sup> and Leonetti et al.<sup>70</sup> used engineered spatial profile of the pump beam in order to control the RL emission direction and mode selection. Directional RL emission was also observed in Anderson localizing optical fiber<sup>71</sup> and hollow core photonic crystal fiber filled with scattering particles and dye solution<sup>72, 73</sup>. Later on,

Schönhuber et al. achieved a RL configuration whose directionality of emission can be controlled.<sup>74</sup> Moreover, the authors even created a collimated RL, while at the same time maintaining its spectral behavior.

## 2.4 Random lasing in nematic liquid crystals

Liquid crystals are mesophases, where the molecules favor a certain orientation because of intermolecular forces. In the nematic phase, the rod-like molecules possess a negligible positional order, while the long axis of the molecules orients in an average direction named as the molecular director<sup>7</sup>  $\mathbf{n}(r, t)$ . In the absence of any dopant materials, NLC are very good dielectrics, transparent from ultraviolet (UV) to mid-infrared lights.<sup>75, 76</sup> In the presence of an applied field, the reaction of the induced-dipoles tends to align (reorientation) the NLC molecules toward the field direction (for details see Chapter 3). Such reorientation exhibits a threshold known as Freedericksz's transition threshold.<sup>75, 76</sup>

The spontaneous fluctuations of the molecular director in NLC can be represented as  $\mathbf{n}(r, t) = \mathbf{n}_0 + \delta\mathbf{n}(r, t)$ . These fluctuations of the molecular director lead to fluctuations in the local dielectric tensor given by the equation  $\varepsilon_{\alpha\beta} = \varepsilon_{\parallel} \delta_{\alpha\beta} + (\varepsilon_{\parallel} - \varepsilon_{\perp})n_{\alpha}n_{\beta}$ . The fluctuations in the dielectric properties support recurrent multiple scattering events as light propagates through the NLC medium. The fluctuations of  $\varepsilon_{\alpha\beta}$  arise from two sources: (i) fluctuations in  $\varepsilon_{\parallel}$  and  $\varepsilon_{\perp}$  due to small, local changes in the temperature and density; (ii) fluctuations in the orientation of the molecular director  $\mathbf{n}$ . The latter one is the dominant one. The scattering strength of visible light in NLC due to its dielectric fluctuations is about  $10^6$  times larger than in normal isotropic fluids.<sup>76</sup> NLC can provide even more scattering by doping it with dye molecules, due to the internal interaction between dye molecules and nematic host occurring under optical excitation.<sup>77</sup> More specifically, in dye-doped NLC the local thermal fluctuations add to the strong photo-induced perturbations providing enhanced light scattering.

Dye-doped NLC are an excellent platform for the realization of RLs due to their tunable scattering properties, which provide the feedback mechanism for lasing. The main drawback of NLC as host material for dye-dopants is that they need to be integrated into glass cells to have macroscopic order of the molecules. In order to have a uniform alignment, the glass surfaces are usually mechanically rubbed with polymers to favor long-range order. This ordering increases the pumping efficiency and polarization ratio of the emission. Several researchers have studied extensively the random lasing properties of NLC doped with pump-resonant active dye molecules (Pyrromethene 597, Pyrromethene 650 and DCM) enclosed in various confinement geometries such as wedge cells, cylindrical capillary tubes, freestanding films and micro droplets.<sup>4, 78-80</sup> Dye-doped NLC emit highly polarized light with good conversion efficiency through resonant feedback upon optical

pumping within the absorption region of the dye. When pumped above a given threshold value, discrete sharp peaks emerge from the residual fluorescence spectrum with a linewidth of less than 0.5 nm, corresponding to a quality factor of  $>1000$  for the random system. Certain periodicity has also been observed in the emission spectrum.<sup>81, 82</sup>

Strangi et al. have studied the polarization dependence of the RL emission. They observed that the emission intensity reduces significantly when the pump light is polarized perpendicular to the NLC director (ordinary polarization) compared to the light polarized parallel to the director (extraordinary polarization), while the emission polarization remains independent of the pump polarization. This effect has been explained by the large diffusion constant of the emitted photons for the extraordinary polarization compared to the ordinary polarization.<sup>83</sup>

The emission polarization of the NLC RLs depends on the rubbing direction or the alignment of the liquid crystal molecules. Ye et al.<sup>84</sup> and Chen et al.<sup>85</sup> explored this by constructing NLC cells with different rubbing directions on the forward and backward light emitting surfaces and observed a bidirectional RL with orthogonal polarizations emitted in two directions. In addition to this, the influence of an external electric field on the polarization degree was also studied.

Further, Ferjani et al. investigated the temperature dependence of the RL emission from dye-doped NLC<sup>79</sup> and found that the slope efficiency and threshold of lasing can be effectively tuned by temperature. The enhancement of thermal fluctuations leads to increased scattering, which shortens the scattering mean free path and hence the volume of the random cavities. They also extended their studies into the spatial profile of the emitted photons and the statistics of the intensity fluctuations. The spatial intensity distribution showed a pattern with rich structure composed of several bright spots. In the statistical analysis, the occurrence of lasing was minimum as the temperature increased. This was in good agreement with temperature dependent coherent backscattering measurements in dye-doped NLC, where the backscattering intensity decreases with increasing temperature. They also explained the chaos of the amplification mechanism in dye-doped NLC through the Shannon entropy and the existence of correlations in the emission properties.<sup>86</sup>

Bian et al. demonstrated an all-optically controllable RL configuration based on the photo-thermal effect, where a continuous-wave (CW) beam nonresonant with the dye was used to control the emission properties.<sup>87</sup> Lee et al. experimentally showed an electrically controlled NLC RL below the Fréedericksz transition threshold.<sup>88</sup> They showed that the lasing intensities and the energy thresholds of the RLs can be adjusted by using applied voltage below the Fréedericksz transition threshold. Wang et al. demonstrated that adding gold nanoparticles in NLC can enhance and control the random lasing properties especially in the presence of applied electric fields.<sup>89</sup>

## 2.5 Applications of random lasers

RLs have applications in a variety of fields ranging from information technology to biomedicine. Micro RL is one of the newly discovered light sources, which can be used inside an electric circuit or can be used as optical tags. RLs can be used for the detection of cancer cells or tumors and in photodynamic therapy.<sup>23</sup> Wiersma et al. have developed a temperature-tunable RL based on liquid crystals.<sup>90</sup> Such a light source exhibits a temperature-tunable emission spectrum and is expected to find applications in photonics, temperature-sensitive displays and screens, as well as remote temperature sensing. Recently Cao et al. demonstrated that RLs can be engineered to provide low spatial coherence, very useful for speckle-free full-field imaging.<sup>91</sup> It has also been shown that RLs can act as optical diodes.<sup>92</sup> A capillary filled with dye with graded gain permits the transmission of light at certain wavelengths in one direction but not in the other. Addition of scattering particles into the dye then allows tailoring the passband. Very recently, RLs have been used as optical sensors<sup>93</sup> e.g., for measuring pH value<sup>94</sup> and milk fat content.<sup>95</sup>



### 3 Nonlinear optics in nematic liquid crystals

Nonlinear optics is an extension of linear optics, boosted by the invention of laser technology. The invention of the laser gave rise to the study of optical properties of materials at high intensities, leading to new phenomena not visible with ordinary light. Such nonlinear effects include the generation of new colors from monochromatic light in transparent crystals and the self-focusing of optical beams in a homogeneous liquid.<sup>96, 97</sup> At the intensities used to generate these types of effects, the usual optical parameters of materials cannot be considered constant but become functions of the light intensity, hence, the area is called nonlinear optics. In this Chapter, the optical properties of NLC and the main features of the propagation of spatial optical solitons in NLC will be discussed.

#### 3.1 Nematic liquid crystals

Liquid crystals are particular states of matter that show properties of both liquids and crystalline solids. They may flow like liquids, nevertheless, possess some degree of long-range order like crystals.<sup>6</sup> There are many different types of liquid crystal phases. Thermotropic are the most widely used liquid crystals. Based on the type of molecular order, thermotropic liquid crystals are classified to nematic, smectic and cholesteric.

NLC are organic compounds consisting of elongated molecules.<sup>98</sup> Fig. 3.1 shows the nematic phase and its difference with respect to the isotropic phase of a normal liquid. In the nematic phase, the long axis of the molecule is aligned in an average direction called the molecular director,  $\mathbf{n}$ , but the molecules lack a positional order. Any liquid crystal phase with some orientational order and negligible positional order can be considered as nematic. In this phase, the orientational order parameter describes the angular distribution of the molecules around the director.<sup>99</sup> The order parameter varies from 0 (isotropic) to 1 (crystal-like order).

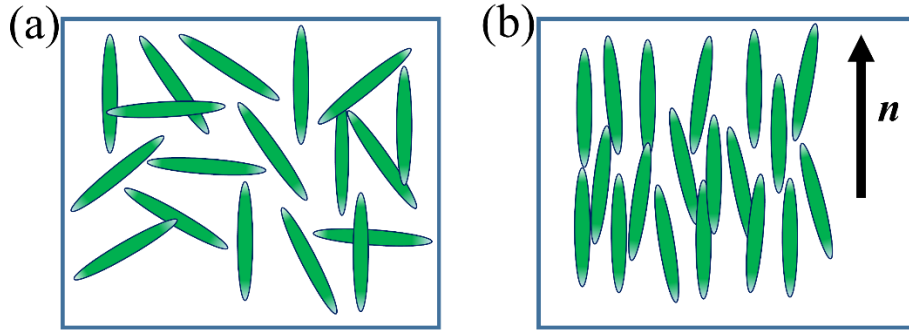


**Figure 3.1.** (a) Pictorial representation of the isotropic phase. Molecules are randomly arranged in space, i.e., both positional and orientational order are absent. (b) In the nematic phase, positional order is negligible, while a long-range orientational order along the director  $\mathbf{n}$  is present.

### 3.2 Optical properties of nematic liquid crystals

In the nematic phase, molecules give rise to a direction dependent response (anisotropy) at the macroscopic level. Therefore, the NLC response to external stimuli can be described with a tensor with two (uniaxial) or three (biaxial) distinct eigenvalues. Typical liquid crystals exhibit a uniaxial nematic phase.

Consider a plane wave propagating with a wavevector  $\mathbf{k}$  in a homogeneously aligned NLC sample. Since NLC are anisotropic materials, the propagating field will experience a refractive index that depends on the angle between the polarization vector of the optical wave and the molecular director. When  $\mathbf{n}$  lies along  $\mathbf{k}$  the light sees refractive index of a wave polarized in a plane perpendicular to the plane containing the wavevector  $\mathbf{k}$  and the director  $\mathbf{n}$ , i.e., ordinary refractive index ( $n_{\perp} = n_o = \sqrt{\epsilon_{\perp}}$ ). For a non-vanishing angle the refractive index is known as extraordinary refractive index, and given by:

$$n_e = \frac{n_{\parallel} n_{\perp}}{\sqrt{n_{\parallel}^2 \cos^2 \theta + n_{\perp}^2 \sin^2 \theta}} \quad (3.1)$$

where  $n_{\parallel} = n_e = \sqrt{\epsilon_{\parallel}}$  is the extreme value of the extraordinary index, valid for light polarized along the director. Typically for NLC,  $n_{\parallel} > n_{\perp}$ , and the material is equivalent to a positive uniaxial crystal with anisotropy  $\Delta\epsilon = \epsilon_{\parallel} - \epsilon_{\perp}$  and optic axis  $\mathbf{n}$ . Moreover, the large birefringence ( $\Delta n = n_{\parallel} - n_{\perp} \approx 0.2$ ) causes the Poynting vector  $\mathbf{S}$  to propagate at a non-negligible walk-off angle  $\delta$  with respect to  $\mathbf{k}$ , being

$$\tan \delta(\theta) = \frac{(n_{\parallel}^2 - n_{\perp}^2) \sin \theta \cos \theta}{n_{\perp}^2 + (n_{\parallel}^2 - n_{\perp}^2) \cos^2 \theta} \quad (3.2)$$

A plot of the extraordinary refractive index and walk-off angle dependence on angle  $\theta$  between molecular director  $\mathbf{n}$  and wavevector  $\mathbf{k}$  in E7 NLC is shown in Fig. 3.2.

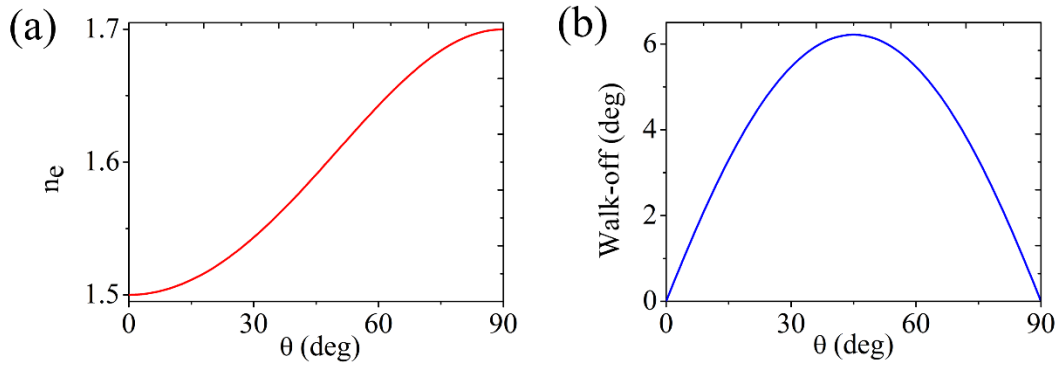


**Figure 3.2.** (a) Extraordinary refractive index and (b) walk-off angle versus the angle  $\theta$  between  $\mathbf{n}$  and  $\mathbf{k}$ . Typical values of  $n_{\parallel}$  and  $n_{\perp}$  are chosen for the E7 NLC.

### 3.3 Continuum theory and reorientational nonlinearity

Liquid crystals molecules are very sensitive to external stimuli such as electric or magnetic fields. In NLC, when an external electric field is present, the electrons in the molecular orbitals tend to follow the field and give rise to dipoles. The molecules therefore tend to align with the applied field in order to minimize the resulting Coulombian torque (see Fig. 3.3).<sup>7, 75, 76</sup> This torque is counteracted by the elastic forces originating from intermolecular links. An equilibrium state is reached when the free energy of the system is minimized. The NLC response towards external stimuli was described by De Gennes and is known as the continuum theory.<sup>6</sup>

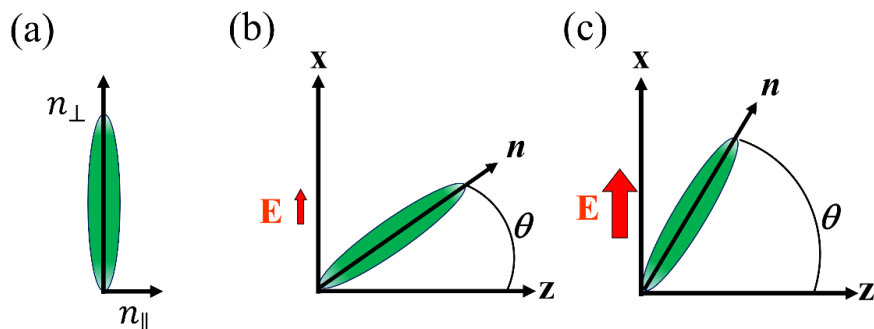


**Figure 3.3.** (a) Representation of refractive indices parallel and perpendicular to the long axis (molecular director) of the NLC molecule. (b) Interaction of NLC with a low intensity field. The angle  $\theta$  is independent of the field intensity. (c) Interaction of NLC with a high intensity field. The molecules tend to reorient towards the field direction.



When an external electromagnetic field interacts with NLC molecules, the torque from the field modifies the director distribution until a new equilibrium state is reached. This can be found by calculating the energy provided by the field in order to reorient the director distribution. The field provides its contribution to the free energy, given by

$$F_E = \frac{\Delta\varepsilon}{2} (\mathbf{n} \cdot \mathbf{E}) \quad (3.3)$$

where  $\Delta\varepsilon$  is the anisotropy. When the field amplitude becomes larger, the elongated NLC molecules tend to align along the externally applied field until the torque from the field is balanced out by the elastic forces present. The contribution of elastic forces to the free energy (Oseen-Zöcher-Frank formula) is given by<sup>100</sup>

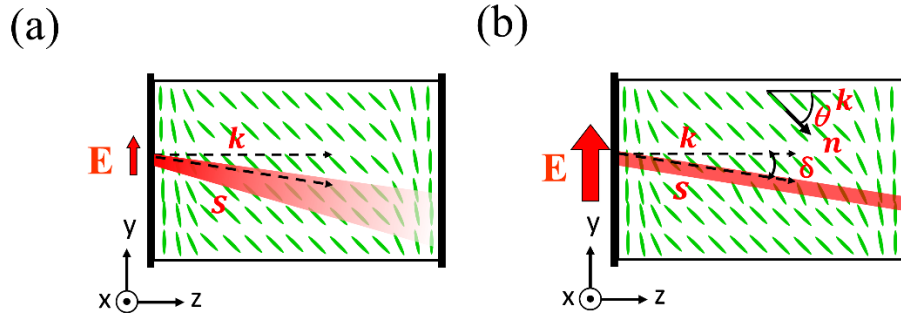
$$F_{elastic} = \frac{1}{2} \{ K_1 (\nabla \cdot \mathbf{n})^2 + K_2 (\mathbf{n} \cdot \nabla \times \mathbf{n})^2 + K_3 (\mathbf{n} \times (\nabla \times \mathbf{n}))^2 \} \quad (3.4)$$

where  $K_1$ ,  $K_2$  and  $K_3$  are the Frank elastic constants for the three elementary deformations of liquid crystals, i.e., splay, twist, and bend respectively. Considering planar deformations ( $K_2 = 0$ ) and a single-constant approximation ( $K_1 \approx K_3 \approx K$ ) and using the Euler-Lagrange equations for the free energy minimization, we can find the reorientational equation<sup>7</sup>

$$K \nabla^2 \theta + \frac{\varepsilon_0 \Delta\varepsilon}{2} \sin 2\theta |\mathbf{E}|^2 = 0 \quad (3.5)$$

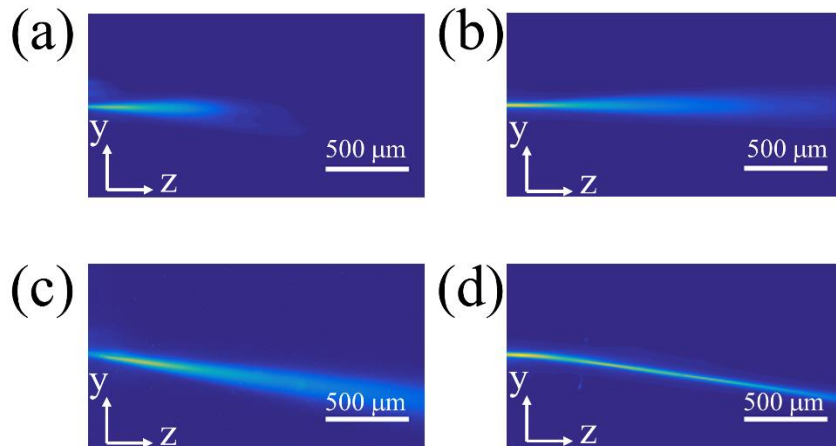
### 3.4 Soliton formation in nematic liquid crystals

Figure 3.4 shows a finite-size fundamental Gaussian beam propagating with wavevector  $\mathbf{k}$  along  $z$  in an NLC sample. The NLC molecules are arranged in plane  $yz$  at angle  $\theta_0$  with respect to  $z$ . When excited by ordinarily polarized beam, the beam will propagate straight, on the other hand, an extraordinarily polarized beam propagate with a walk-off angle  $\delta$ , defining a direction lying between  $\mathbf{n}$  and  $\mathbf{k}$ . At very low powers (linear regime), both beam components diffract with their characteristic Rayleigh length  $L = n_i \pi w_0^2 / \lambda$  where  $n_i$  is the ordinary or extraordinary refractive index,  $w_0$  is the input beam waist and  $\lambda$  is the excitation wavelength. The ordinary polarization (electric field along  $x$ ) cannot produce any reorientation, due to the high value of the Freedericksz's transition threshold.<sup>6</sup> For the extraordinary polarization (electric field in plane  $yz$ ), the Freedericksz's transition threshold is zero and light with sufficient intensity can reorient the molecular director.<sup>101</sup> The molecular director reorientation increases the effective refractive index  $n_e(\theta)$  according to Eq. (3.3)<sup>102, 103</sup> Because of this, the NLC perturbed by the beam will act as a focusing lens, in turn yielding self-focusing of a finite-size beam. This self-focusing



**Figure 3.4.** Pictorial sketch of (a) linear diffraction and (b) soliton generation of an extraordinarily polarized beam in an NLC cell.

effect balances out the linear diffraction and hence supports the propagation of self-confined light beams, so-called optical solitons. The spatial optical solitons in NLC are also called nematicons. An experimental demonstration of the nematicon formation is shown in Fig. 3.5.



**Figure 3.5.** Behavior of light beam propagation in NLC sample captured through the experimental setup described in Section 4.2. Propagation of an ordinarily polarized beam at powers (a) 0.6 mW and (b) 5mW. Propagation of an extraordinarily polarized beam at powers (c) 0.6 mW and (d) 5mW.

The theoretical model describing the soliton formation can be obtained from Maxwell's equation under the paraxial approximation and considering the anisotropy. The beam propagation in the paraxial approximation is given by<sup>104</sup>

$$2ik_0n_e \left( \frac{\partial A}{\partial z} + \tan\delta \frac{\partial A}{\partial y} \right) + D_y \frac{\partial^2 A}{\partial y^2} + \frac{\partial^2 A}{\partial x^2} + k_0^2 \Delta n_e^2 A = 0 \quad (3.6)$$

$$\nabla^2\theta + \gamma\sin(2(\theta - \delta))|A|^2 = 0 \quad (3.7)$$

where  $z$  is the propagation direction,  $A$  is the electric field envelope,  $D_y$  is the diffraction coefficient along  $y$ ,  $\delta$  is the walk-off angle,  $\Delta n_e^2 = n_e^2(\theta) - n_e^2(\theta_m)$  is the nonlinear index well, where  $\theta_m$  is the maximum orientation angle, and  $\gamma = \varepsilon_0 \Delta\varepsilon/4K$  is the effective nonlinear strength, where  $\varepsilon_0$  is the vacuum dielectric constant. Eq. (3.6) is a nonlinear Schrödinger type equation that accounts the beam walk-off and saturation, in the reorientational medium. Eq. (3.7) is the reorientational equation, which describes the balance between the optical torque and the elastic force.<sup>105</sup>

Due to the elastic intermolecular forces, the refractive index perturbation is much wider than the input beam width. Moreover, this optical perturbation extends over a range in the transverse direction, determined by the boundary separation in standard planar cells. This high nonlocality of the nonlinear response prevents catastrophic collapse and stabilizes the nematicon.<sup>106-108</sup>

## 4 Nematicon-assisted random lasing

As mentioned earlier, nematicons are light-induced waveguides for extraordinarily polarized signals of relatively arbitrary wavelengths, powers and profiles.<sup>109-114</sup> Owing to their large numerical aperture,<sup>109</sup> nematicons have been used in various experiments to efficiently collect and inject fluorescence or ASE into optical fibers.<sup>115-116</sup> This Chapter is based such opportunities and provides one of the core parts of this Thesis. We report that by the combination of solitons and collinear optical pumping in dye-doped NLC can provide random lasing with enhanced features. The main results of **Publication I**, **Publication II** and **Publication III** are discussed here.

### 4.1 Sample

The sample used in our experiments is a planar glass cell made up of two parallel indium tin oxide (ITO) covered Borosilicate glass slides.<sup>117</sup> Mylar spacers were inserted between the glass slides to define the thickness of the cell. The cell is about 100  $\mu\text{m}$  thick ( $x$ ), 30 mm wide ( $y$ ) and 2 mm long ( $z$ ). The surfaces of the glass plates were covered with polyimide and mechanically rubbed to favor homogeneous alignment of the NLC molecular director in the plane  $yz$  at  $45^\circ$  with respect to  $z$ . This anchoring maximizes the walk-off angle and the nonlinearity experienced by an extraordinarily polarized beam propagating with  $\mathbf{k}$  parallel to  $z$ .<sup>118</sup> This also forces the NLC to have a long range order even in the bulk of the sample. Another set of microscope cover slides of 100  $\mu\text{m}$  thickness were glued orthogonal to  $z$  in order to seal the cell and define input and output facets. These glass plates were also surface treated with Polyimide and mechanically rubbed along  $y$  to optimize the coupling of  $y$ -polarized input beams to extraordinary waves in the NLC cell. Moreover, the presence of these extra interfaces suppresses the formation of menisci and depolarization effects.<sup>119</sup> A pictorial representation of the planar cell is shown in Fig. 4.1.

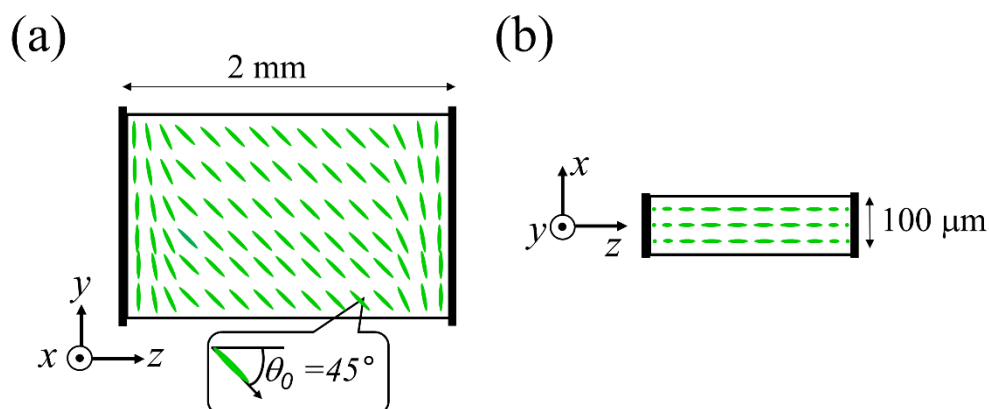


**Figure 4.1.** Pictorial representation of the planar cell filled with NLC sample. (a) Top view (b) Side view.

A mixture of commercially available E7 (Merck) and 0.3 wt% of pyrromethene 597 (PM 597) dye (Exciton) is used as the RL material. The above fabricated cells were filled with this mixture using the capillary action. E7 is a liquid crystalline mixture in the nematic phase and it has large birefringence. The molecular composition of E7 is illustrated in Fig. 4.2 (a). The Frank's constants for E7 at 1064 nm are  $K_1 = 11.7$  pN,  $K_2 = 9.10$  pN and  $K_3 = 19.5$  pN and the refractive indices along the principal axes are  $n_{||} = 1.71$  and  $n_{\perp} = 1.52$ .<sup>7</sup> PM 597 is based on the fluoroboration of two pyrrole rings associated by a conjugated  $\pi$ -system chain, yielding Dipyrrromethene-BF<sub>2</sub> complexes. PM597 belongs to the group of cyclic cyanine dyes. It has absorption and emission maxima at 530 nm and 575 nm, respectively. It also has a fluorescence quantum yield approaching unity and can lase more efficiently than rhodamine.<sup>120, 121</sup>

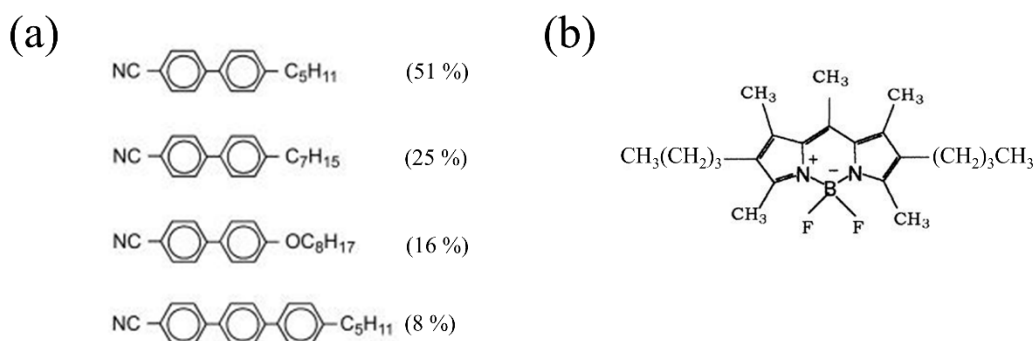


**Figure 4.2.** Molecular structure of (a) E7 mixture and its relative composition and (b) PM 597 dye.

## 4.2 Experimental setup

As sketched in Fig. 4.3, the experimental setup consist of two laser sources. One is a continuous-wave (CW) source operating at the near-infrared (NIR) wavelength of 1064 nm and the second one is a Q-switched Nd:YAG pulsed laser with 6 ns pulse length, 20 Hz pulse repetition rate, and emitting at its second-harmonic wavelength of 532 nm. The former laser is used to create the soliton waveguide, while the latter is used to pump the guest-host medium. Both beams were collinearly focused in the midplane ( $x = 50 \mu\text{m}$ ) of the cell using an objective lens (infinity corrected) with a comparable focal spot radius of about  $3 \mu\text{m}$  to avoid reflections from the upper and lower interfaces. Polarizers and waveplates were used to control the polarization and power of the launched laser beams. The NIR soliton and the generated fluorescence/ASE/RL emission were imaged by NLC light scattering out the of the plane  $yz$  and also, the transverse plane  $xy$  at the cell output using microscopes and high-resolution CMOS cameras.

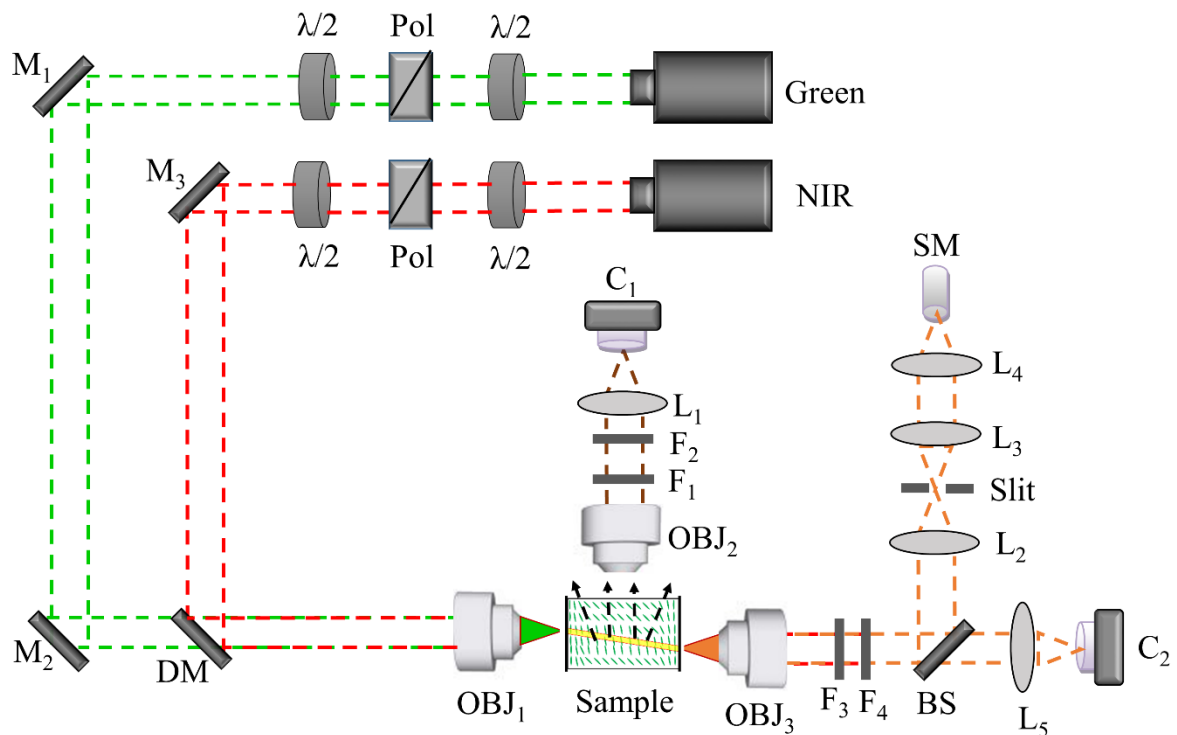


**Figure 4.3.** Schematic of the experimental setup.  $\lambda/2$ : Half waveplate; Pol: Polarizer;  $M_1$ ,  $M_2$ ,  $M_3$ : Mirrors; DM: Dichroic mirror;  $OBJ_1$ ,  $OBJ_2$ ,  $OBJ_3$ : Objective lenses (infinity corrected);  $F_1$ ,  $F_2$ ,  $F_3$ ,  $F_4$ : Notch filters;  $L_1$ ,  $L_2$ ,  $L_3$ ,  $L_4$ ,  $L_5$ : Lenses;  $C_1$ ,  $C_2$ : CMOS cameras; BS: Beam splitter; SM: Spectrometer. This experimental setup was used in **Publication III** and **IV** and a simplified version of this was used in **Publication I** and **II**.

A fiber equipped spectrometer (Ocean optics) with resolution  $\Delta\lambda = 0.15$  nm was used to collect and spectrally resolve the emitted light. Additionally, filtering elements such as notch filters and a slit were used whenever appropriate to eliminate the residual pump, NIR and scattered light from the cell boundaries. A silicon detector was used to measure the RL output energy.

### 4.3 Interaction geometry

The interactions of the green pump, RL emission and the NIR soliton in the NLC cell are sketched in Fig. 4.4. As explained in Section 4.2, both green and NIR beams were collinearly injected with wave vectors ( $\mathbf{k}_g // \mathbf{k}_{NIR}$ ) along  $z$  at the cell mid-plane. The former one generates fluorescence and also stimulated emission and lasing action via random scattering and feedback, while the latter one excites a reorientational spatial soliton at mW powers. The pump-pulse duration (6 ns), repetition rate (20 Hz) and the pulse energy used in the experiments prevented significant reorientational and thermal nonlinear effects in the guest-host. It has been shown that the emission from NLC doped with PM597 tends to be polarized in the plane of the director alignment and, independent of the pump polarization.<sup>78, 6, 115</sup> Hence, the generated photons are extraordinarily polarized waves in the geometry investigated and they propagate with their characteristic walk-off in the uniaxial guest-host (see Fig. 4.4). Since the generated photons are co-polarized with the soliton, they can trap inside the soliton waveguide and are conveyed at the exit without any spatial dispersion of the emitted light. The pump beam can also undergo soliton confinement depending on its polarization. If the pump is polarized along  $y$  (extraordinary) at the input, it can be guided along the soliton, yielding an extended interaction of the pump (limited by the absorption) inside the soliton waveguide compared to an ordinarily polarized pump (see Fig. 4.4). However, we experimentally found that, in this geometry defined by the boundary conditions (see Section 4.1), an ordinarily polarized pump is more efficient in terms of emission yield (see Section 4.4). These observations were published in **Publication I**.

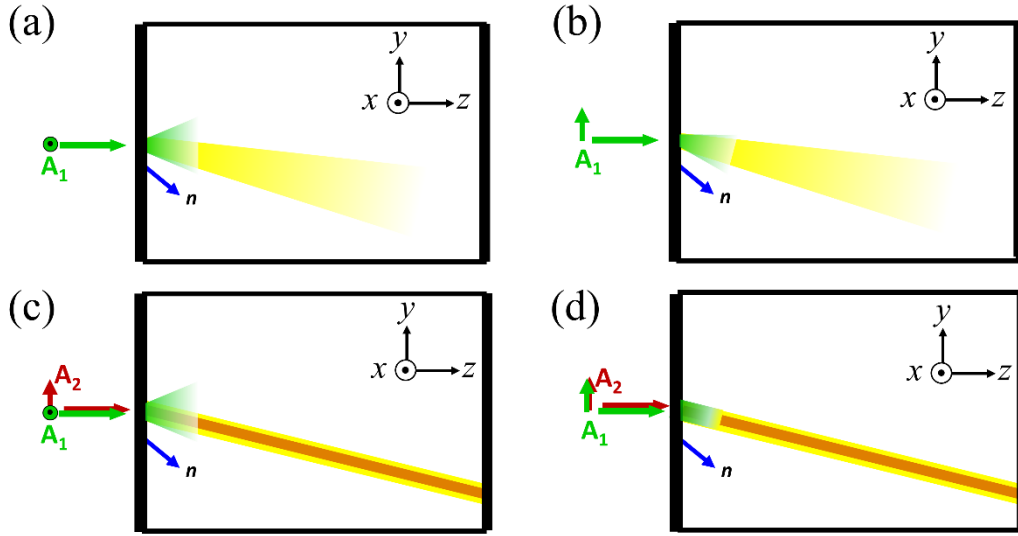


**Figure 4.4.** Pictorial representation of the interaction geometry. Interaction of an (a) ordinary and (b) extraordinary wave pump (amplitude  $A_1$ ). The emitted light, represented as a yellow beam, is generated in the initial region of the pumped area where the pump remains intense despite absorption. Sketch of the interaction of an extraordinary wave soliton (amplitude  $A_2$ ) with an (c) ordinary and (d) extraordinary wave pump.

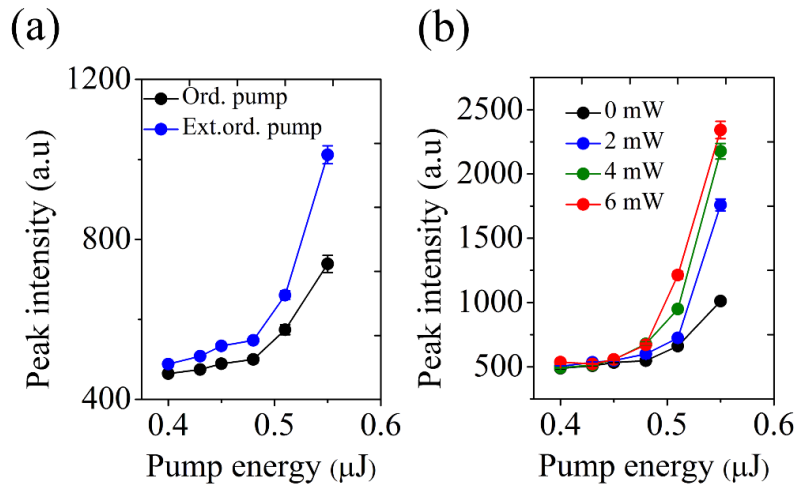
#### 4.4 Input versus output characteristics

Figure 4.5 (a) shows the measured output peak intensity versus input pump pulse energy characteristics of the RL acquired from the emitted light for ordinarily and extraordinarily polarized pump in the absence of soliton. The peak intensity  $\bar{I}_{Max}$ , calculated as

$$\bar{I}_{Max} = \frac{1}{N} \sum_{K=1}^N Max_{\lambda} I_K(\lambda) \quad (4.1)$$

with  $I_k(\lambda)$  being an individual emission spectrum in intensity and averaged over  $N=200$  gated acquisitions. The curves exhibit a standard lasing character with an energy threshold around  $0.48 \mu\text{J}$  and higher slope efficiency for an ordinarily polarized pump. For the ordinarily polarized pump, the threshold is slightly lower and lasing more efficient. This is consistent with a previous observation in the same material.<sup>78, 115</sup> Clearly, despite the spatial spreading (limited by absorption) of the ordinarily polarized pump, the nematicon-assisted RL operates better in a configuration with orthogonal pump and nematicon. These observations were first published in **Publication I** along with other preliminary results. In **Publication I** we used a low-resolution ( $\Delta\lambda = 4 \text{ nm}$ ) spectrometer for characterizing random laser emission. However, evidence of random lasing such as lasing threshold and spectral narrowing was present.





**Figure 4.5.** Measured peak intensity of the emission spectra versus pump energy. (a) Ordinarily and extraordinarily polarized pump without soliton. (b) Ordinary-wave pump with solitons of various powers. These results were published in **Publications I, II** and **III**.

Figure 4.5 (b) displays the input versus output characteristics of the nematicon-assisted RL in the most efficient configuration for various nematicon powers as indicated by the legends. The in-out curves give a lasing threshold at energies around 0.48  $\mu\text{J}$  and slope efficiencies clearly improved by the nematicon. The presence of nematicon slightly decreases the threshold energy as apparent from Fig. 4.5 (b). Representative RL emission spectra above threshold are shown in Fig. 4.6. The lasing spectrum consists of several discrete narrow sharp peaks (full width at half-maximum (FWHM)  $\sim 0.3$  nm) emerging from the fluorescence and ASE background. They vary shot-to-shot and exhibit characteristic fluctuations in intensity and frequency as typical for most RLs (Fig. 4.6 (a)). The lasing peaks for various realizations exhibit random intensity fluctuations but remain regularly spaced versus wavelength when averaging over a large number of pump shots with peak spacing of about 0.7 nm (Fig. 4.6 (b)).

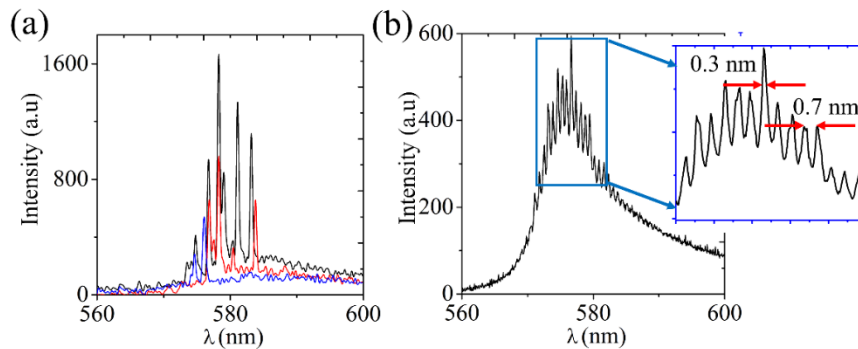


**Figure 4.6.** (a) Emission spectra collected from different shots at the same pump energy above lasing threshold. (b) Emission spectrum averaged over  $N=200$  shots.

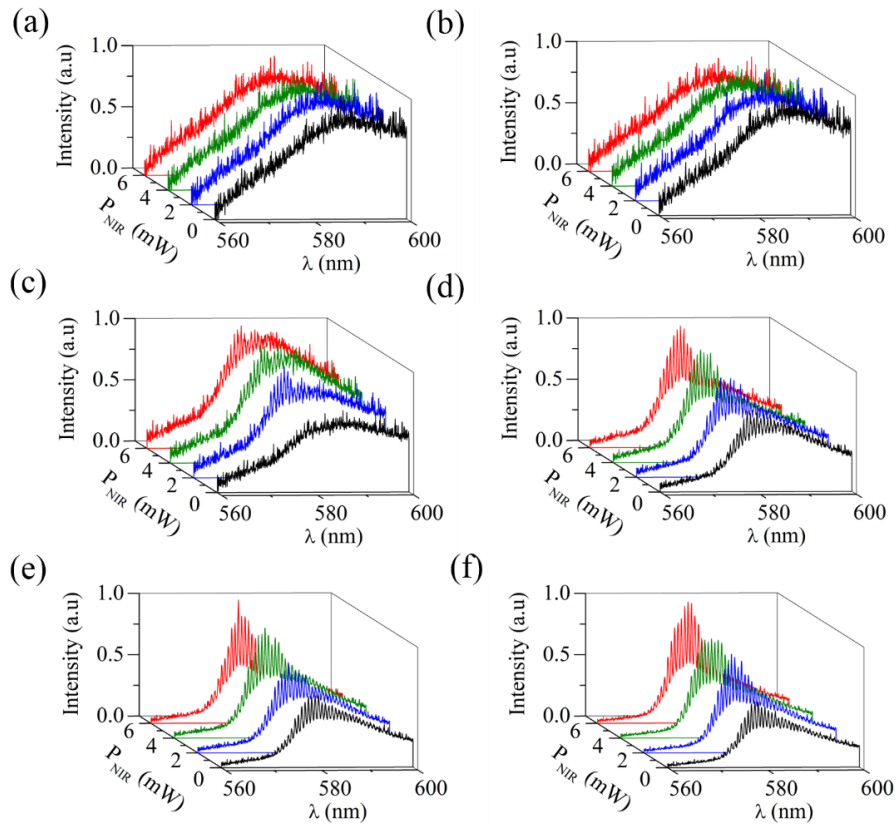


**Figure 4.7.** Emission spectra normalized to unity for various nematocion powers (colors) co-injected with the ordinarily polarized pump of various pulse energies. The spectra are averaged over  $N=200$  gated acquisitions. Pump pulse energy (a)  $E_p = 0.40 \mu\text{J}$ . (b)  $E_p = 0.45 \mu\text{J}$ . (c)  $E_p = 0.48 \mu\text{J}$ . (d)  $E_p = 0.51 \mu\text{J}$ . (e)  $E_p = 0.55 \mu\text{J}$ . (f)  $E_p = 0.6 \mu\text{J}$ . These results were published in **Publication III**

Fig. 4.7 represents the emitted spectra collected at the output averaged over  $N=200$  gated acquisitions with and without nematocions of various powers co-injected with the ordinarily polarized pump below and above lasing threshold. This illustrates the transition from fluorescence (characterized by broad emission spectrum, Fig. 4.7 (a)) to ASE (characterized by spectral narrowing, Fig. 4.7 (b)) to random lasing (characterized by sharp features, Fig. 4.7 (c-d)) upon increasing both pump energy and soliton power. The effect of nematocions of various powers is negligible at low energies (well below lasing threshold) as the light induced waveguide simply increases the collection efficiency of the emitted fluorescence or ASE measured at the exit of the cell.<sup>115</sup> However the presence of the collinear nematocion becomes much more pronounced at pump energies close to lasing threshold and above. At pump energy close to threshold (Fig. 4.7 (b)) and above threshold (Fig. 4.7 (c-d)) nematocions contribute to narrower multihump spectra, more intense and numerous sharp lasing peaks and global spectral narrowing compared to the emission spectra without nematocion. It is worth noting that at pump energy close to threshold

(below lasing threshold without nematicon), the presence of nematicons even brings the system above threshold by modulating the scattering and feedback and improving the collection efficiency associated with the all-optical waveguide.

As discussed in Fig. 4.6 (b), the average spectra presented in Fig. 4.7 consists narrow peaks (FWHM  $\sim 0.3$  nm) with random amplitude but regularly spaced versus wavelength (peak spacing  $\sim 0.7$  nm). This observation is in contrast with ideal random lasers where the peaks appears more randomly versus wavelength.<sup>33, 35, 46, 66, 70, 71</sup> However, this is in perfect agreement with random lasing emission observed in Refs. 44, 81 and 82. The nearly constant spectral spacing of lasing modes, which resembles that of a regular Fabry-Perot laser cavity, suggests the existence of an effective cavity even in the absence of real mirrors.<sup>122</sup> Using the formula of a Fabry-Perot cavity, we can extract the length of the cavity  $L_c$  as

$$L_c = \lambda^2 / 2n\Delta\lambda \quad (4.2)$$

where  $\Delta\lambda$  is the peak spacing and  $n$  is the refractive index of the medium. The peak spacing in our case suggest an equivalent cavity length  $L_c \sim 130$   $\mu\text{m}$ . This estimated length is comparable to the spatial extent of the excited region where the pump is absorbed as observed from the top of the cell. Furthermore, the change in  $\Delta\lambda$  is negligible versus soliton power which pinpoints the role of absorption in limiting the extent of the effective cavity, enabling scattering and feedback only in the initial fraction of the pumped volume.<sup>44</sup> However, it was a tedious task to closely examine the presence of an effective cavity as higher pump energies required to lengthen the effective cavity resulted in saturation and bleaching, as observed in **Publication II**. The above observations appear consistent with weak scattering close to under-coupling regime (i.e., an effective cavity much shorter than the nematicon), where the modes are formed mainly by the feedback from the scatterers near the system boundary.<sup>44, 123</sup>

## 4.5 Statistical analysis of emitted spectra

Since the focus of this work is on random lasers, the integrated average intensity versus pump energy plot (Fig. 4.8 (a)) does not exhibit any threshold despite the presence of spikes in the emission spectra or the presence of threshold when mapping the peak intensity (see Fig. 4.5 and Eq. (4.1)). It is very important to note that, in such cases, there is a co-existence of RL and ASE, where the RL threshold is masked by ASE, which does not necessarily exhibit a clear a threshold. It should be noted that the integrated intensity plots exhibit a plateau and then a sharp rise in the vicinity of pump threshold. This might be due to the random variation of the experimental conditions such as pump energy fluctuations as it did not appear in any other measurements. Therefore, in order to display

a threshold, we rely on statistical analysis of the spectral fluctuations quantified by variance.<sup>33, 124</sup>

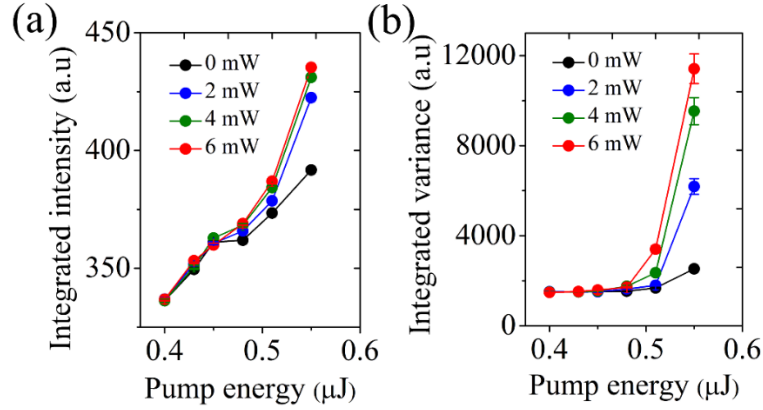


**Figure 4.8.** (a) Integrated intensity and (b) integrated variance of the emission spectra versus pump energy for various soliton powers. These results were published in **Publication III**.

To analyze the emission properties and threshold behavior of the random laser, we thus calculated the average intensity and the variance over  $N = 200$  output spectra (gated over 100 ms window) defined as

$$\bar{I}(\lambda) = \frac{1}{N} \sum_{K=1}^N I_K(\lambda) \quad (4.3)$$

$$\sigma_I^2 = \frac{1}{N-1} \sum_{K=1}^N (I_K(\lambda) - \bar{I}(\lambda))^2 \quad (4.4)$$

respectively. To analyze the system behavior and gain more insight on the global operation of the random laser, the average intensity and the variance can be integrated over the spectral window defined as  $\Delta\lambda = \lambda_{Max} - \lambda_{Min}$ . The integrated average intensity and integrated variance, respectively,

$$\bar{I} = \frac{1}{\Delta\lambda} \int_{\lambda_{Min}}^{\lambda_{Max}} \bar{I}(\lambda) d\lambda \quad (4.5)$$

$$\sigma_I^2 = \frac{1}{\Delta\lambda} \int_{\lambda_{Min}}^{\lambda_{Max}} \sigma_I^2(\lambda) d\lambda \quad (4.6)$$

The integrated variance described in Eq. 4.6 is remarkably sensitive to the emergence of spectral peaks and their characteristic fluctuations. Hence, a threshold on the fluctuations in Fig. 4.8 reveals the onset of laser action as it appears in the mean peak intensity (see Fig. 4.5 (b)). Sample data of the quantities such as average spectra and variance versus wavelength for various pump energies and soliton powers are shown in Fig. 4.9.

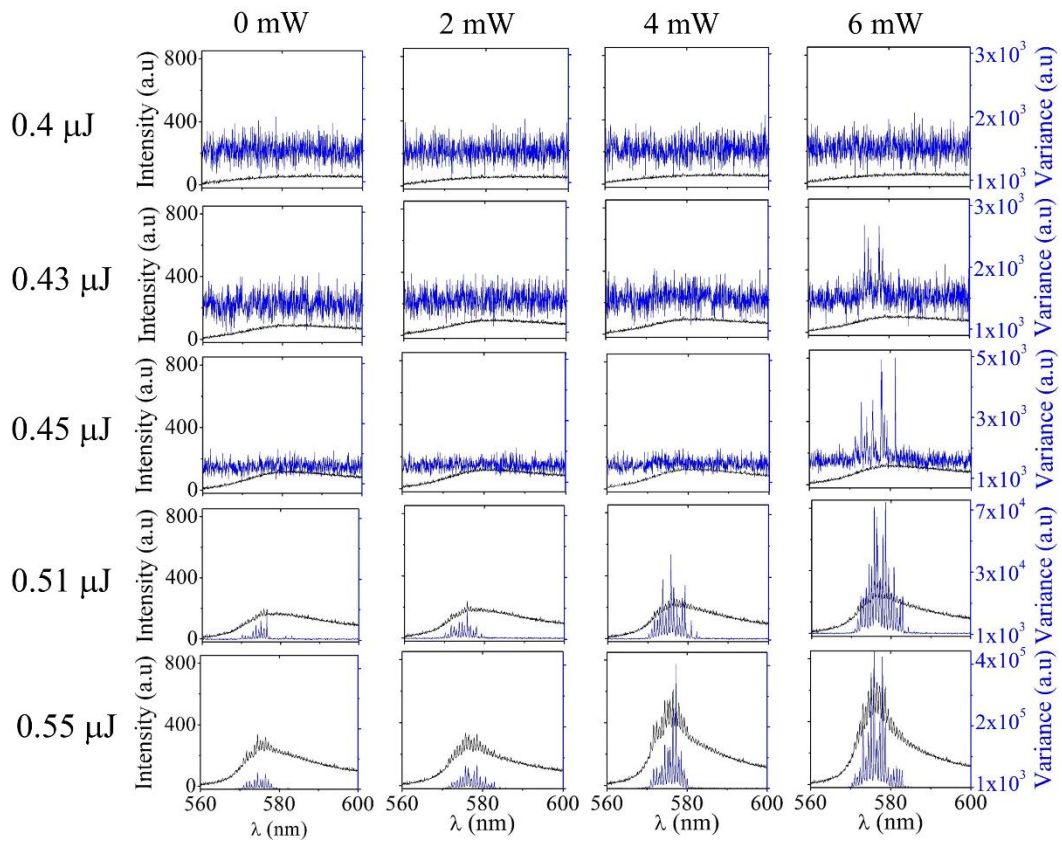


**Figure 4.9.** Average intensity and the corresponding variance of the emission spectra over 200 gated acquisitions plotted versus wavelength for various soliton powers and pump energies. Plots are arranged in rows of equal pump energy and columns of equal soliton powers. These results were published in **Publication III**.

## 4.6 Transistor-like operation of nematicon random laser

As discussed in Section 4.4, it is possible to all-optically modulate the RL operation by injecting a collinear low power NIR input. When setting the pump energy slightly below the lasing threshold without nematicon, turning on the nematicon brings the system above threshold and makes the system more efficient through improved photon collection and modified scattering. This is apparent not only from Figs. 4.5 (b), 4.7, 4.8 (b) and 4.9, but also from individual spectra collected at the output. Fig. 4.10 shows examples of several individual spectral realizations for various pump energies and nematicon powers. It is clear that, for a given pump energy/pulse, the presence of a nematicon enhances the occurrence of numerous highly intense sharp peaks over the background fluorescence and ASE.

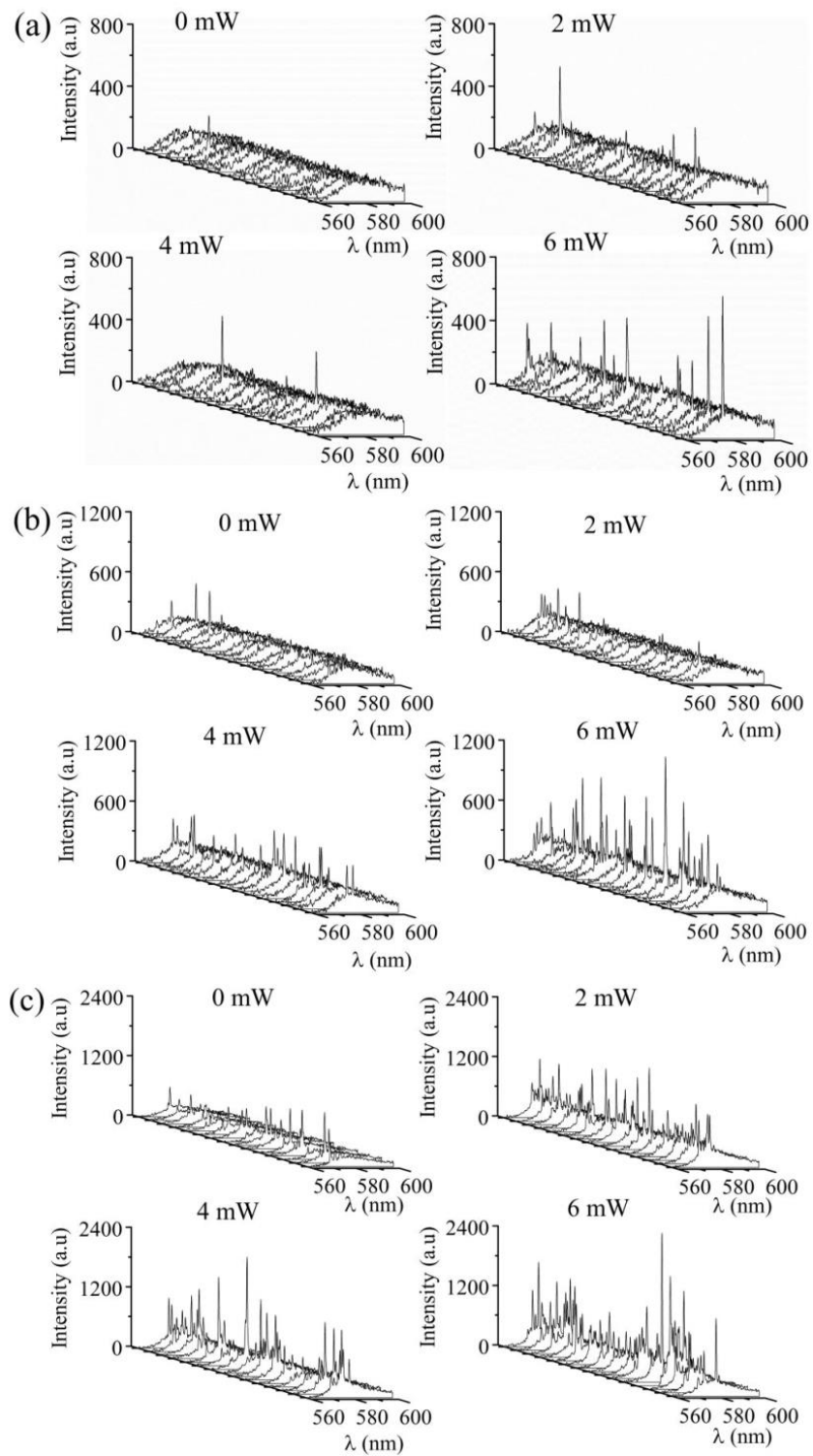


**Figure 4.10.** Individual realizations of the RL emission spectra collected at the output for various powers of nematicon and pump energies (a)  $0.48 \mu\text{J}$ , (a)  $0.51 \mu\text{J}$ , and (a)  $0.55 \mu\text{J}$ .

It is very important to note that the all-optical modulation is visible in every single realization despite the random nature of the emission versus time. It is also worth noting that the above demonstrated all-optical switching is not based on any absorptive and photo-thermal response<sup>87, 90</sup> or light induced trans-cis isomerization,<sup>125</sup> but, exclusively based on a nonresonant effect.

## 4.7 Beaming the random laser emission

Most of the RLs lack predetermined directionality and well-defined beam characteristics due to their random nature. To address this issue, we have measured the beam characteristics of the nematicon-assisted random laser.

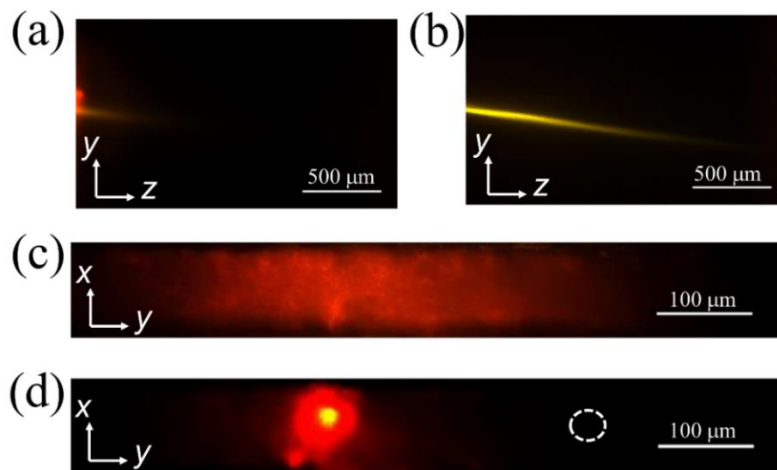


**Figure 4.11.** Acquired photographs of emitted light in the principal plane  $yz$  (a) in the absence of nematicon (b) in the presence of a collinear 6 mW nematicon at pump energy of  $0.55 \mu\text{J}/\text{pulse}$ . (c-d) Images of the output profiles corresponding to (a) and (b), respectively. The white dashed circle represent the location of the input wavevector. These results were published in **Publication III**.

As shown in Fig. 4.11, we managed to image the RL beam evolution in the principal plane  $yz$  and in the transverse plane  $xy$ . Fig. 4.11 (a) and (b) represent the RL beam evolution in plane  $yz$  and the corresponding output profiles measured in the transverse plane  $xy$  without and with a collinear 5 mW nematicon, respectively, at pump energy well above threshold ( $0.55 \mu\text{J}$ ). The generated extraordinarily polarized RL light diffracts and gives rise to a diffuse intensity pattern with low intensity at the output. When injecting a 5 mW nematicon, RL emission acquires beam characteristics. The emitted extraordinary light is confined in the nematicon waveguide, beamed along its inherent walk-off and exits the cell with a relatively smooth output profile. This is in contrast to a spiky and noisy profile as observed for usual RLs. The transversely localized RL modes interact

inside the nematicon waveguide and provide smooth output profile invariant over time. To get an insight into the beam features of the nematicon-assisted lasing, we also imaged the RL emission in the backward direction (towards the input light). Typical results are shown in Fig. 4.12. The output profile consist of several hotspots fluctuating in time and space as typical for thin samples.<sup>78-80, 126, 127</sup>

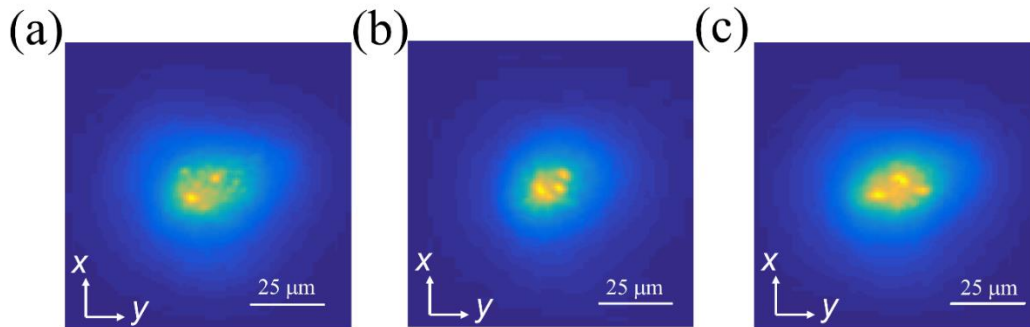


**Figure 4.12.** Acquired photographs of the backward emitted RL light in the  $xy$  plane at pump energy  $0.8 \mu\text{J}$  and  $6 \text{ mW}$  soliton. (a-c) represent three different realizations to describe the random nature of the emission. These results were published in **Publication III**.

## 4.8 Efficiency of the random laser

The practical uses of RLs are mainly hampered by their low lasing efficiency. Therefore, generating highly efficient RLs is very important for applications. In order to estimate the efficiency of the random laser configuration demonstrated here, the measured output energy versus input energy above the lasing threshold for various nematicon powers are shown in Fig. 4.13. The measured output energy values are averaged over 200 shots and corrected for Fresnel losses at the output interface (4%) and at the optical components (17.6%) before the detector (OBJ<sub>3</sub>, F<sub>3</sub>, F<sub>4</sub> in Fig. 4.3). Fresnel losses of the pump at the input interface (4%) are also considered. As can be seen from Fig. 4.13, the nematicons clearly improve the lasing efficiency. When pumping at  $0.6 \mu\text{J}/\text{pulse}$ , the presence of a  $6 \text{ mW}$  soliton improves the lasing efficiency at the output from 0.1% (without soliton) to 2.6%. Since most of the RL light is generated in the initial region of the soliton (actively pumped region of  $\sim 130 \mu\text{m}$ ), it experiences absorption and scattering losses during propagation. Assuming the absorption and scattering losses of  $\sim 6.95 \text{ cm}^{-1}$  at visible wavelengths in the host NLC, the extrapolated RL efficiency reaches a relatively high value 9.6%. The measured RL output energies and estimated efficiencies for various pump energies above threshold and various nematicon powers are presented in Table 4.1. However higher RL efficiency has been achieved in various other materials such as Sulforhodamine B with  $\text{TiO}_2$  (10%),<sup>128</sup> Nd:YAG crystal powder (12.5%),<sup>129</sup>  $\text{NdAl}_3(\text{BO}_3)_4$  power (30%),  $\text{NdPO}_4$  powder (25%) and  $\text{NdVO}_4$  powder (20%).<sup>130</sup>



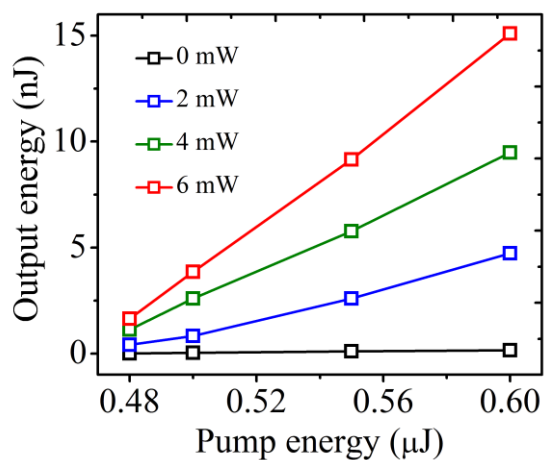


**Figure 4.13.** Emission energy versus pump energy/pulse above lasing threshold for various soliton powers. The measured values are averaged over 200 shots and corrected for Fresnel reflection losses.

**Table 4.1.** Measured RL output energies and estimated conversion efficiencies corrected for Fresnel losses and transmission losses for various pump energies and nematicon powers. Extrapolated output energy and efficiency are also given considering the active lasing volume and scattering and absorption losses during propagation in the guest-host. A summary of these results were published in **publication III**.

$E_P$ ( $\mu\text{J}$ )	$P_{\text{NIR}}$ (mW)	$E_{\text{out}}$ (nJ)	$\eta$ (%)	$(E_{\text{out}})_{\text{max}}$ (nJ)	$\eta_{\text{max}}$ (%)
0.48	0	0.012	0.003	0.044	0.01
	2	0.422	0.092	1.546	0.336
	4	1.128	0.245	4.139	0.9
	6	1.65	0.358	6.052	1.31
0.5	0	0.041	0.009	0.15	0.03
	2	0.831	0.173	3.048	0.64
	4	2.601	0.542	9.541	1.98
	6	3.854	0.803	14.135	2.95
0.55	0	0.106	0.02	0.389	0.074
	2	2.601	0.493	9.541	1.81
	4	5.768	1.093	21.158	4.01
	6	9.152	1.733	33.57	6.36
0.6	0	0.16	0.028	0.588	0.102
	2	4.733	0.822	17.36	3.01
	4	9.477	1.646	34.76	6.04
	6	15.101	2.622	55.39	9.62

## 5 Random laser steering with nematicons

One of the greatest advantages of NLC is their response towards external stimuli. Therefore, their optical properties, from index of refraction to nonlinearity and anisotropy, can be adjusted by electromagnetic perturbations<sup>131</sup> that in turn affect the nematicon propagation. The trajectories of the nematicon waveguides can therefore be steered by using external stimuli acting on the director distribution. These stimuli include refractive perturbations,<sup>132, 133</sup> applied voltage,<sup>134-139</sup> applied magnetic field,<sup>140</sup> boundaries of the NLC cell<sup>141</sup> and external light beams.<sup>131, 142, 143</sup> In this Chapter two examples of nematicon-guided RL angular steering will be discussed. These results are the core parts of **Publication III** and **Publication IV**.

### 5.1 Voltage-controlled angular steering

In order to demonstrate electro-optic angular steering of the nematicon-confined RL, a voltage bias from a 1 kHz generator was applied across the cell thickness (see Section 4.1 for sample description). When a low-frequency voltage is applied, it alters the director distribution and the nematicon can be steered.<sup>134</sup> As the applied voltage (perpendicular to the optic axis  $\mathbf{n}$ ) increases, the resulting torque on the induced dipoles tends to reorient the NLC molecules out of plane  $yz$  and therefore the molecular director is pulled out of the alignment plane  $yz$  towards the vertical axis  $x$ . This rotates the principal plane, which defines the extraordinary wave, and thereby reduces the walk-off angle. When the applied bias becomes large enough to completely reorient the molecular director along  $x$ , the walk-off angle vanishes and the extraordinarily polarized nematicon propagates with Poynting vector ( $\mathbf{S}$ ) parallel to its own wavevector  $\mathbf{k}$ .<sup>8, 134</sup> Therefore, the walk-off can be electrically adjusted and the nematicon angularly steered versus applied bias. It is important to note that the nematicon remains as extraordinarily polarized when it adiabatically evolves in polarization through the transition region near the input interface of

the NLC cell.<sup>119</sup> Figures 5.1 provide a pictorial representation of this mechanism. Here an extraordinarily polarized nematicon is steered due to the voltage-induced reorientation of the molecular director, resulting in a semicircular trajectory in the transverse plane  $xy$ . The observable walk-off ( $\alpha$ ) in the  $yz$  plane can be calculated as,<sup>8, 100, 134</sup>

$$\alpha = \arctan\left(\frac{\tan \delta \cos \xi}{\sqrt{1 + \sin^2 \xi \cot^2 \theta_0}}\right) \quad (5.1)$$

where  $\xi$  is the elevation angle and  $\theta_0$  is the initial NLC orientation.

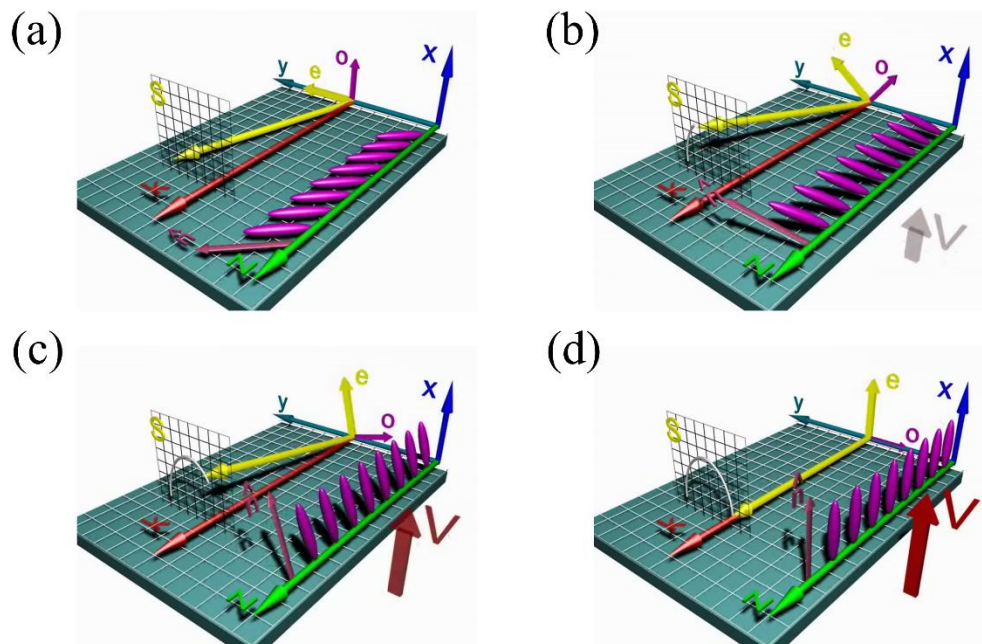


**Figure 5.1.** (a-d) pictorial representation of voltage-driven angular steering of nematicon-guided RL. The walk-off (angle between  $S$  (yellow) and  $k$  (red)) progressively reduces as the voltage increases. The walk-off vanishes when  $S$  and  $k$  become collinear.

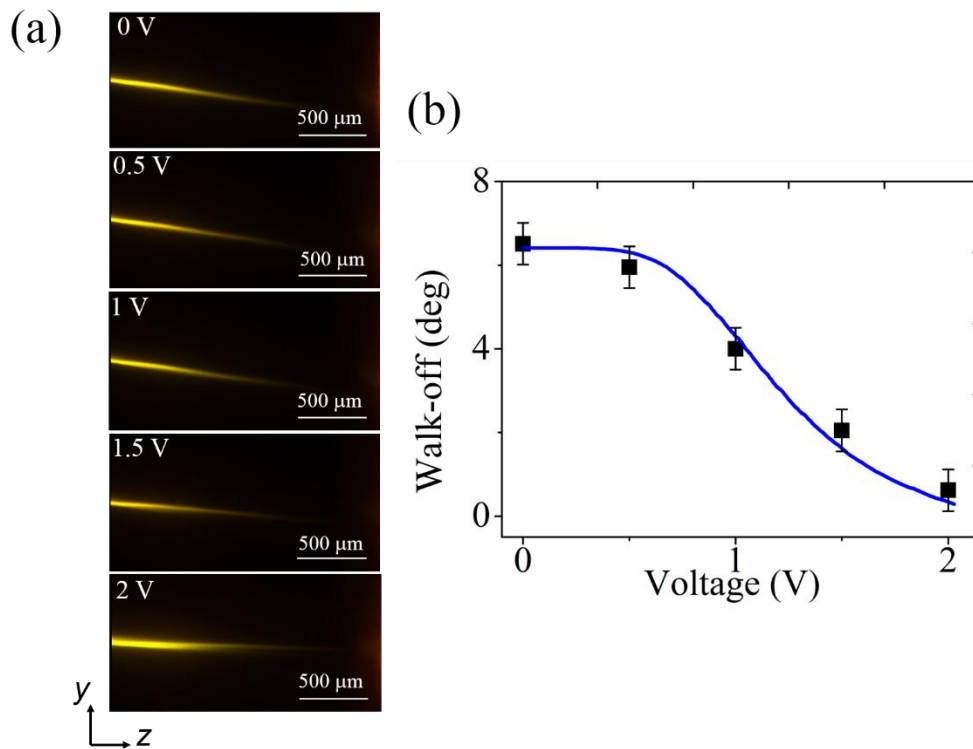


**Figure 5.2.** (a) Photographs of RL streaks in the observation plane  $yz$  for various values of the applied voltage. The NIR beam and residual pump were filtered out. (b) Measured (symbols) and calculated (solid line, using Eq. 5.1) walk-off versus applied voltage. These results were published in **Publication III**.

Typical results of voltage-controlled angular steering of the RL emission in the presence of a 5 mW nematicon and pump energy well above threshold are shown in Fig. 5.2. As the applied voltage increased from  $V = 0$  V to  $V = 2$  V, the RL beam steered from  $7^\circ$  to nearly  $0^\circ$  (Fig. 5.2 (a)). A plot of the measured and calculated walk-off of the RL beam observed in the  $yz$  plane is presented in Fig. 5.3 (b). It should be noted that some of the RL light diffuses out of the nematicon waveguide at high voltages as apparent from Fig. 5.2 (a). As a fixed power nematicon evolves versus voltage towards the ordinary-wave configuration ( $S//k$ ), it becomes progressively less confined as the associated waveguide has a lower refractive-index profile. Moreover, when the walk-off becomes zero, the reorientational nonlinear response of the NLC tends to zero. Correspondingly, the emitted spectra (averaged) collected at the cell output (Fig. 5.3) exhibit lower intensities at high voltages.

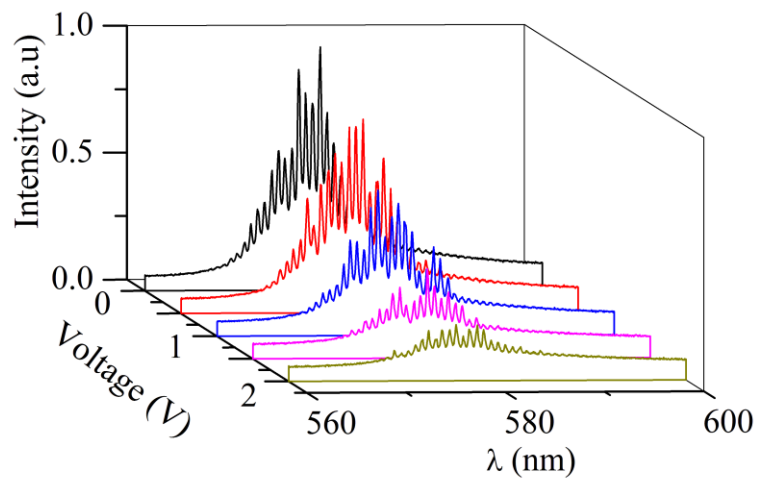


**Figure 5.3.** Measured averaged RL output spectra for various applied voltages. The nematicon power was 5 mW and pump energy well above threshold. These results were published in **Publication III**.

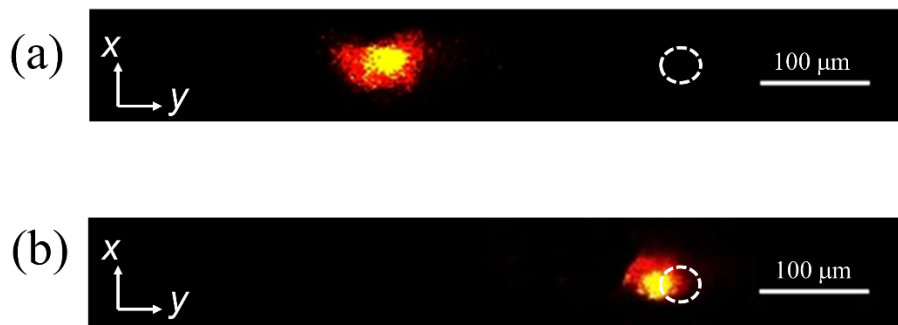


**Figure 5.4.** Photographs of the RL output measured at the transverse plane  $xy$  for applied voltages (a)  $V = 0$  V and (b)  $V = 2$  V. The white dashed circle represent the direction of the input wavevector. The NIR light was filtered out. These results were published in **Publication III**.

Fig. 5.4. represents photographs of the RL output spot measured at the transverse plane  $xy$  for applied voltages  $V = 0$  V and  $V = 2$  V. As the RL beam steered from  $7^\circ$  to nearly  $0^\circ$ , the output spot of the RL beam is laterally displaced in the transverse plane  $xy$  with an overall displacement of about  $245 \mu\text{m}$  at the output.

## 5.2 In-plane angular steering using external magnetic field

The voltage-driven angular steering of the RL beam described above is not effective for RL steering at large angles. Moreover, voltage steering causes the principal plane to rotate and the output spot to move out of the plane. In order to overcome this issue, an

alternative way can be used to steer the RL by exploiting the response of NLC's towards external magnetic fields.<sup>140</sup> An externally applied magnetic field can effectively reorient the NLC molecular director and control the soliton trajectories.

In order to demonstrate magnetic steering of the nematicon-confined RL, we applied a magnetic field co-planar with  $\mathbf{k}$  and  $\mathbf{n}$ , to alter the initial homogeneous alignment of the NLC molecular director ( $\theta = 45^\circ$ ) with respect to  $\mathbf{k}/z$ . For this purpose, we applied a permanent cylindrical magnet (diameter 25 mm, thickness 12 mm) mounted on a rotation stage (rotation around  $x$ ) with  $yz$  translation close to the output facet of the sample. The magnetic field strength at about 2 mm away from the cell output was  $\sim 0.23$  T. This magnetic field strength was large enough to reorient the NLC molecules in the whole volume of interest despite the spatial distribution of the magnetic field and the size of the cell.<sup>140</sup>

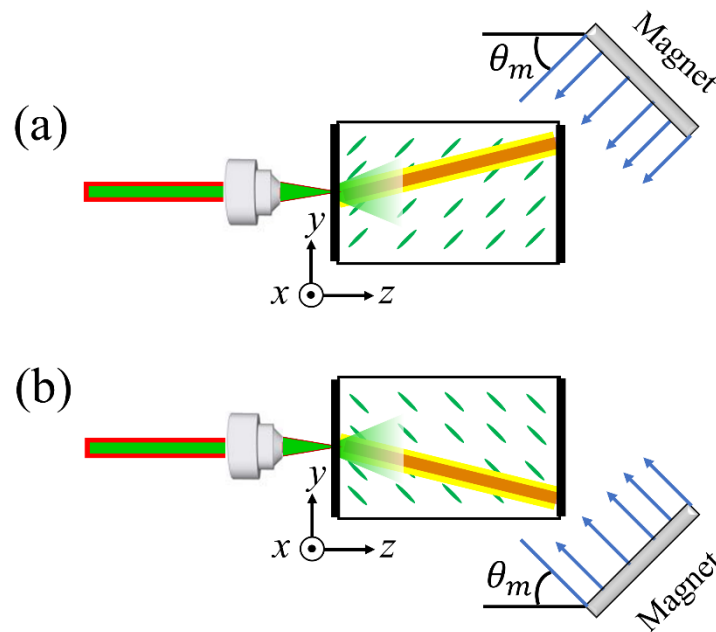


**Figure 5.5.** Pictorial representation of relative orientations of the magnetic field and the cell for two cases (a)  $\theta_m = -50^\circ$  and (b)  $\theta_m = 50^\circ$ .

In order to steer the RL beam we varied the angular direction of the applied magnetic field with respect to  $\mathbf{k}/z$  in the  $yz$  plane (by rotating around  $x$ ). The angle  $\theta_m$  between the magnetic field vector and  $\mathbf{k}/z$  determines the walk-off angle  $\delta(\theta)$ , with  $\theta = \theta_m$  (see Eq. 3.4). Two examples of the magnet-cell orientation are illustrated in Fig. 5.5. When the magnetic field is present, it forces the molecular director to reorient at angle  $\theta = \theta_m$ , the NIR beam remains an extraordinary wave and the resulting walk-off experienced by the NIR soliton-guided RL gets modified according to Eq. 3.4.

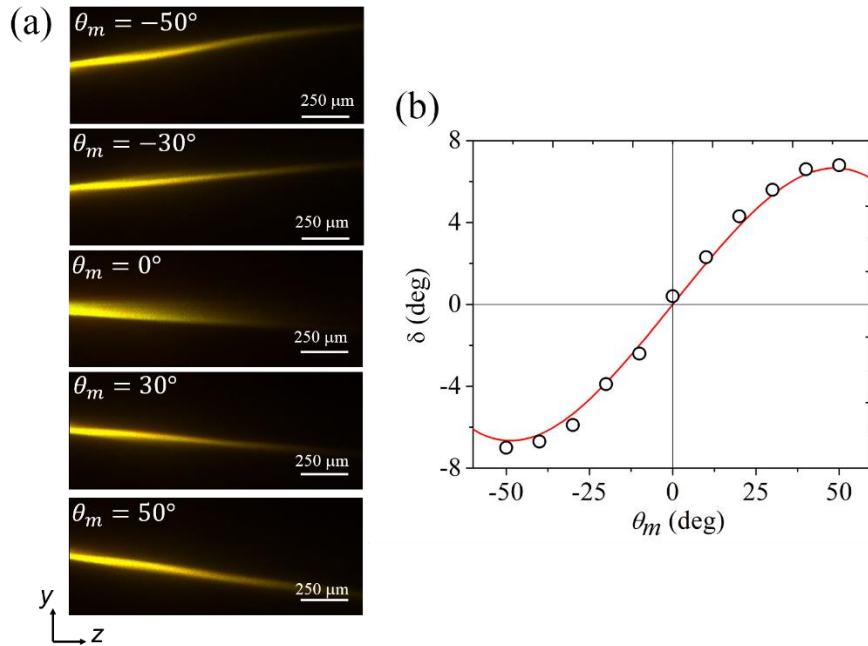


**Figure 5.6.** (a) Photographs of RL streaks in the observation plane  $yz$  for various magnetic field orientations  $\theta_m$ . The NIR beam and residual pump were filtered out. (b) Measured (symbols) and calculated (solid line) walk-off angles  $\delta$  for various  $\theta_m$  values. These results were published in **Publication IV**.

Typical results of the RL beam steering observed from the principal plane  $yz$  when pumping at  $0.6 \mu\text{J}$  and in the presence of a  $7 \text{ mW}$  nematicon for various  $\theta_m$  values are shown in Fig. 5.6 (a). By varying  $\theta_m$  from  $-50^\circ$  to  $50^\circ$ , the walk-off experienced by the RL beam varies from  $-7^\circ$  to  $7^\circ$ . The measured walk-off angles within plane  $yz$  are in perfect agreement with the calculated values using Eq. 3.4 as apparent from Fig. 5.6 (b). It should be noted that as the walk-off angle approaches zero when  $\theta_m \rightarrow 0$ , the nonlinearity tends to vanish and the resulting guided beam tends to diffract due to the lowered index contrast. However, for  $\theta_m$  values other than zero, the characteristics of the RL beam remains the same.

The acquired photographs of the magnetically steered RL beam at the output facet of the cell for the cases of  $\theta_m = \pm 50^\circ$  are displayed in Fig. 5.7. Note that it was difficult to acquire photographs of the output beam for  $\theta_m$  approaching zero as the magnet eclipsed the output beam. As the nematicon-guided RL beam is magnetically steered, the output spot remains essentially in the same plane with an overall displacement of about  $490 \mu\text{m}$  across  $y$ . Note that the RL output spot does not exhibit any shift in the transverse direction  $x$  as it is magnetically steered in-plane. This is contrast to the voltage-driven angular steering.

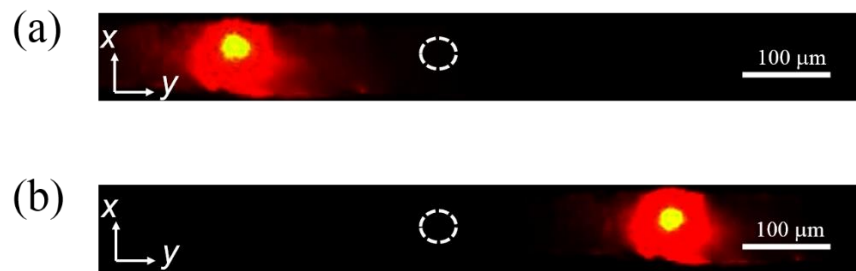


**Figure 5.7.** Photographs of the RL output measured at the transverse plane  $xy$  for magnetic field orientations (a)  $\theta_m = 50^\circ = 0$  V and (b)  $\theta_m = -50^\circ$ . The white dashed circle represents the direction of the input wavevector. The NIR light was filtered out. These results were published in **Publication IV**.

Fig. 5.8. displays the RL emission spectra (averaged) for various magnetic field orientations. The spectra corresponding to symmetric orientations of the applied magnetic field are essentially the same despite the random intensity fluctuations of the RL emission. A small reduction in the emission intensity is visible for  $\theta_m \rightarrow 0$ . This can be attributed to the lowered nonlinear response of the NLC, as the optical reorientation tends to vanish, making the nematicon less effective in collecting and confining the RL emission.

In the absence of the external magnetic field, the molecular director  $\mathbf{n}$  of the NLC is pre-aligned according to the boundary conditions (see Section 4.1.). We also monitored the response time of the RL beam to the magnetic field and the time required for it to relax back to its original trajectory. In the absence of the magnetic field, the RL beam propagates at a walk-off  $\delta \sim +7^\circ$ . When applying a magnetic field at  $\theta_m = -50^\circ$  the time needed for the RL beam to reach  $\delta \sim -7^\circ$  was about 60 s. Conversely, nearly 200 s was required for the RL beam to relax to its original trajectory, i.e., from  $\delta \sim -7^\circ$  to  $\delta \sim +7^\circ$  after the magnet was removed. This slow response can be attributed to the large thickness of the pre-aligned NLC and the modest strength of the applied magnetic field.



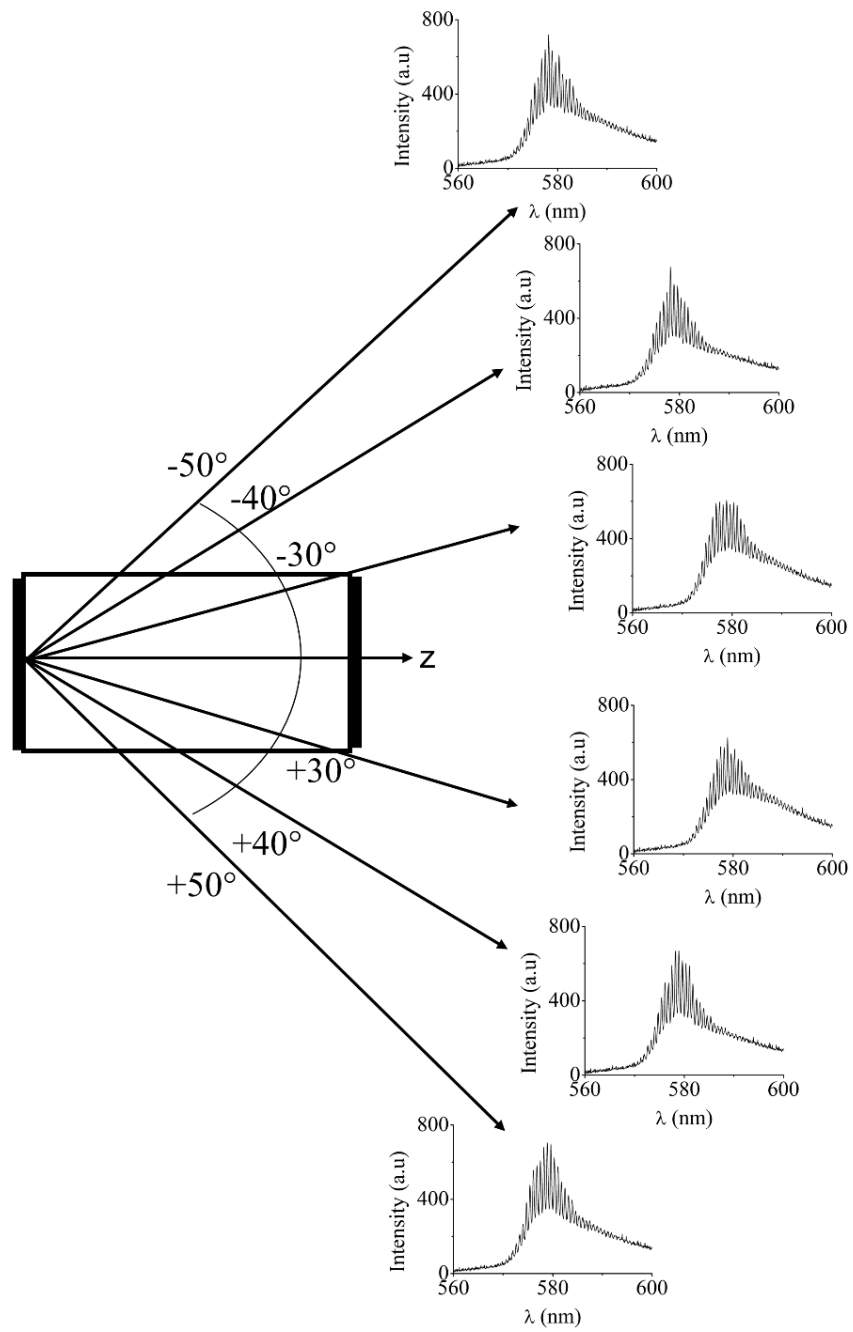


**Figure 5.8.** Averaged emission spectra for various  $\theta_m$  values. These results were published in Publication IV.

### 5.3 Comparison of RL steering methods

As demonstrated in previous sections, RL beam can be steered at will by means of external low-frequency voltage and moderate magnetic field. Compared to voltage-controlled steering, magneto-optic steering of RL was more efficient as the emission properties such as efficiency are less dependent on the applied field. Table 5.1. describes a meaningful comparison between these two methods. It is evident that magnetic steering has several benefits over voltage steering.

**Table 5.1.** Comparison between voltage-controlled and magnetic steering of RL beam

Characteristics	Voltage steering	Magnetic steering
Type of steering	Angular steering	In-plane steering
Walk-off angle	Varies from $7^\circ$ to $0^\circ$	Varies from $+7^\circ$ to $-7^\circ$
Displacement of the output spot	245 $\mu\text{m}$	490 $\mu\text{m}$
Lasing efficiency	Strongly depend on applied voltage	less dependent on applied magnetic field orientation
response time	Comparable to magnetic steering	Comparable to voltage steering



## 6 Summary and outlook

In this Thesis, we have demonstrated a novel random laser configuration in dye-doped nematic liquid crystals, based on the interplay between two diverse nonlinear optical responses, namely, beam self-confinement through molecular reorientation and scattering mediated light amplification and lasing. Through this synergy, the demonstrated nematicon-controlled random laser improved the overall lasing efficiency and allowed several additional features to be demonstrated, resulting in a highly controllable cavity-less light source in soft-matter. At variance with the standard thin sample and one beam configuration, our NLC cell provided additional degrees of freedom to control the RL emission. First, we investigated the basic features of the nematicon-assisted random laser. The spatial soliton confines the emitted light and contributes to tuning of the laser features such as slope efficiency, lasing threshold and emission spectra, as witnessed in **Publications I and II**.

These basic properties led us to investigate the more advanced features of the system by taking advantage of the properties of the nematicon waveguides as demonstrated in **Publication III**. Previous demonstrations of RLs in various materials have found limited applications due to their multi-directionality. We showed that our approach is able to beam the random laser emission and to provide a smooth transverse output profile. Moreover, this nematicon-assisted configuration enhances the conversion efficiency, by improving the photon collection and scattering properties. Furthermore, the approach provides all-optical modulation, driven by a continuous-wave beam operating at mW power levels.

Our next aim was to overcome the uncontrollable nature of the emission direction of random lasers. Towards this, in **Publications III and IV**, we introduced a direction adjustable random laser. We showed that the output beam of the random laser can be steered at will within the active medium itself (rather than acting on the emitted beam) by exploiting the response towards external stimuli. We demonstrated the first random

laser operating in a voltage-controlled direction. By applying a voltage across the sample thickness, the output of the random laser can be angularly steered over  $7^\circ$ . However, the angular steering moves the random laser output spot out of the original operation plane. We therefore introduced an alternative strategy to modify the random laser beam trajectory within the observation plane and to steer the output at large angles. In order to do this, we took advantage of the magneto-optic response of nematicons. We thus used an external magnetic field and varied its orientation to steer the random laser beam. This was the first demonstration of a random laser steering by acting with a magnetic field on the active medium itself. By adjusting the applied magnetic field orientation, we achieved in-plane random laser beam steering as large as  $14^\circ$ . These results open up new routes towards practical applications of cavity-less light sources.

However, several aspects of nematicon-assisted random laser are still unclear. These aspects need to be investigated, requiring extensive future work. Since the localized random laser modes tend to evolve along the waveguide resulting in a smooth transverse profile, the role of the nematicon waveguide needs to be thoroughly investigated. A simple way for doing this is to compare the random laser characteristics and to measure the spectral features at each point within the emitted random laser beam profiles. A detailed study of the random laser mode profile and its coherence properties will be useful to understand its applicability in, e.g., full-field speckle-free imaging. A proper theoretical model accounting for the different properties of the system would also be helpful for answering several questions. However, building such a model will be extremely demanding due to the complex interactions that take place in the liquid-crystal based system.

## References

- [1] H. Cao, "Random Lasers: Development, Features and Applications," *Optics and Photonics News*, vol.16, pp. 24-29 (2005).
- [2] A. Ishimaru, "Wave propagation and scattering in random media," Academic Press New York, (1978).
- [3] D. S. Wiersma, "The physics and applications of random lasers," *Nature Physics*, vol. 4, pp. 359-367 (2008).
- [4] G. Strangi, V. Barna, A. De Luca, S. Ferjani and C. Versace, "Liquid Crystal Microlasers," 1st ed., Transworld Research network, pp. 43-65 (2010).
- [5] S. Chandrasekhar, "Liquid Crystals," Cambridge University, (1977).
- [6] P. G. de Gennes and J. Prost, "The Physics of Liquid Crystals," 2nd ed. Oxford, (1993).
- [7] I. C. Khoo, "Liquid Crystals: Physical Properties and Nonlinear Optical Phenomena," Wiley, (1995).
- [8] M. Peccianti and G. Assanto, "Nematicons," *Physics Reports*, vol. 516 (4-5), pp. 147-208 (2012).
- [9] M. Segev, Y. Silberberg, D. and N. Christodoulides, "Anderson localization of light," *Nature Photonics*, vol. 7, pp. 197-204 (2013).
- [10] M. Bahoura and M. A. Noginov, "Determination of the transport mean free path in a solid-state random laser," *Journal of Optical Society of America B*, vol. 20, pp. 2389-2394 (2003).
- [11] D. S. Wiersma, "Disordered photonics," *Nature Photonics*, vol. 7, pp. 188-196 (2013).
- [12] K. M. Yoo, G. C. Tang, and R. R. Alfano, "Coherent backscattering of light from biological tissues," *Applied Optics*, vol. 29, pp. 3237-3239 (1990).
- [13] Y. Kuga and A. Ishimaru, "Retro reflection from a Dense Distribution of Spherical Particles," *Journal of Optical Society of America A*, vol. 1, pp. 831-835 (1984).

- [14] M. van Albada and A. Lagendijk, "Observation of Weak Localization of Light in a Random Medium," *Physical Review Letters*, vol. 55, pp. 2692-2695 (1985).
- [15] G. Maret and P. Wolf, "Weak Localization and Coherent Backscattering of Photons in Disordered Media," *Physical Review Letters*, vol. 55, pp. 2696-2699 (1985).
- [16] R. Sapienza, S. Mujumdar, C. Cheung, A. G. Yodh, and D. Wiersma, "Anisotropic Weak Localization of Light," *Physical Review Letters*, vol. 92, p. 033903 (2004).
- [17] A. E. Siegman, "Lasers," University science book, Mill valley, (1986).
- [18] L. W. Casperson, "Threshold characteristics of mirrorless lasers," *Journal of Applied Physics*, vol. 48, pp. 256-262 (1977).
- [19] O. Svelto, S. Taccheo, and C. Svelto, "Analysis of amplified spontaneous emission: some corrections to the linford formula," *Optics Communications*, vol. 149, pp. 277-282 (1998).
- [20] G. Heliotis, D. Bradley, G. Turnbull, and I. Samuel, "Light amplification and gain in polyfluorene waveguides," *Applied Physics Letters*, vol. 81, pp. 415-417 (2002).
- [21] L. Blinov, G. Cipparrone, V. Lazarev, P. Pagliusi, and T. Rugiero, "Liquid crystal as laser medium with tunable gain spectra," *Optics Express*, vol. 16, pp. 6625-6630 (2008).
- [22] D. L. Matthews, P. L. Hagelstein, M. D. Rosen, M. J. Eckart, N. M. Ceglio, A. U. Hazi, H. Medeck, B. J. MacGowan, J. E. Trebes, B. L. Whitten, E. M. Campbell, C. W. Hatcher, A. M. Hawryluk, R. L. Kauffman, L. D. Pleasance, G. Rambach, J. H. Scofield, G. Stone, and T. A. Weaver, "Demonstration of a soft x-ray amplifier," *Physical Review Letters*, vol. 54, pp. 110-113 (1985).
- [23] H. Cao, "Lasing in random media," *Waves in Random Media*, vol. 13, pp. R1-R39 (2003).
- [24] H. Cao, "Review on latest developments in random lasers with coherent feedback," *Journal of Physics A: Mathematical and General*, vol. 38, pp. 10497-10535 (2005).
- [25] V. S. Latokhov, "Stimulated emission of an ensemble of scattering particles with negative absorption," *Journal of Experimental and Theoretical Physics Letters*, vol. 5, pp. 212-215 (1967).
- [26] V. S. Latokhov, "Generation of light by a scattering medium with negative resonance absorption," *Journal of Experimental and Theoretical Physics Letters*, vol. 26, pp. 835-840 (1968).

- [27] R. Ambartsumyan, N. Basov, P. Kryukov, and V. Letokhov, "A laser with a nonresonant feedback," *IEEE Journal of Quantum Electronics*, vol. 2, pp. 442–446 (1966).
- [28] V. M. Markushev, V. F. Zolin, and C. M. Briskina, "Luminescence and stimulated emission of neodymium in sodium lanthanum molybdate powders," *Soviet Journal of Quantum Electronics*, vol. 16, p. 281 (1986).
- [29] V. M. Markushev, N. E. Ter-Garielyyan, C. M. Briskina, V. R. Belan and V. F. Zolin, "Stimulated emission kinetics of neodymium powder lasers" *Soviet Journal of Quantum Electronics*, vol. 20, p. 773 (1990).
- [30] N. M. Lawandy, R. M. Balachandra, A. S. L. Gomes, and E. Sauvain, "Laser action in strongly scattering media," *Nature*, vol. 368, pp. 436–438 (1994).
- [31] N. M. Lawandy and R. M. Balachandran, "Random laser," *Nature*, vol. 373, p. 204 (1995).
- [32] S. M. Morris, A. D. Ford, M. N. Pivnenko and H. J. Coles, "Electronic control of nonresonant random lasing from dye-doped smectic A\* liquid crystal scattering device," *Applied Physics Letters*, vol. 86, p. 141103 (2005).
- [33] N. Ghofraniah, I. Viola, A. Zacheo, V. Arima, G. Gigli, and C. Conti, "Transition from nonresonant to resonant random lasers by the geometrical confinement of disorder," *Optics Letters*, vol. 38, pp. 5043-5046 (2013).
- [34] R. Uppu and S. Mujumdar, "Statistical fluctuations of coherent and incoherent intensity in random lasers with nonresonant feedback," *Optics Letters*, vol. 35, pp. 2831-2833 (2010).
- [35] R. Uppu and S. Mujumdar, "On the coherent modes of ultranarrowband random lasers with nonresonant feedback," *Applied Optics*, vol. 50, pp. E13-E19 (2011).
- [36] H. Cao, Y. G. Zhao, H. C. Ong, S. T. Ho, J. Y. Dai, J. Y. Wu and R. P. H. Chang, "Ultraviolet lasing in resonator formed by scattering in semiconductor polycrystalline films," *Applied Physics Letters*, vol. 73, p. 3656 (1998).
- [37] H. Cao, Y. G. Zhao, H. C. Ong, S. T. Ho, E. Q. Seelig, Q. H. Wang, and R. P. H. Chang, "Random laser action in semiconductor powder," *Physical Review Letters*, vol. 82, p. 2278 (1999).
- [38] S. V. Frolov, Z. V. Vardeny, K. Yoshino, A. Zakhidov, and R.H. Baughman, "Stimulated emission in high-gain organic media," *Physical Review B*, vol. 59, p. R5284 (1999).
- [39] S. V. Frolov, Z. V. Vardeny, A. Z. Zakhidov, and R. H. Baughman, "Laser like emission in opal photonic crystals," *Optics Communication*, vol. 162, p. 241 (1999).
- [40] S. V. Frolov, M. Shkunov, A. Fujii, K. Yoshino, and Z. V. Vardeny, "Lasing and Stimulated Emission in  $\pi$ -Conjugated Polymers," *IEEE Journal of Quantum Electronics*, vol. 36, p. 2 (2000).



- [41] Y. Ling, H. Cao, A. L. Burin, M. A. Ratner, X. Liu, and R. P. H. Chang, "Investigation of random lasers with resonant feedback," *Physical Review A*, vol. 64, p. 063808 (2001).
- [42] R. C. Polson and Z. V. Vardeny, "Organic random lasers in the weak-scattering regime," *Physical review B*, vol. 71, p. 045205 (2005).
- [43] M. Anni, S. Lattante, R. Cingolani, G. Gigli, G. Barbarella and L. Favaretto, "Far-field emission and feedback origin of random lasing in oligothiophene dioxide neat films," *Applied Physics Letters*, vol. 83, p. 2754 (2003).
- [44] X. Wu, W. Fang, A. Yamilov, A. A. Chabanov, A. A. Asatryan, L. C. Botten, and H. Cao, "Random lasing in weakly scattering systems," *Physical Riview A*, vol. 74, p. 053812 (2006).
- [45] S. Mujumdar, M. Ricci, R. Torre, and D. S. Wiersma, "Amplified extended modes in random lasers," *Physical Review letters*, vol. 93, p. 053903 (2004).
- [46] S. Mujumdar, V. Tuerck, R. Torre, and D. S. Wiersma, "Chaotic behavior of random lasers with static disorder," *Physical Review A*, vol. 98, p. 033807 (2007).
- [47] J. Fallert, R. J. B. Dietz, J. Sartor, D. Schneider, C. Klingshirn and H. Kalt, "Co-existence of strongly and weakly localized random laser modes," *Nature Photonics*, vol. 3, pp. 279-282 (2009).
- [48] H. Cao, J. Y. Xu, D. Z. Zhang, S-H. Chang, S. T. Ho, E. W. Seelig, X. Liu, and R. P. H. Chang, "Spatial confinement of laser light in active random media," *Physical review Letters*, vol. 84, pp. 5584-5587 (2000).
- [49] H. Cao, J. Y. Xu, S-H Chang, S. T. Ho, "Transition from amplified spontaneous emission to laser action in strongly scattering media," *Physical Review E*, vol. 61, pp. 1985-1989 (2000).
- [50] T. Nakamura, T. Hosaka, S. Adachi, "Gold-nanoparticle-assisted random lasing from powdered GaN," *Optics Express*, vol. 9, pp. 467-475 (2011).
- [51] M. Bahoura, K.J. Morris, M. A. Noginov, "Threshold and slope efficiency of Nd<sub>0.5</sub>La<sub>0.5</sub>Al<sub>3</sub>(BO<sub>3</sub>)<sub>4</sub> ceramic random laser: effect of the pumped spot size," *Optics Communication*, vol. 201, pp. 405-411 (2002).
- [52] S. J. Marinho, L. M. Jesus, L. B. Barbosa, D. R. Ardila, M. A. R. C. Alencar, J. J. Rodrigues Jr, "Bi-chromatic random laser from alumina porous ceramic infiltrated with rhodamine B," *Laser Physics Letters*, vol. 12, p. 055801 (2015)
- [53] F. Quochi, F. Cordella, A. Mura, G. Bongiovanni, F. Balzer, H-G. Rubahn, "One-Dimensional Random Lasing in a Single Organic Nanofiber," *Journal of Physical Chemistry B*, vol. 109, pp. 21690-21693 (2005).
- [54] S. Gottard, R. Sapienza, P. D. Garcia, A. Blanco, D. S. Wiersma, C. Lopez, "Resonance-driven random lasing," *Nature Photonics*, vol. 2, pp. 429-432 (2008).

- [55] Q. Song, S. Xiao, Z. Xu, J. Liu, X. Sun, V. Drachev, V.M. Shalaev, O. Akkus, Y. L. Kim, "Random lasing in bone tissue," *Optics Letters*, vol. 35, pp. 1425-1427 (2010).
- [56] Q. Song, Z. Xu, S. H. Choi, X. Sun, S. Xiao, O. Akkus, Y. L. Kim, "Detection of nanoscale structural changes in bone using random lasers," *Biomedical Optics Express*, vol. 1, pp. 1401-1407 (2010).
- [57] R. C. Polson, Z. V. Vardeny, "Random lasing in human tissues," *Applied Physics Letters*, vol. 85, p. 1289 (2004).
- [58] F. Lahoz, I. R. Martín<sup>1</sup>, M. Urgellés, J. Marrero-Alonso, R. Marín, C. J. Saavedra, A. Boto, M. Díaz, "Random laser in biological tissues impregnated with a fluorescent anticancer drug," *Laser Physics Letters*, vol. 12, p. 045805 (2015).
- [59] L. Florescu and S. John, "Photon Statistics and Coherence in Light Emission from a Random Laser," *Physical Review Letters*, vol. 93, p. 013602 (2004).
- [60] H. Cao, Y. Ling, J. Y. Xu, C. Q. Cao, and P. Kumar, "Photon Statistics of Random Lasers with Resonant Feedback," *Physical Review Letters*, vol. 86, pp. 4524–4527 (2001).
- [61] X. Jiang and C. M. Soukoulis, "Time Dependent Theory for Random Lasers," *Physical Review Letters*, vol. 85, pp. 70–73 (2000).
- [62] C. Vanneste and P. Sebbah, "Selective Excitation of Localized Modes in Active Random Media," *Physical Review Letters*, vol. 87, p. 183903 (2001).
- [63] J. Andreasen, A. A. Asatryan, L. C. Botten, M. A. Byrne, H. Cao, L. Ge, L. Labonté, P. Sebbah, A. D. Stone, H. E. Tureci, and C. Vanneste, "Modes of random lasers," *Advances in Optics and Photonics*, vol. 3, pp. 88–127 (2011).
- [64] B. Liu, A. Yamilov, Y. Ling, J. Y. Xu, and H. Cao, "Dynamic nonlinear effects on lasing in a random medium," *Physical Review Letters*, vol. 91, p. 063903 (2003).
- [65] M. A. Noginov, J. Novak, and S. Williams, "modelling of photon density dynamics in random lasers," *Physical Review A*, vol. 70, p. 063810 (2004).
- [66] M. Leonetti, C. Conti, and C. Lopez, "The mode-locking transition of random lasers," *Nature Photonics*, vol. 15, pp. 615–617 (2011).
- [67] K. C. Jorge, M. A. Alvarado, E. G. Melo, M. N. P. Careno, M. I. Alayo, and N. U. Wetter, "Directional random laser source consisting of a HC-ARROW reservoir connected to channels for spectroscopic analysis in microfluidic devices," *Applied optics*, vol. 55, pp. 5393-5398 (2016).
- [68] N. Bachelard, J. Andreasen, S. Gigan, and P. Sebbah, "Taming random lasers through active spatial control of the pump," *Physical Review Letters*, vol. 109, p. 033903 (2012).
- [69] N. Bachelard, S. Gigan, X. Noblin and P. Sebbah, "Adaptive pumping for spectral control of random lasers," *Nature Physics*, vol. 10, pp. 426-431 (2014).

- [70] M. Leonetti and C. Lopez, "Active subnanometer spectral control of a random laser," *Applied Physics Letters*, vol. 102, p. 071105 (2013).
- [71] B. Abaie, E. Mobini, S. Karbasi, T. Hawkins, J. Ballato and A. Mafi, "Random lasing in an Anderson localizing optical fibre" *Light: Science & Applications*, vol. 6, p. e17041 (2017).
- [72] Y. Yonenaga, R. Fujimura, M. Shimojo, A. Kubono, and K. Kajikawa, "Random laser of dye-injected holey photonic-crystal fiber," *Physical Review A*, vol. 92, p. 013824 (2015).
- [73] C. J. S. de Matos, L. de S. Menezes, A. M. Brito-Silva, M. A. M. Gamez, A. S. L. Gomes, and C. B. de Araujo, "Random fiber laser," *Physical Review Letters*, vol. 99, p. 153903 (2007).
- [74] S. Schönhuber, M. Brandstetter, T. Hisch, C. Deutsch, M. Krall, H. Detz, A. M. Andrews, G. Strasser, S. Rotter, and K. Unterrainer, "Random lasers for broadband directional emission," *Optica*, vol. 3, pp. 1035–1038 (2016).
- [75] F. Simoni, "Nonlinear optical properties of Liquid crystals," World Scientific, (1997).
- [76] P. G. de Gennes and J. Prost, "The Physics of the Liquid Crystals," Clarendon Press, Oxford, (1993).
- [77] I. Janossy, "Molecular interpretation of the absorption-induced optical reorientation of nematic liquid crystals," *Physical Review E*, vol. 49, p. 2957 (1994).
- [78] G. Strangi, S. Ferjani, V. Barna, A. De Luca, N. Scaramuzza, C. Versace, C. Umeton and R. Bartolino, "Random lasing and weak localization of light in dye-doped nematic liquid crystals," *Optics Express*, vol. 14, pp. 7737-7744 (2006).
- [79] S. Ferjani, V. Barna, A. De Luca, N. Scaramuzza, C. Versace, C. Umeton, R. Bartolino and G. Strangi, "Thermal behavior of random lasing in dye doped nematic liquid crystals," *Applied Physics Letters*, vol. 89, p. 121109 (2006).
- [80] S. Ferjani, V. Barna, A. De Luca, C. Versace and G. Strangi, "Random lasing in freely suspended dye-doped nematic liquid crystals," *Optics Letters*, vol. 33, p. 557 (2008).
- [81] L. Ye, C. Hou, C. Lv, C. Zhao, Z. Yin, Y. Cui, and Y. Lu, "Tailoring of random lasing characteristics in dye doped nematic liquid crystals," *Applied physics B*, vol. 115, pp. 303-309 (2014).
- [82] L. Ye, B. Liu, C. Zhao, Y. Wang, Y. Cui, and Y. Lu, "The electrically and magnetically controllable random lasers from dye-doped liquid crystals," *Journal of Applied Physics*, vol. 116, p. 053103 (2014).
- [83] P. Johnson, B. J. Bret, J. G. Rivas, J. J. Kelly, and A. Langendijk, "Anisotropic Diffusion of Light in a Strongly Scattering Material," *Physical Review Letters*, vol. 89, p. 243901 (2002).

- [84] L. Ye, C. Zhao, Y. Feng, B. Gu, Y. Cui and Y. Lu, "Study on the polarization of random lasers from dye-doped nematic liquid crystals," *Nanoscale Research Letters*, vol. 12, pp. 1-8, (2017).
- [85] C. W. Chen, H. P. Huang, H. C. Jau, C. Y. Wang, C. W. Wu, and T. H. Lin, "Polarization-asymmetric bidirectional random laser emission from a twisted nematic liquid crystal," *Journal of Applied Physics*, vol. 121, p. 033102 (2017).
- [86] S. Ferjani, L-V. Sorriso, V. Barna, A. De Luca, R. De Marco, G. Strangi, "Statistical analysis of random lasing emission properties in nematic liquid crystals," *Physical Review E*, vol. 78, p. 011707 (2008).
- [87] H. Bian, F. Yao, H. Liu, F. Huang, Y. Pei, C. Hou and X. Sun, "Optically controlled random lasing based on photothermal effect in dye-doped nematic liquid crystals," *Liquid crystals*, vol. 41, pp. 1436-1441 (2014).
- [88] C. R. Lee, J. D. Lin, B. Y. Huang, S. H. Lin, T. S. Mo, S. Y. Huang, C. T. Kuo, and H. C. Yeh, "Electrically controllable liquid crystal random lasers below the Fréedericksz transition threshold," *Optics Express*, vol. 19, pp. 2391-2400 (2011).
- [89] L. Wang, Y. Wan, L. Shi, H. Zhong and L. Deng, "Electrically controllable plasmonic enhanced coherent random lasing from dye-doped nematic liquid crystals containing Au nanoparticles," *Optics Express*, vol. 24, pp. 17593-17602 (2016).
- [90] D. S. Wiersma, "Light emission: A temperature-tunable random laser," *Nature*, vol. 414, pp. 708-709 (2001).
- [91] B. Redding, M. A. Choma, and H. Cao, "Speckle-free laser imaging using random laser illumination," *Nature Photonics*, vol. 6, p. 355 (2012).
- [92] S. Mujumdar, and H. Ramachandran, "Use of a graded gain amplifier as an optical diode," *Optics Letters*, vol. 26, pp. 929-931 (2001).
- [93] E. Ignesti, F. Tommasi, L. Fini, F. Martelli, N. Azzali, and S. Cavalieri, "A new class of optical sensors: a random laser based device," *Scientific Reports*, vol. 6, p. 35225 (2016).
- [94] M. Gaio, S. Caixeiro, B. Marelli, F. G. Omenetto, and R. Sapienza, "Gain-based mechanism for pH sensing based on random lasing," *Physical Review Applied*, vol. 7, p. 034005 (2017).
- [95] L. M. G. Abegao, A. A. C. Pagani, S. C. Zilio, M. A. R. C. Alencar, and J. J. Rodrigues Jr., "Measuring milk fat content by random laser emission," *Scientific Reports*, vol. 6, p. 35119 (2016).
- [96] P. A. Franken, A. E. Hill, C. W. Peters and G. Weinreich, "Generation of optical harmonics," *Physical Review letters*, vol. 7, pp. 118-119 (1961).
- [97] R. W. Boyd, *Nonlinear Optics*, San Diego: Academic press, (2008).
- [98] L. Blinov, *Structure and properties of Liquid crystals*, Springer Netherlands (2011).

- [99] P. G. De Gennes, "Short range order effects in the isotropic phase of nematics and cholesterics, *Molecular Crystals and Liquid Crystals*, vol. 12, pp. 193-214 (1971).
- [100] G. Assanto, *Nematicons*, Wiley (2012).
- [101] M. Peccianti, A. De Rossi, G. Assanto, A. De Luca, C. Umeton, and I. C. Khoo, "Electrically assisted self-confinement and waveguiding in planar nematic liquid crystal cell," *Applied Physics Letters*, vol. 77, pp. 7-9 (2000).
- [102] N. Tabiryan and B. Zeldovich, "The orientational optical nonlinearity of liquidcrystals," *Molecular Crystals Liquid Crystals*, vol. 62, pp. 237–250, (1980).
- [103] E. Braun, L. P. Faucheux, and A. Libchaber, "Strong self-focusing in nematic liquid crystals," *Physical Review A*, vol. 48, pp. 611–622, (1993).
- [104] N. Karimi, A. Alberucci, O. Buchnev, M. Virkki, M. Kauranen, and G. Assanto, "Phase-front curvature effects on nematicon generation," *Journal Optical Society of America B*, vol. 33, pp. 903-909 (2016).
- [105] M. Kwasny, A. Piccardi, A. Alberucci, M. Peccianti, M. Kaczmarek, M. A. Karpierz, and G. Assanto, "Nematicon-nematicon interactions in a medium with tunable nonlinearity and fixed nonlocality," *Optics Letters*, vol. 36, pp.2566–2568 (2011).
- [106] C. Conti, M. Peccianti, and G. Assanto, "Route to nonlocality and observation of accessible solitons," *Physical Review Letters*, vol. 91, p. 073901 (2003).
- [107] C. Conti, M. Peccianti, and G. Assanto, "Observation of optical spatial solitons in a highly nonlocal medium," *Physical Review Letters*, vol. 92, p.113902 (2004).
- [108] C. Conti, M. Peccianti, and G. Assanto, "Spatial solitons and modulational instability in the presence of large birefringence: the case of highly nonlocal liquid crystals," *Physical Review E*, vol. 72, p. 066614 (2005).
- [109] M. Peccianti and G. Assanto, "Signal readdressing by steering of spatial solitons in bulk nematic liquid crystals," *Optics Letters*, vol. 26, pp. 1690-1692 (2001).
- [110] X. Hutsebaut, C. Cambournac, M. Haelterman, J. Beeckman, and K. Neyts, "Measurement of the self-induced waveguide of a solitonlike optical beam in a nematic liquid crystal," *Journal of Optical Society of America B*, vol. 22, pp. 1424-1431 (2005).
- [111] A. Alberucci, M. Peccianti, G. Assanto, A. Dyadyusha, and M. Kaczmarek, "Two color vector solitons in nonlocal media," *Physical Review Letters*, vol. 97, p. 153903 (2006).
- [112] Y. Izdebskaya, G. Assanto, and W. Krolikowski, "Observation of stable-vector vertex solitons" *Optics Letters*, vol. 40, pp. 4182-4185 (2015).
- [113] Y. Izdebskaya, V. Shvedov, A. Desyatnikov, W. Krolikowski, M. Belic, G. Assanto, and Y. Kivshar, "Counterpropagating nematicons in bias-free liquid crystals," *Optics Express*, vol. 18, pp. 3258-3263 (2010).

- [114] Y. Izdebskaya, A. Desyatnikov, G. Assanto, and Y. Kivshar, "Multimode nematic waveguides," *Optics Letters*, vol. 36, pp.184-186 (2011).
- [115] S. Bolis, T. Virgili, S. K. Rejendran, J. Beeckman, and P. Kockaert, *Optics Letters*, vol. 41, p. 2245 (2016).
- [116] J. F. Henninot, J. F. Blach, and M. Warenghem, "Enhancement of dye fluorescence recovery in nematic liquid crystals using a spatial optical soliton," *Journal of Applied Physics*, vol. 107, p. 113111 (2010).
- [117] A. Alberucci, A. Piccardi, N. Kravets, O. Buchnev, and G. Assanto, "Soliton enhancement of spontaneous symmetry breaking," *Optica* 2, 783-789 (2015).
- [118] A. Alberucci, A. Piccardi, M. Peccianti, M. Kaczmarek, and G. Assanto, "propagation of spatial optical solitons in dielectric with adjustable nonlinearity," *Physical Review A*, vol. 82, p. 023806 (2010).
- [119] A. Alberucci, M. Peccianti, G. Assanto, G. Goschignano, A. De Luca, and C. Umeton, "Self-healing generation of spatial solitons in liquid crystals," *Optics Letters*, vol. 30, pp. 1381-1383 (2005).
- [120] E. Yariv, and R. Reisfeld, "laser properties of Pyrromethene dyes in sol-gel glasses," *Optical Materials*, vol. 13, p. 49 (1999).
- [121] K. K. Jagtap, D. K. Maity, A. K. Ray, K. Dasgupta, and S. K. Ghosh, "High efficiency dye laser with low fluorescence yield pyrromethene dyes: experimental and theoretical studies," *Applied Physics B*, vol. 103, pp. 917-924 (2011).
- [122] I. Nys, J. Beeckman, and K. Neyts, "Electrically tunable Fabry-Perot lasing in nematic liquid crystal cells," *Journal of Optical Society of America B*, vol. 31, pp. 1516-1524 (2014).
- [123] H. Kogelnik, and C. V. Shank, "Coupled-wave theory of distributed feedback lasers," *Journal of Applied Physics*, vol. 43, p. 2327 (1972).
- [124] F. Tommasi, E. Ignesti, S. Lepri, and S. Cavalieri, "Robustness of replica symmetry breaking phenomenology in random laser," *Scientific Reports*, vol. 6, p. 37113 (2016).
- [125] C. R. Lee, S. H. Lin, C. H. Guo, S. H. Chang, T. S. Mo, and S. C. Chu, "All-optically controllable random lasing based on dye-doped polymer-dispersed liquid crystals with nano-sized droplets," *Optics Express*, vol. 18, pp. 2406-2412 (2010).
- [126] M. Leonetti, C. Conti, and C. Lopez, "Random laser tailored by directional stimulated emission," *Physical Review A*, vol. 85, p. 043841 (2012).
- [127] M. Leonetti, C. Conti, and C. Lopez, "Tunable degree of localization in random lasers with controlled interaction," *Applied Physics Letters*, vol. 101, p. 051104 (2012).

- [128] G. V. Soest, and Ad Lagendijk, " $\beta$  factor in a random laser," *Physical Review E*, vol. 65, p. 047601 (2002).
- [129] J. Azkargorta, I. Iparraguirre, M. Barredo-Zuriarrain, S. García-Revilla, R. Balda, and J. Fernández, "Random laser action in Nd:YAG crystal powders," *Materials*, vol. 9, p. 369 (2016).
- [130] J. Azkargorta, I. Iparraguirre, M. Bettinelli, E. Cavalli, M. Barredo-Zuriarrain, S. García-Revilla, R. Balda, and J. Fernandez, "Effects of pumping wavelength and pump density on the random laser performance of stoichiometric Nd crystal powders," *Optics Express*, vol. 22, p. 27356 (2014).
- [131] A. Piccardi, A. Alberucci, U. Bortolozzo, S. Residori, and G. Assanto, "Readdressable interconnects with spatial soliton waveguides in liquid crystal light valves," *IEEE Photonic Technology Letters*, vol. 22, pp. 694-696 (2010).
- [132] Y. Izdebskaya, A. Desyatnikov, G. Assanto and Y. Kivshar, "Deflection of nematicons through interaction with dielectric particles," *Journal of Optical Society of America B*, vol. 30, pp. 1432-1437 (2013).
- [133] U. Laudyn, M. Kwasny, F. Sala, M. Karpierz, N. F. Smyth, and G. Assanto, "Curved solitons subject to transverse acceleration in reorientational soft matter," *Scientific Reports*, vol. 7, p. 12385 (2017).
- [134] M. Peccianti, C. Conti, G. Assanto, A. De Luca and C. Umeton, "Routing of Anisotropic Spatial Solitons and Modulational Instability in liquid crystals," *Nature*, vol. 432, pp. 733-737 (2004).
- [135] G. Assanto, C. Umeton, M. Peccianti, and A. Alberucci, "Nematicons and their angular steering," *Journal of Nonlinear Optical Physics & Materials*, vol. 15, pp. 33-42 (2005).
- [136] M. Peccianti, A. Dyadyusha, M. Kaczmarek and G. Assanto, "Tunable refraction and reflection of self-confined light beams," *Nature Physics*, vol. 2, pp. 737-742 (2006).
- [137] A. Piccardi, M. Peccianti, G. Assanto, A. Dyadyusha and M. Kaczmarek, "Voltage-driven in-plane steering of nematicons," *Applied Physics Letters*, vol. 94, p. 091106 (2009).
- [138] J. Beeckman, K. Neyts and M. Haeltermann, "Patterned electrode steering of nematicons," *Journal of Optics A - Pure and Applied Optics*, vol. 8, pp. 214-220 (2006).
- [139] Y. V. Izdebskaya, "Routing of spatial solitons by interaction with rod microelectrodes," *Optics Letters*, vol. 39, pp. 1681-1684 (2014).
- [140] Y. Izdebskaya, V. Shvedov, G. Assanto, and W. Krolikowski, "Magnetic routing of light-induced waveguides," *Nature Communications*, vol. 8, p. 14452 (2017).
- [141] A. Alberucci, M. Peccianti, and G. Assanto, "Nonlinear bouncing of nonlocal spatial solitons at the boundaries," *Optics Letters*, vol. 32, pp. 2795-2797 (2007).

[142] A. Pasquazi, A. Alberucci, M. Peccianti, and G. Assanto, "Signal processing by opto-optical interactions between self-localized and free propagating beams in liquid crystals," *Applied Physics Letters*, vol. 87, p. 261104 (2005).

[143] A. Piccardi, G. Assanto, L. Lucchetti, and F. Simoni, "All-optical steering of soliton waveguides in dye-doped liquid crystals," *Applied Physics Letters*, vol. 93, p. 171104 (2008).





## **ORIGINAL PAPERS**

## Soliton-assisted random lasing in optically-pumped liquid crystals

Sreekanth Perumbilavil,<sup>1</sup> Armando Piccardi,<sup>2</sup> Oleksandr Buchnev,<sup>3</sup> Martti Kauranen,<sup>1</sup> Giuseppe Strangi,<sup>4,5</sup> and Gaetano Assanto<sup>1,2,6,a)</sup>

<sup>1</sup>Optics Laboratory, Tampere University of Technology, FI-33101 Tampere, Finland

<sup>2</sup>NooEL - Nonlinear Optics and OptoElectronics Lab, University "Roma Tre," IT-00146 Rome, Italy

<sup>3</sup>Optoelectronics Research Centre, University of Southampton, SO17 1BJ Southampton, United Kingdom

<sup>4</sup>Department of Physics, Case Western Reserve University, Cleveland, Ohio 44106-7079, USA

<sup>5</sup>CNR Nanotec, 87036 Rende and Italian Institute of Technology, 16163 Genova, Italy

<sup>6</sup>CNR-ISC, Institute for Complex Systems, IT-00185 Rome, Italy

(Received 25 July 2016; accepted 8 October 2016; published online 21 October 2016)

We demonstrate a guided-wave random laser configuration by exploiting the coexistence of optical gain and light self-localization in a reorientational nonlinear medium. A spatial soliton launched by a near-infrared beam in dye-doped nematic liquid crystals enhances and confines stimulated emission of visible light in the optically-pumped gain-medium, yielding random lasing with enhanced features. *Published by AIP Publishing.* [<http://dx.doi.org/10.1063/1.4965852>]

In random lasers, a disordered distribution of scattering centers provides the required feedback for oscillations in optically amplifying media. In recent years, they have attracted a great deal of attention, mainly due to the versatility stemming from cavity-less geometries and the ease of realization.<sup>1–9</sup> In liquid crystals, suitable dopants can provide the gain action through optical pumping, while optical birefringence in conjunction with intense fluctuations of the dielectric tensor yield the required recurrent multiple scattering for random resonances to occur.<sup>10–17</sup> In the nematic phase, moreover, liquid crystals are positive uniaxial materials subject to optic axis reorientation under the action of electric fields, either at low or optical frequencies.<sup>18</sup> The latter response provides a low-power mechanism for nonlinear optics<sup>19</sup> and light localization into self-confined light-beams, the so-called “nematocons”.<sup>20</sup> Nematocons are bright spatial solitons (solitary waves) which are stable in two transverse dimensions due to the nonlocal response associated with the elastic intermolecular links in the liquid state;<sup>21,22</sup> they support graded-index waveguides able to confine additional (incoherent) signals/beams of different wavelengths as well as powers and profiles,<sup>23–30</sup> and are robust against refractive index perturbations<sup>31–35</sup> and collisional interactions.<sup>36–38</sup> Aided by nematocons, reorientational and electronic nonlinear responses, characterized by distinct time- and power-scales, can synergistically be combined.<sup>39,40</sup> Owing to their large numerical aperture,<sup>41</sup> nematocon waveguides solitons have also been employed in experiments involving incoherent light generation by fluorescence<sup>42</sup> or amplified spontaneous emission,<sup>43</sup> offering a means to better collect and couple the emitted light into optical fibers.

In this Letter, we demonstrate an example of synergy between diverse nonlinear responses: the combination of spatial solitons and random lasing into a “nematocon random laser”, whereby a low-power self-confined beam provides a guided-wave landscape for the stimulated emission induced by collinear optical pumping of dye-doped nematic liquid crystals (NLC).

Several benefits can be expected from adopting such light-induced guided-wave configuration for random lasing. At variance with standard thin film geometries, the thick NLC cell provides an extended volume where optical pumping can produce fluorescence, and in turn, stimulated emission and lasing action via random scattering and feedback. The large interaction volume can exploit several feedback paths through scattering, support many coupled lasing modes<sup>44</sup> and their competition/thermalization,<sup>45</sup> producing smoother spectrum and spatial profile as compared to “standard” random lasers. Furthermore, owing to anisotropic light scattering in uniaxials,<sup>46</sup> the spontaneous as well as the stimulated emissions in NLC doped with pyromethene-dye tend to be polarized in the plane of the director alignment,<sup>10,18,43</sup> hence, the generated photons are co-polarized with the reorientational soliton and can be trapped in the light-induced waveguide, the nematocon. At variance with a standard one-beam configuration (see Fig. 1(a)), the confinement afforded by the nematocon on extraordinary-polarized (e-) waves can balance out the spatial dispersion of the involved wavepackets and result in reduced diffraction through index change as well as modified distribution of the emission through disorder confinement<sup>47</sup> and altered scattering. In standard NLC random lasers, localized and extended modes in the active volume overlap and compete; in our geometry transversely confined modes are sustained by the waveguide landscape and conveyed at the exit. Finally, the pump beam can also undergo nematocon confinement depending on its polarization: if polarized along  $y$  at the input, even the e-pump can be guided along the nematocon, yielding an extended interaction with light emitted along the waveguide and only limited by absorption. The latter pump polarization, however, turns out to be the least efficient in terms of fluorescence in the uniaxial guest-host material. For this reason, we conducted experiments with either (i) an ordinary-wave (o-) pump with polarization orthogonal to the optic axis or (ii) an extraordinary pump copolarized with (and guided by) the soliton and the emitted light (Figs. 1(b) and 1(c)).

We prepared and employed planar glass cells with mechanically rubbed polyimide/NLC interfaces to prepare 100  $\mu\text{m}$  thick samples of nematic liquid crystals E7 doped

<sup>a)</sup>assanto@uniroma3.it

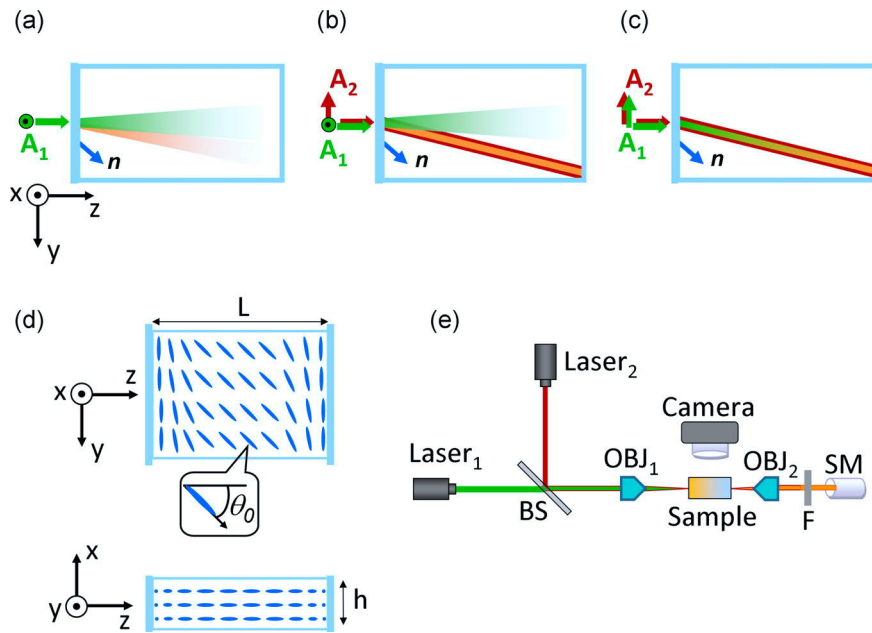


FIG. 1. (a) Sketch of the interaction without nematicon. (b) and (c) Sketch of the interaction with nematicon (amplitude  $A_2$ ) and (b) ordinary or (b) extraordinary wave pump (amplitude  $A_1$ ). The emitted light, represented here as a beam, is actually generated in the region where the pump remains intense despite the absorption. (d) Sample geometry and director alignment.  $\theta_0$  is the bulk orientation due to the boundary conditions. (e) Experimental setup: SM, spectrometer; OBJ, microscope objective; Laser<sub>1</sub>, pulsed pump laser at 532 nm; Laser<sub>2</sub>, cw laser at 1064 nm.

with 0.3 wt. % pyromethene dye (PM597). Such guest-host mixture, when resonantly pumped by nanosecond laser pulses at 532 nm, is able to provide fluorescence and optical amplification in the visible spectrum around 570–580 nm.<sup>10,43</sup> When excited by mW-power e-wave beams, through non-resonant reorientation it can also support the formation and propagation of self-guided spatial optical solitons of arbitrary wavelength.<sup>20</sup> The NLC cell was 3 mm-long in propagation and equipped with input and output glass interfaces to prevent meniscus formation and undesired beam depolarization (see sample geometry in Fig. 1(d)). The NLC optic axis was aligned in the plane  $yz$  at  $\theta = 45^\circ$  with respect to the wave vector direction  $\mathbf{k}/z$  in order to avoid a power (Fréedericksz) threshold effect for all-optical reorientation, while maximizing the nonlinear optical response.<sup>48</sup>

A cw near-infrared beam of wavelength  $1.064 \mu\text{m}$  was e-polarized with electric field parallel to  $y$ , focused at the input interface to a waist  $3 \mu\text{m}$  and launched with wave vector along  $z$  in the cell mid-plane ( $x=0$ ) in order to excite a self-trapped nematicon (see Fig. 1(e)). The latter, stabilized by nonlocality in two-dimensions, is able to propagate with a nearly invariant profile in the plane  $yz$  at the walkoff angle  $\delta$  defined by the birefringence,<sup>20,21</sup> i.e.,

$$\delta = \arctan \left[ \frac{(n_{\parallel}^2 - n_{\perp}^2) \sin \theta \cos \theta}{n_{\parallel}^2 \sin^2 \theta + n_{\perp}^2 \cos^2 \theta} \right],$$

with  $n_{\parallel}$  and  $n_{\perp}$  the refractive indices for electric fields parallel and orthogonal to the optic axis  $\hat{\mathbf{n}}$ , respectively. A 20 Hz rep-rate train of  $\approx 6$  ns pulses from a frequency-doubled Q-switched Nd:YAG laser was focused and injected in the cell mid-plane collinearly with the cw beam, with particular care to ensure that, despite walkoff, the two (green and near-infrared) beams had parallel Poynting vectors. The experimental setup was completed by a microscope, a CCD camera to check the beam alignment and a spectrometer to collect the emission from the cell output, as sketched in Fig. 1(e).

Figure 2(a) shows the measured output versus input characteristics of the random laser, acquired from the emitted light without (black) and with (red) a 5 mW nematicon,

injecting the pump in the e-polarization. The emission, collected after a bandpass filter and spatially integrated, exhibits the standard lasing character with an energy threshold around  $0.85 \mu\text{J}$  and a higher slope (efficiency) when the nematicon is present. Fig. 2(b) displays the corresponding results for an ordinary-polarized pump: as before, the nematicon increases the lasing efficiency. For o-polarized pump light the threshold is slightly lower and a marked increase in the output-vs-input slope and lasing efficiency is clearly visible, consistently with previous observations in the same material<sup>10,43</sup> In the latter geometry, the o-pump is not confined but interacts more efficiently with the guest-host, whereas the e-wave emission is confined within the near-infrared nematicon and propagates along its walkoff angle (Fig. 1(b)). Clearly, despite the spatial spreading incurred by the o-polarized pump, the random laser operates better in this configuration with orthogonal pump and soliton. When calculating the  $\beta$ -factor (rate of spontaneous emission radiated into lasing modes over total rate of spontaneous emission) according to the procedure outlined in Ref. 49 and used, e.g., in Ref. 50, the  $\beta$  reduction observed for an o-wave pump became more apparent in the presence of

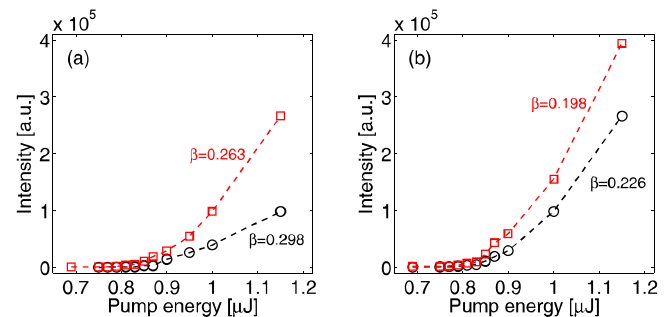


FIG. 2. Output intensity of emitted light (units correspond to spectrometer counts) at wavelengths around 575 nm the energy of the pump pulse. (a) e-wave pump in bulk interaction without nematicon (black symbols and line) and guided-wave interaction in the presence of a 5 mW nematicon (red squares and line); (b) o-wave pump without (black circles and line) and with a 5 mW nematicon (red symbols and line). The calculated  $\beta$ -factors are indicated next to each line.

the nematicon, as indicated by the values next to each curve in Fig. 2. This confirms that the fraction of spontaneous emission that triggers random lasing is significantly less with than without soliton, i.e., the nematicon-assisted configuration is more efficient.

Figure 3 illustrates the spectral narrowing afforded by this random laser with/without a collinear spatial soliton. The full-width half-maximum data points, plotted versus pump energy/pulse, clearly show the lasing characteristics corresponding to Fig. 2, with a marked improvement when the nematicon contributes to the confinement of the emitted light. A narrowing of the emitted spectrum is visible in (a) without soliton as the system goes from fluorescence to above lasing threshold, from 43.4 nm (45.6 nm) to 11.0 nm (19.8 nm) for o- (e-) pump; the spectral narrowing is more marked with nematicon assistance, particularly for a pump orthogonal to the optic axis of the guest-host medium: from 42.9 nm (43.8 nm) to 7.2 nm (12.3 nm) for o- (e-) pump. The spectral width in the presence of a nematicon is consistently lower above threshold, confirming the beneficial role of our soliton assisted geometry in an extended interaction region.

Figure 4 shows various lasing spectra when the guest-host system is pumped (o-polarization) in the presence/absence of a collinear nematicon. When the pump energy is below threshold ( $0.75 \mu\text{J}$ ) no laser action takes place and a 5 mW nematicon barely increases the emitted intensity by collecting photons at the output (Fig. 4(a)). Conversely, when pumping above threshold ( $1.2 \mu\text{J}$ ), the index contrast introduced by the nematicon through reorientation assists the emission process by changing the scattering paths and the interaction efficiency, resulting in wavelength tuning and spectral narrowing (Fig. 4(b)). The smooth spectral features of the lasing emission might be ascribed to the overlap of several modes, as discussed in Ref. 16. Figs. 4(c) and 4(d) illustrates the nematicon role on spectral profiles, width, and random laser intensity for  $1.2 \mu\text{J}$  o-wave pumping and nematicon power varying up to 6 mW. Such all-optical tuning can be ascribed to changes in the local scattering cross-section that, in turn, modify the transport distance of the generated photons and the size of the random loops responsible for random resonances and lasing.

Finally, Fig. 5 graphs the spatial profile of the emitted light. The curves, plotted against the transverse coordinate  $y$ , indicate that the soliton confines the laser light and improves its transverse distribution and spatial coherence, consistently with the expected benefits of a nematicon random laser. When exploited in conjunction with nematicon steering and

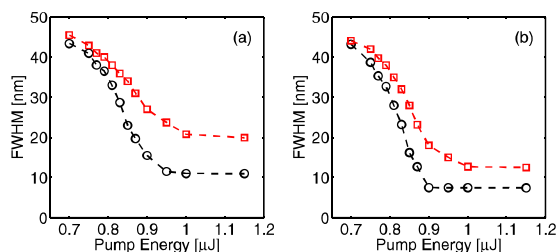


FIG. 3. Measured full-width half-maxima (FWHM) of the spectral emission (see Fig. 4) versus energy of the pump pulses, for an ordinary (black circles and lines) or extraordinary (red squares and lines) wave pump (a) in a bulk interaction (no soliton), (b) in the presence of a collinear 5 mW nematicon.

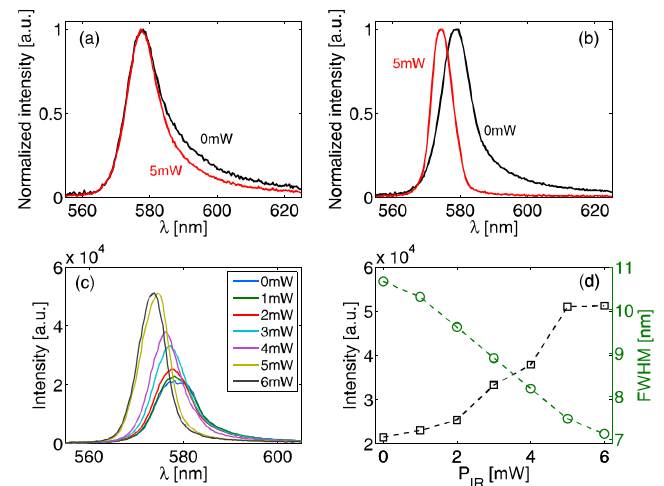


FIG. 4. Soliton effects on spectral emission, for a pump orthogonal to the optic axis. (a) Emission spectrum with pump energy below threshold ( $0.75 \mu\text{J}$ ), without (black) and with a 5 mW soliton (red). (b) Spectrum with pump energy above threshold ( $1.2 \mu\text{J}$ ), without (black) and with (red) a 5 mW nematicon: the latter shifts the wavelength peak and narrows the spectrum. (c) Emission spectra for a pump at  $1.2 \mu\text{J}$  and various nematicon powers. (d) Tuning of lasing efficiency (output intensity, squares) and spectral width (FWHM, circles) versus nematicon power, for a pump at  $1.2 \mu\text{J}$ .

readdressing, these features can allow one to engineer random lasing with increased spatial coherence and controlled direction of emission.

In conclusion, we have designed and demonstrated a nematicon-assisted random laser, where the graded index region defined by the spatial soliton through reorientation confines the emitted radiation and contributes to tune the features of random lasing in terms of spectrum and overall efficiency, as witnessed by changes in  $\beta$ -factor, laser wavelength, and linewidth. While these preliminary results are sensitive to details of sample preparation and definitely subject to improvement through a better control of beam alignment and guest-host composition, they prove that the benefits of a cavity-less random laser can be combined with those of an optical control of scattering and diffraction by a light-induced guided-wave geometry, towards better laser coherence and directionality, narrower lines, and lower threshold with higher slope efficiency. We plan to investigate additional properties

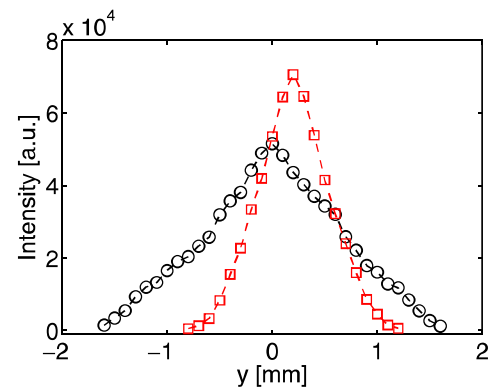


FIG. 5. Measured spatial distribution of the random laser emission, imaged with a microscope objective by translating a slit and filtering out near-infrared and green light, with (red squares and line) and without (black circles and line) a collinear 5 mW nematicon. The peak emission is at the wavelength 578.1 nm without soliton and at 573.9 nm with soliton, respectively.

of nematic random lasers and to derive a suitable model accounting for the large number of lasing modes and their competition in an extended and confined interaction region.

This work was supported by the Academy of Finland through the Finland Distinguished Professor Grant No. 282858. The authors also thank C. Conti for enlightening discussions and the European Union COST Action IC1208.

- <sup>1</sup>D. S. Wiersma and S. Cavaleri, *Nature* **414**, 708 (2001).
- <sup>2</sup>D. S. Wiersma, *Nat. Phys.* **4**, 359 (2008).
- <sup>3</sup>M. Leonetti, C. Conti, and C. Lopez, *Nat. Photonics* **5**, 615 (2011).
- <sup>4</sup>N. Bachelard, J. Andreasen, S. Gigan, and P. Sebbah, *Phys. Rev. Lett.* **109**, 033903 (2012).
- <sup>5</sup>Y. Bliokh, E. I. Chaikina, N. Lizárraga, E. R. Méndez, V. Freilikher, and F. Nori, *Phys. Rev. B* **86**, 054204 (2012).
- <sup>6</sup>M. Leonetti and C. Lopez, *Appl. Phys. Lett.* **102**, 071105 (2013).
- <sup>7</sup>S. Turitsyn, S. A. Babin, D. Churkin, I. D. Vatik, M. Nikulin, and E. Podivilov, *Phys. Rep.* **542**, 133 (2014).
- <sup>8</sup>C. T. Dominiques, M. A. Gomes, Z. S. Macedo, C. B. de Araujo, and A. S. L. Gomes, *Nanoscale* **7**, 317 (2015).
- <sup>9</sup>L. V. Gerasimov, D. V. Kuprianov, and M. D. Havey, *Opt. Spectrosc.* **119**, 377 (2015).
- <sup>10</sup>G. Strangi, S. Ferjani, V. Barna, A. D. Luca, C. Versace, N. Scaramuzza, and R. Bartolino, *Opt. Express* **14**, 7737 (2006).
- <sup>11</sup>S. Ferjani, L. Sorriso-Valvo, A. De Luca, V. Barna, R. De Marco, and G. Strangi, *Phys. Rev. E* **78**, 011707 (2008).
- <sup>12</sup>B. He, Q. Liao, and Y. Huang, *Opt. Mater.* **31**, 375 (2008).
- <sup>13</sup>Q. Song, L. Liu, L. Xu, Y. Wu, and Z. Wang, *Opt. Lett.* **34**, 298 (2009).
- <sup>14</sup>C.-R. Lee, J.-D. Lin, B.-Y. Huang, T.-S. Mo, and S.-Y. Huang, *Opt. Express* **18**, 25896 (2010).
- <sup>15</sup>C.-R. Lee, J.-D. Lin, B.-Y. Huang, S.-H. Lin, T.-S. Mo, S.-Y. Huang, C.-T. Kuo, and H.-C. Yeh, *Opt. Express* **19**, 2391 (2011).
- <sup>16</sup>S. M. Morris, D. J. Gardiner, M. M. Qasim, P. J. W. Hands, T. D. Wilkinson, and H. J. Coles, *J. Appl. Phys.* **111**, 033106 (2012).
- <sup>17</sup>H. Biana, F. Yaoa, H. Liuc, F. Huang, Y. Peiab, C. Houab, and X. Sunab, *Liq. Cryst.* **41**, 1436 (2014).
- <sup>18</sup>P. G. DeGennes and J. Prost, *The Physics of Liquid Crystals* (Oxford Science, New York, 1993).
- <sup>19</sup>I. C. Khoo, *Phys. Rep.* **471**, 221 (2009).
- <sup>20</sup>M. Peccianti and G. Assanto, *Phys. Rep.* **516**, 147 (2012).
- <sup>21</sup>C. Conti, M. Peccianti, and G. Assanto, *Phys. Rev. Lett.* **92**, 113902 (2004).
- <sup>22</sup>A. Alberucci, C. P. Jisha, N. Smyth, and G. Assanto, *Phys. Rev. A* **91**, 013841 (2015).
- <sup>23</sup>M. Peccianti and G. Assanto, *Opt. Lett.* **26**, 1791 (2001).
- <sup>24</sup>X. Hutsebaut, C. Cambournac, M. Haelterman, J. Beeckman, and K. Neyts, *J. Opt. Soc. Am. B* **22**, 1424 (2005).
- <sup>25</sup>A. Alberucci, M. Peccianti, G. Assanto, A. Dyadyusha, and M. Kaczmarek, *Phys. Rev. Lett.* **97**, 153903 (2006).
- <sup>26</sup>J. F. Henninot, J. F. Blach, and M. Warengem, *J. Opt. A: Pure Appl. Opt.* **9**, 20 (2007).
- <sup>27</sup>Y. Izdebskaya, V. Shvedov, A. Desyatnikov, W. Krolikowski, M. Belic, G. Assanto, and Y. Kivshar, *Opt. Express* **18**, 3258 (2010).
- <sup>28</sup>A. Piccardi, A. Alberucci, and G. Assanto, *Phys. Rev. Lett.* **104**, 213904 (2010).
- <sup>29</sup>Y. Izdebskaya, A. Desyatnikov, G. Assanto, and Y. Kivshar, *Opt. Lett.* **36**, 184 (2011).
- <sup>30</sup>Y. Izdebskaya, G. Assanto, and W. Krolikowski, *Opt. Lett.* **40**, 4182 (2015).
- <sup>31</sup>A. Pasquazi, A. Alberucci, M. Peccianti, and G. Assanto, *Appl. Phys. Lett.* **87**, 261104 (2005).
- <sup>32</sup>A. Piccardi, G. Assanto, L. Lucchetti, and F. Simoni, *Appl. Phys. Lett.* **93**, 171104 (2008).
- <sup>33</sup>A. Piccardi, A. Alberucci, U. Bortolozzo, S. Residori, and G. Assanto, *IEEE Photonics Technol. Lett.* **22**, 694 (2010).
- <sup>34</sup>Y. Izdebskaya, V. Shvedov, A. Desyatnikov, W. Krolikowski, and Y. Kivshar, *Opt. Lett.* **35**, 1692 (2010).
- <sup>35</sup>A. Piccardi, A. Alberucci, U. Bortolozzo, S. Residori, and G. Assanto, *Appl. Phys. Lett.* **96**, 071104 (2010).
- <sup>36</sup>M. Peccianti, K. Brzadkiewicz, and G. Assanto, *Opt. Lett.* **27**, 1460 (2002).
- <sup>37</sup>C. P. Jisha, A. Alberucci, R.-K. Lee, and G. Assanto, *Opt. Lett.* **36**, 1848 (2011).
- <sup>38</sup>A. Piccardi, S. Residori, and G. Assanto, *J. Opt.* **18**, 07LT01 (2016).
- <sup>39</sup>I. B. Burgess, M. Peccianti, G. Assanto, and R. Morandotti, *Phys. Rev. Lett.* **102**, 203903 (2009).
- <sup>40</sup>M. Peccianti, A. Pasquazi, G. Assanto, and R. Morandotti, *Opt. Lett.* **35**, 3342 (2010).
- <sup>41</sup>M. Peccianti and G. Assanto, *Opt. Lett.* **26**, 1690 (2001).
- <sup>42</sup>J. F. Henninot, J. F. Blach, and M. Warengem, *J. Appl. Phys.* **107**, 113111 (2010).
- <sup>43</sup>S. Bolis, T. Virgili, S. K. Rajendran, J. Beeckman, and P. Kockaert, *Opt. Lett.* **41**, 2245 (2016).
- <sup>44</sup>M. Leonetti, C. Conti, and C. Lopez, *Light Sci. Appl.* **2**, e88 (2013).
- <sup>45</sup>C. Conti, M. Leonetti, A. Fratolocci, L. Angelani, and G. Ruocco, *Phys. Rev. Lett.* **101**, 143901 (2008).
- <sup>46</sup>S. Gottardo, S. Cavaleri, O. Yaroshchuk, and D. S. Wiersma, *Phys. Rev. Lett.* **93**, 263901 (2004).
- <sup>47</sup>N. Ghofraniha, I. Viola, A. Zacheo, V. Arima, G. Gigli, and C. Conti, *Opt. Lett.* **38**, 5043 (2013).
- <sup>48</sup>M. Peccianti, C. Conti, and G. Assanto, *Opt. Lett.* **30**, 415 (2005).
- <sup>49</sup>G. van Soest and A. Lagendijk, *Phys. Rev. E* **65**, 047601 (2002).
- <sup>50</sup>S. Ferjani, A. D. Luca, V. Barna, C. Versace, and G. Strangi, *Opt. Express* **17**, 2042 (2009).

## Erratum: “Soliton-assisted random lasing in optically-pumped liquid crystals” [Appl. Phys. Lett. 109, 161105 (2016)]

Sreekanth Perumbilavil,<sup>1</sup> Armando Piccardi,<sup>2</sup> Oleksandr Buchnev,<sup>3</sup> Martti Kauranen,<sup>1</sup> Giuseppe Strangi,<sup>4,5</sup> and Gaetano Assanto<sup>1,2,6,a)</sup>

<sup>1</sup>Optics Laboratory, Tampere University of Technology, FI-33101 Tampere, Finland

<sup>2</sup>NooEL - Nonlinear Optics and OptoElectronics Lab, University “Roma Tre,” IT-00146 Rome, Italy

<sup>3</sup>Optoelectronics Research Centre, University of Southampton, SO17 1BJ Southampton, United Kingdom

<sup>4</sup>Department of Physics, Case Western Reserve University, Cleveland, Ohio 44106-7079, USA

<sup>5</sup>CNR Nanotec, 87036 Rende and Italian Institute of Technology, 16163 Genova, Italy

<sup>6</sup>CNR-ISC, Institute for Complex Systems, IT-00185 Rome, Italy

(Received 16 December 2016; accepted 27 December 2016; published online 6 January 2017)

[<http://dx.doi.org/10.1063/1.4973864>]

We recently reported our experimental findings on the use of a passive Kerr-like nonlinear optical response, namely, reorientational self-focusing and spatial soliton generation, in conjunction with optically pumped random lasing in nematic liquid crystals (E7) doped with Pyrromethene dye (PM597).<sup>1</sup> In Ref. 1, for the emission spectra at pump energies of  $0.75 \mu\text{J}/\text{pulse}$  (below threshold), we mistakenly used the wrong data and curves in Fig. 4(a). The amended figure (to replace Fig. 4 in Ref. 1) is presented here. This correction does not affect the discussion of the results and the conclusions presented in the article.

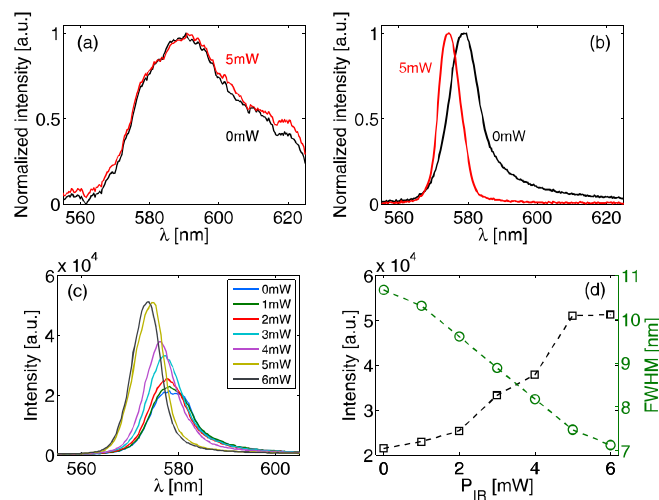


FIG. 1. Soliton effects on spectral emission, for a pump orthogonal to the optic axis. (a) Emission spectrum with pump energy below threshold ( $0.75 \mu\text{J}$ ), without (black) and with a 5 mW soliton (red). (b) Spectrum with pump energy above threshold ( $1.2 \mu\text{J}$ ), without (black) and with (red) a 5 mW nematicon: the latter shifts the wavelength peak and narrows the spectrum. (c) Emission spectra for a pump at  $1.2 \mu\text{J}$  and various nematicon powers. (d) Tuning of lasing efficiency (output intensity, squares) and spectral width (FWHM, circles) versus nematicon power, for a pump at  $1.2 \mu\text{J}$ .

<sup>1</sup>S. Perumbilavil, A. Piccardi, O. Buchnev, M. Kauranen, G. Strangi, and G. Assanto, *Appl. Phys. Lett.* **109**, 161105 (2016).

<sup>a)</sup>assanto@uniroma3.it





II

**ALL-OPTICAL GUIDED-WAVE RANDOM LASER IN NEMATIC  
LIQUID CRYSTALS**

by

Sreekanth Perumbilavil, Armando Piccardi, Oleksandr Buchnev, Martti Kau-  
ranen, Giuseppe Strangi and Gaetano Assanto, March 2017

Optics Express vol. 25, pp. 4672-4679

© 2017 Optical Society of America

Reproduced with permission.



# All-optical guided-wave random laser in nematic liquid crystals

SREEKANTH PERUMBILAVIL,<sup>1</sup> ARMANDO PICCARDI,<sup>2</sup> OLEKSANDR BUCHNEV,<sup>3</sup> MARTTI KAURANEN,<sup>1</sup> GIUSEPPE STRANGI<sup>4</sup> AND GAETANO ASSANTO<sup>1,2,\*</sup>

<sup>1</sup>Photonics Laboratory, Tampere University of Technology, FI-33101 Tampere, Finland

<sup>2</sup>NooEL - Nonlinear Optics and OptoElectronics Lab, University "Roma Tre", I-00146 Rome, Italy

<sup>3</sup>Optoelectronics Research Centre, University of Southampton, SO17 1BJ, Southampton, United Kingdom

<sup>4</sup>Dept. of Physics, Case Western Reserve University, Cleveland, Ohio 44106-7079, USA

\*[assanto@uniroma3.it](mailto:assanto@uniroma3.it)

**Abstract:** Spatial solitons can affect and enhance random lasing in optically-pumped dye-doped nematic liquid crystals. Upon launching two collinear beams in the sample, the first to pump the fluorescent guest molecules and the second to induce a reorientational soliton, strikingly the second beam not only guides the emitted photons in the soliton waveguide, but also enhances the lasing efficiency and modulates its spectral width. By altering the scattering paths of the emitted photons, the soliton also contributes to the selection of the lasing modes, as further confirmed by the observed kinks in the input/output characteristics. These experimental results demonstrate that random lasing can be efficiently controlled by a light beam which does not interact with the gain molecules, opening a route towards light-controlled random lasers.

© 2017 Optical Society of America

**OCIS codes:** (190.5940) Self-action effects; (190.6135) Spatial solitons; (160.3380) Laser materials; (160.3710) Liquid crystals.

## References and links

1. H. Cao, "Lasing in random media," *Waves in Random Media* **13** (3), R1–R39 (2003).
2. V. S. Letokhov, "Generation of light by a scattering medium with negative resonance absorption," *Sov. Phys. JETP* **26**, 835 (1968).
3. N. M. Lawandy, R. M. Balachandran, A. S. L. Gomes, and E. Sauvain, "Laser action in strongly scattering media," *Nature* **36**, 436–438 (1994).
4. D. S. Wiersma, "The physics and applications of random lasers," *Nature Phys.* **4** (10), 359–367 (2008).
5. H. Cao, J. Y. Xu, D. Z. Zhang, S.-H. Chang, S. T. Ho, E. W. Seelig, X. Liu, and R. P. H. Chang, "Spatial confinement of laser light in active random media," *Phys. Rev. Lett.* **84**, 5584–5587 (2000).
6. M. Leonetti and C. Lopez, "Active subnanometer spectral control of a random laser," *Appl. Phys. Lett.* **102**, 071105 (2013).
7. M. Pang, X. Bao, L. Chen, Z. Qin, Y. Lu, and P. Lu, "Frequency stabilized coherent Brillouin random fiber laser: theory and experiments," *Opt. Express* **21** (22), 27155–27168 (2013).
8. R. C. Polson and Z. V. Vardeny, "Random lasing in human tissues," *Appl. Phys. Lett.* **85** (7), 1289–1291 (2004).
9. G. Strangi, S. Ferjani, V. Barna, A. De Luca, C. Versace, N. Scaramuzza, and R. Bartolino, "Random lasing and weak localization of light in dye-doped nematic liquid crystals," *Opt. Express* **14** (17), 7737–7744 (2006).
10. D. S. Wiersma and S. Cavaliere, "Light emission: a temperature-tunable random laser," *Nature* **414**, 708–709 (2001).
11. S. M. Morris, D. J. Gardiner, M. M. Qasim, P. J. W. Hands, T. D. Wilkinson, and H. J. Coles, "Lowering the excitation threshold of a random laser using the dynamic scattering states of an organosiloxane smectic A liquid crystal," *J. Appl. Phys.* **111**, 033106 (2012).
12. S. Mujumdar, S. Cavaliere, and D. S. Wiersma, "Temperature-tunable random lasing: numerical calculations and experiments," *J. Opt. Soc. Am. B* **21** (1), 201–207 (2004).
13. T. Nakamura, B. P. Tiwari, and S. Adachi, "Control of random lasing in  $ZnOAl_2O_3$  nanopowders," *Appl. Phys. Lett.* **99**, 231105 (2011).
14. X. H. Wu, A. Yamilov, H. Noh, H. Cao, E. W. Seelig, and R. P. H. Chang, "Random lasing in closely packed resonant scatterers," *J. Opt. Soc. Am. B* **21** (1), 159–167 (2004).
15. S. Gottardo, S. Cavaliere, O. Yaroshchuk, and D. S. Wiersma, "Quasi-two-dimensional diffusive random laser action," *Phys. Rev. Lett.* **93**, 263901 (2004).
16. N. Bachelard, J. Andreasen, S. Gigan, and P. Sebbah, "Taming random lasers through active spatial control of the pump," *Phys. Rev. Lett.* **109**, 033903 (2012).

17. H. Cao, Y. G. Zhao, S. T. Ho, E. W. Seelig, Q. H. Wang, and R. P. H. Chang, "Random laser action in semiconductor powder," *Phys. Rev. Lett.* **82**, 2278–2281 (1999).
18. S. Mujumdar, M. Ricci, R. Torre, and D. S. Wiersma, "Amplified extended modes in random lasers," *Phys. Rev. Lett.* **93**, 053903 (2004).
19. M. Leonetti, C. Conti, and C. Lopez, "The mode locking transition of random lasers," *Nat. Photon.* **5**, 615–617 (2011).
20. P. G. DeGennes and J. Prost, *The physics of liquid crystals* (Oxford Science, 1993).
21. I. C. Khoo, *Liquid crystals: physical properties and nonlinear optical phenomena* (Wiley, 1995).
22. S. Ferjani, V. Barna, A. De Luca, C. Versace, N. Scaramuzza, R. Bartolino, and G. Strangi, "Thermal behavior of random lasing in dye-doped nematic liquid crystals," *Appl. Phys. Lett.* **89**, 121109 (2006).
23. M. Peccianti and G. Assanto, "Nematicons," *Phys. Rep.* **516**, 147–208 (2012).
24. M. Peccianti, C. Conti, G. Assanto, A. De Luca, and C. Umeton, "Routing of anisotropic spatial solitons and modulational instability in nematic liquid crystals," *Nature* **432**, 733 (2004).
25. M. Warengem, J.F. Henninot, and G. Abbate, "Non linearly induced self waveguiding structure in dye doped nematic liquid crystals confined in capillaries," *Opt. Express* **2** (12), 483–490 (1998).
26. J. Beeckman, K. Neyts, X. Hutsebaut, C. Cambournac, and M. Haelterman, "Simulations and experiments on self-focusing conditions in nematic liquid-crystal planar cells," *Opt. Express* **12** (6), 1011–1018 (2004).
27. M. Peccianti, G. Assanto, A. De Luca, C. Umeton, and I. C. Khoo, "Electrically assisted self-confinement and waveguiding in planar nematic liquid crystal cells," *Appl. Phys. Lett.* **77** (1), 7–9 (2000).
28. G. Assanto, A. Fratolocchi, and M. Peccianti, "Spatial solitons in nematic liquid crystals: from bulk to discrete," *Opt. Express* **15** (8), 5248–5259 (2007).
29. Y. V. Izdebskaya, V. G. Shvedov, A. S. Desyatnikov, W. Z. Krolikowski, M. BeliÄĀ, G. Assanto, and Y. S. Kivshar, "Counterpropagating nematicons in bias-free liquid crystals," *Opt. Express* **18** (4), 3258–3263 (2010).
30. A. Alberucci, A. Piccardi, M. Peccianti, M. Kaczmarek, and G. Assanto, "Propagation of spatial optical solitons in a dielectric with adjustable nonlinearity," *Phys. Rev. A* **82** (2), 023806 (2010).
31. A. Piccardi, A. Alberucci, and G. Assanto, "Self-turning self-confined light beams in guest-host media," *Phys. Rev. Lett.* **104**, 213904 (2010).
32. J. F. Henninot, J. F. Blach, and M. Warengem, "Enhancement of dye fluorescence recovery in nematic liquid crystals using a spatial optical soliton," *J. Appl. Phys.* **107**, 113111 (2010).
33. S. Bolis, T. Virgili, S. K. Rajendran, J. Beeckman, and P. Kockaert, "Nematicon-driven injection of amplified spontaneous emission into an optical fiber," *Opt. Lett.* **41** (10), 2245–2248 (2016).
34. I. Burgess, M. Peccianti, G. Assanto, and R. Morandotti, "Accessible light bullets via synergetic nonlinearities," *Phys. Rev. Lett.* **102**, 203903 (2009).
35. M. Peccianti, A. Pasquazi, G. Assanto, and R. Morandotti, "Enhancement of third-harmonic generation in nonlocal spatial solitons," *Opt. Lett.* **35** (20), 3342–3344 (2010).
36. U. A. Laudyn, M. Kwasny, A. Piccardi, M. A. Karpierz, R. Dabrowski, O. Chojnowska, A. Alberucci, and G. Assanto, "Nonlinear competition in nematicon propagation," *Opt. Lett.* **40** (22), 5235–5238 (2015).
37. J. Yi, Y. Yu, J. Shang, X. An, B. Tu, G. Feng, and S. Zhou, "Waveguide random laser based on a disordered ZnSe-nanosheets arrangement," *Opt. Express* **24** (5), 5102–5109 (2016).
38. S. Perumbilavil, A. Piccardi, O. Buchnev, M. Kauranen, G. Strangi, and G. Assanto, "Soliton-assisted random lasing in optically-pumped liquid crystals," *Appl. Phys. Lett.* **102**, 203903 (2016).
39. E. Yariv and R. Reisfeld, "Laser properties of pyrromethene dyes in sol-gel glasses," *Opt. Mater.* **13**, 49 (1999).
40. J. H. Lin, Y. L. Hsiao, B. Y. Ciou, S. H. Lin, Y. H. Chen, and J. J. Wu, "Manipulation of random lasing action from dye-doped liquid crystals infilling two-dimensional confinement single core capillary," *IEEE Photon. J.* **7** (3), 1501809 (2015).
41. I. Jánossy and T. Kósa, "Influence of anthraquinone dyes on optical reorientation of nematic liquid crystals," *Opt. Lett.* **17** (17), 1183–1185 (1992).
42. L. Sznitko, K. Kaliciak, A. Adamow, and J. Mysliwiec, "A random laser made of nematic liquid crystal doped with a laser dye," *Opt. Mat.* **56**, 121–128 (2016).
43. T. Nakamura, S. Sonoda, T. Yamamoto, and S. Adachi, "Discrete-mode ZnO microparticle random laser," *Opt. Lett.* **40** (11), 2661–2664 (2015).
44. B. He, Q. Liao, and Y. Huang, "Random lasing in a dye doped cholesteric liquid crystal polymer solution," *Opt. Mat.* **31**, 375–379 (2008).
45. G. van Soest and A. Lagendijk, "Beta factor in a random laser," *Phys. Rev. E* **65**, 047602 (2002).

---

## 1. Introduction

Random lasing occurs when disorder in an optically amplifying medium provides multiple scattering events for emitted light, such that the resulting photon paths allow for amplification and stimulated emission, even in the absence of an actual cavity [1]. Since its prediction [2] and the first experimental demonstration [3], several efforts were devoted to obtaining random

lasing (RL), foreseeing the development of low cost coherent sources [4]. To achieve random lasing, the significant scattering required from the active medium or the host was obtained in powders [3,5,6], optical fibers [7], biological tissues [8] and liquid crystals [9–11]. At the same time, the strong dependence of RL emission on environmental parameters offered unprecedented opportunities to tune the lasing properties through, e.g., temperature control [12], concentration of active molecules in host materials [13], grain size in powder systems [14], bias voltage [11, 15], spatial profile of the pump beam [6, 16]. By acting on the favoured scattering paths (equivalent to tuning the cavity in standard lasers), it was possible to select lasing modes [17, 18] and lock them [19].

Liquid crystals are mesophases possessing a finite degree of positional and/or orientational order, due to their relatively weak intermolecular links [20]. In the nematic phase the positional order is negligible, while the long axes of the oriented molecules are aligned in an average direction, termed molecular director  $\mathbf{n}$  and corresponding to the optic axis of the macroscopic uniaxial material [21]. RL can be obtained in nematic liquid crystals (NLC) by doping them with a pump-resonant active dye, as demonstrated in various systems [9, 22]. The director distribution in NLC can be adjusted by the application of electric fields [15], making them excellent candidates for the tuning of random lasers.

Another important property of NLC is their nonlinear optical response, with a dominant contribution from molecular reorientation through the torque provided by the electric field of light on the dipoles induced in the elongated molecules. When all-optical reorientation is produced by a finite size beam, the corresponding increase in refractive index for extraordinarily polarized waves leads to self-focusing and eventually self-confinement, with the propagation of an optical spatial soliton and the formation of a light-induced waveguide [23]. Spatial solitons and their control in nematic liquid crystals ("nematicons") have been extensively reported in the past two decades [23–31]; they form when a finite beam produces a graded director distribution and refractive index profile with self-focusing balancing out linear diffraction [23]. Such light-induced waveguides can confine co-polarized signals at other wavelengths [27], as well as light emitted through fluorescence or spontaneous emission [31–33]; moreover, distinct regimes allow for the effective synergy of diverse nonlinear responses in NLC and their mutual control in the presence of solitons [34–36]. In this work we control the RL emission of a planar dye-doped NLC sample exploiting all-optical reorientation to launch a soliton at a wavelength well removed from the guest-host absorption resonance. We demonstrate that, in analogy to other guiding geometries [37], the light-induced waveguide associated to a soliton can confine the emitted photons in the extraordinary polarization [33, 38], enhancing the overall lasing efficiency. This approach to random lasing, combining a resonant light-matter interaction between the pump and the guest-host with a non-resonant one supporting beam self-confinement via reorientation, can be exploited for a novel generation of controllable cavity-less lasers.

## 2. Experimental setup and sample characterization

The sample we used in the experiments, sketched in Fig. 1(a) and similar to that previously used, e.g., in [24,33,38], consists of two parallel glass slides separated by Mylar spacers, surface treated with polyimide to favor the NLC alignment at  $\theta = \angle \mathbf{n}\hat{z} = \pi/4$ , thus maximizing the birefringent walkoff of the equivalent uniaxial and the nonlinearity experienced by an extraordinary  $e^-$  beam propagating with  $\mathbf{k}$  parallel to  $\hat{z}$  [30]. Two other thinner glass interfaces perpendicular to  $z$  seal the cell and provide anchoring with  $\mathbf{n}$  parallel to  $y$  in order to optimize the coupling of radiation (input laser beam) into the extraordinary wave [24]. The cell is infiltrated by capillarity with a mixture of the commercial E7 NLC with a 0.3wt% of Pyrromethene dye (PM597). The latter dye is based on the fluoroboration of two pyrrole rings linked by a conjugated  $\pi$ -system chain, yielding the dipyrromethene-BF<sub>2</sub> complexes also known as cyclic cyanine dyes; it has a fluorescence quantum yield approaching unity and can lase more efficiently than other

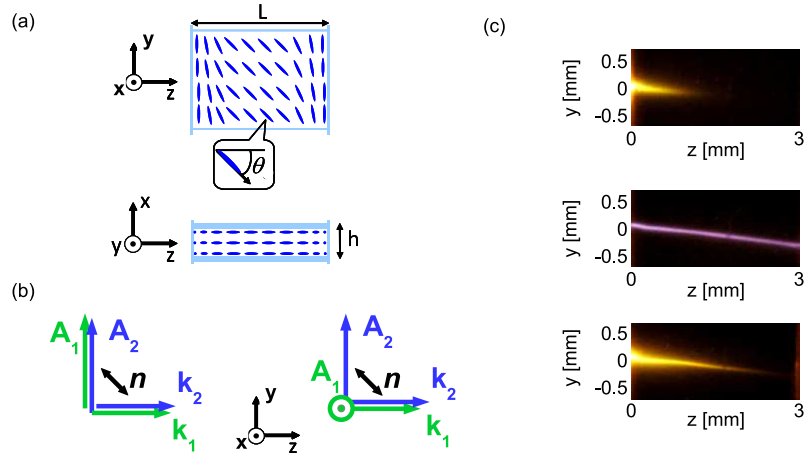


Fig. 1. (a) Sketch of the planar NLC sample. (b) Launch geometries in the principal plane  $yz$ , with  $A_1$  and  $A_2$  the amplitudes of the visible pump beam and the near-infrared solitary beam, respectively. (c) Acquired photographs of fluorescence emitted  $e$ -wave photons without nematicon (top), near-infrared nematicon (center), emitted  $e$ -wave light in the presence of a co-polarized nematicon (bottom). The near-infrared was filtered out in the last case.

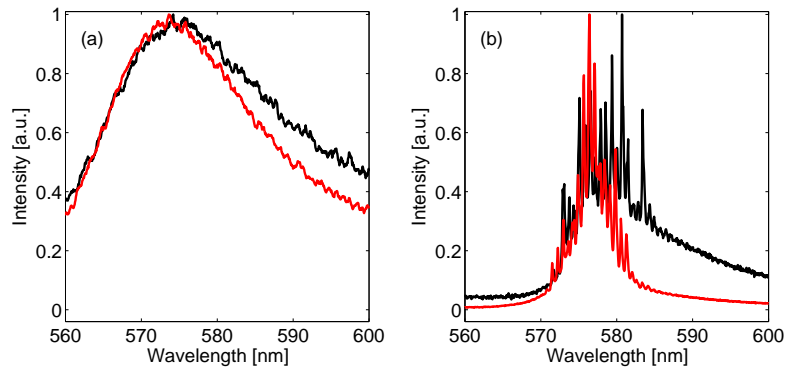


Fig. 2. (a) Typical example of normalized emission spectra below lasing threshold, without (black line) and with (red line) a collinear 3mW nematicon. (b) Same as in (a) but above threshold, for an input pump beam polarized along  $x$  and energy  $E = 1 \mu\text{J}$ .

common dyes such as rhodamine, also because of the low T-T absorption capacity over the lasing spectrum [9, 39]. A similar mixture, with absorption peaked around 530nm, has been demonstrated to random lase in various configurations (wedge cells, drops, capillaries) and allow for temperature tuning [9, 22, 40]. It has been proven that the optically-induced molecular reorientation for wavelengths out of the dye absorption band is not affected by such a low concentration of fluorescent guest molecules in the nematic host [41]. Thus, PM597-E7 is an excellent guest-host system to investigate the interplay between the pumping beam and the reorienting beam for conveying all-optically controlled random laser emission.

We employed two laser beams of different intensities and wavelengths to independently excite the two nonlinear mechanisms, namely fluorescence/lasing and reorientation, focusing them at the cell entrance through a microscope objective and additional optics to obtain comparable waists  $w_0 \approx 4\mu\text{m}$  at the input facet. A microscope imaged the out-of-plane scattered light into a CCD camera, allowing for the acquisition of beam evolution in the principal propagation plane  $yz$ . At the output, a spectrometer equipped with a  $100\mu\text{m}$ -core multimode fiber and a  $100\mu\text{m}$  slit collected the emitted light and acquired the spectra. A continuous-wave near-infrared (NIR)  $y$ -polarized Gaussian beam at  $\lambda = 1.064\mu\text{m}$  was launched in the cell to excite a nematicon at powers  $P > 2\text{mW}$ , propagating with a transverse angular velocity (walkoff)  $\delta = \arctan[\epsilon_a \sin 2\theta / (\epsilon_a + 2n_{\perp}^2 + \epsilon_a \cos 2\theta)]$  with respect to the wavevector ( $\mathbf{k}$  parallel to  $\hat{z}$ ) [24], according to the initial director alignment, with  $\epsilon_a = n_{\parallel}^2 - n_{\perp}^2 > 0$  the optical anisotropy ( $n_{\parallel}$  and  $n_{\perp}$  being the refractive indices for fields parallel and orthogonal to the optic axis, respectively). We generated fluorescence and RL emission with a frequency-doubled Q-switched 6ns-pulse Nd:YAG source at wavelength 532nm and 20Hz repetition rate.

The spectra obtained by pumping the material (in the absence of a NIR nematicon) with either  $\mathbf{k}$  along  $\hat{x}$  (transverse geometry) or  $\mathbf{k}$  parallel to  $\hat{z}$  in the  $yz$  plane (principal plane of the NIR beam) exhibited RL emission peaked around 576nm, non-collinear to the pump beam owing to the optical anisotropy and to the randomness of the resonant feedback [9, 15]. Since material anisotropy affects both the lasing efficiency and the emission polarization [15, 42], the emitted light was an  $e$ -wave in the plane  $\mathbf{n}\hat{z} \equiv \hat{y}\hat{z}$  despite the pump polarization, whereas the emission efficiency was maximum for a pump  $x$ -polarized perpendicular to the director, as previously reported in [38] but at variance with [9]. This polarization dependence suggests that the combined action of the two beams can yield efficient RL for an ordinary-wave ( $o$ -) pump collinear with the  $e$ -wave soliton (Fig. 1(b), right), allowing the latter to confine the emitted light in the waveguide region if a suitable input tilt compensates for the limited beam overlap due to the angular walkoff of the soliton. The alternative configuration, an  $e$ -pump collinear with and confined by the  $e$ -soliton (Fig. 1(b),left), would maximize the overlap of pump and fluorescence in the nematicon region, but at the expenses of the resulting emission. Figure 1(c) shows the acquired pictures of (top) the emitted (green-yellow) photons, (middle) the NIR beam featuring self-confinement and (bottom) the emitted ( $y$ -polarized) photons guided by the nematicon waveguide.

### 3. Results and discussion

As described above, we co-launched two co-planar beams sharing one and the same direction of their Poynting vectors in the medium, an ordinary ( $o$ -) polarized pump (visible) and an  $e$ -wave nematicon (NIR), adjusting their waists and tilt in order to maximize the overlap between the emitted fluorescent light and the green pump within the graded-index waveguide formed by the NIR soliton. As we demonstrated earlier [38], light-induced reorientation alters the scattering paths of the emission and limits diffraction, beneficially affecting the random lasing characteristics. Typical emission spectra of the emitted light (single realizations) below and above lasing threshold are shown in Fig. 2 with and without the presence of a NIR nematicon

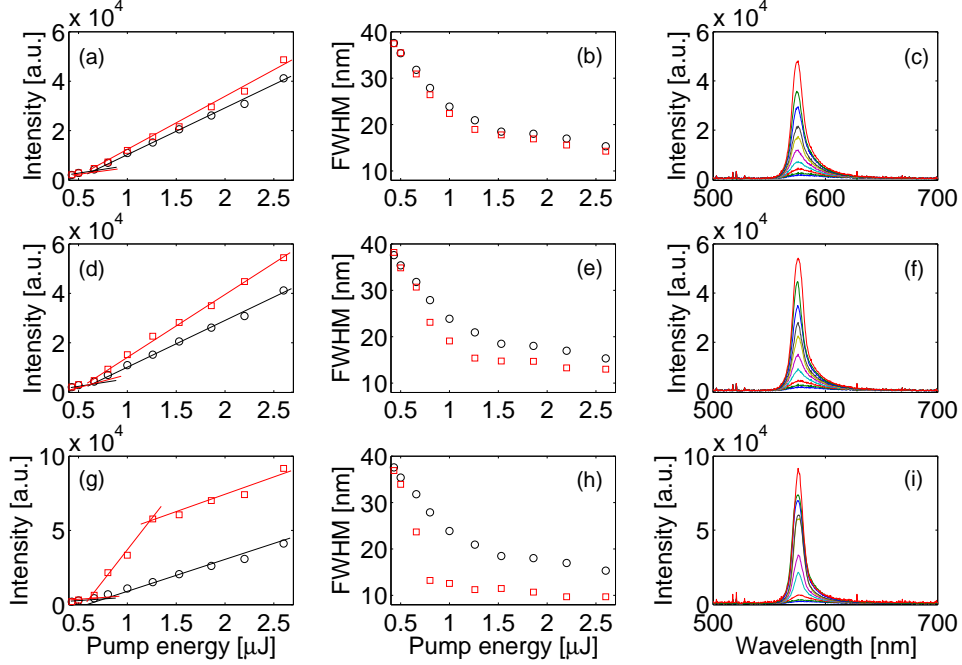


Fig. 3. (a)-(d)-(g) Input/output random lasing characteristics and (b)-(e)-(h) emission spectrum full-widths at half-maximum (FWHM) versus pump energy/pulse; (c)-(f)-(i) Emission spectra versus wavelength at the used pump energies. (a-c) Results for the interaction between RL and a  $P_{NIR} = 2mW$  nematicon (red symbols and line) compared to the case without nematicon (black symbols and line): the soliton waveguide marginally affects RL emission. (d-f) Same as (a-c), but for  $P_{NIR} = 6mW$ : the NIR-induced confinement enhances RL, with a higher gain accompanied by spectral narrowing. (g-i) Same as (a-c), for  $P_{NIR} = 14mW$ : the spectra further narrow down and a kink appears in the input/output characteristic (g). Narrower profiles in (c)-(f)-(i) correspond to increasing pump energies.

collinear with the  $o$ -pump beam. To gain a better insight on the phenomenon, we acquired the input/output characteristics as well as the output spectra of the generated radiation as we varied both the pump pulse energy and the soliton power, as shown in Fig. 3 after averaging over numerous ( $> 60$ ) pulse realizations and employing a spectrometer with limited resolution ( $\approx nm$ ) in order to present and compare smooth (realization-independent) profiles. As a result, Fig. 3 the FWHM values are overestimated.

For  $P_{NIR} = 2mW$  nonlinear reorientation gives rise to an NIR spatial soliton but contributes negligibly to the overall RL performance, as apparent in Figs. 3(a)–(c): the RL spectra without (not shown) and with the nematicon exhibit marginal differences. Things change when the soliton power increases as, e.g., for  $P_{NIR} = 6mW$  (Figs. 3(d)–(f)): soliton induced reorientation features a higher RL efficiency and lowers the  $\beta$ -factor (Fig. 3(d)), with a moderate narrowing of the emission spectra as compared to the bulk case without nematicon (Figs. 3(e)–(f)).

Further increases in soliton power allow to access a the RL regime illustrated, e.g., in Fig. 3(g): for  $P_{NIR} = 14mW$  the input/output curve above threshold initially exhibits a higher gain, later followed by a reduced slope at energies above  $E_k \approx 1.25\mu J$  where a "kink" appears. Consistently with similar effects observed in other random lasing systems [43, 44], this behavior can be attributed to the interaction/competition of several lasing modes in the large interaction volume



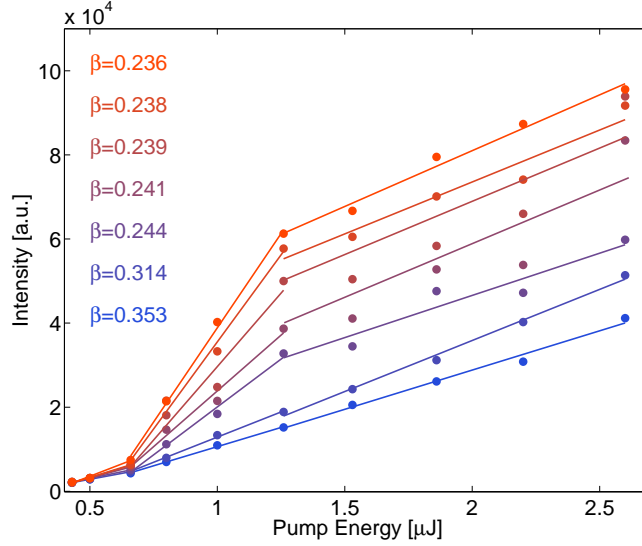


Fig. 4. Input/output random laser characteristics for various soliton powers, with the corresponding  $\beta$ -factors calculated at  $E = 1\mu\text{J}$  and indicated in the legend. Neither the energy threshold nor the kink location change with nematocion power. From bottom to top the curves correspond to  $P_{NIR} = 0, 2, 6, 10, 12, 14, 16, 18\text{mW}$ , respectively.

defined by the cell length  $L$ , with a resulting saturation of the laser gain.

Figure 4 collates RL input/output curves versus pump energy for various NIR soliton powers, up to  $P_{NIR} = 18\text{mW}$ ; at powers of  $18\text{mW}$  and higher, nematocions tend to become less stable and exhibit trajectory fluctuations in the transverse plane. It is apparent that, although soliton-driven reorientation does not affect the RL threshold energy  $E_{th} \approx 0.7\mu\text{J}$ , the transition to lasing gets sharper and the slope of the laser intensity versus pump energy/pulse initially increases with  $P_{NIR}$ . The corresponding enhancement factors  $\beta$ , calculated from the emission spectra before (fluorescence) and after (RL) threshold at a pump energy  $E = 1\mu\text{J}$  according to [45], are indicated in the legend for various nematocion powers. Surprisingly, the kink remains approximately positioned at  $E_k \approx 1.25\mu\text{J}$  and it only appears in the presence of the nematocion, which is likely to trigger a more efficient mode selection. A quantitative estimate of the interaction between the emitted photons and the pump, various scattering paths and their modulation by soliton reorientation, are beyond the scopes of this paper and will be discussed in future work together with a suitable model.

Figure 5 illustrates the role of nematocions on random lasing, graphing RL spectra for various nematocion powers, as well as the corresponding FWHM and the peak emitted intensities (as acquired by the spectrometer). At a pump energy  $E \approx 0.66\mu\text{J}$  (Figs. 5(a)–(b)), below lasing threshold, the presence of a soliton collinear with the pump does not produce dramatic changes, with a moderate enhancement  $G = \frac{I_{P_{Max}}}{I_{P=0}} \approx 2$  due to improved photon collection and a spectral narrowing  $S_n = \left| \frac{(FWHM_{P_{Max}} - FWHM_{P=0})}{FWHM_{P=0}} \right| > 0.25$ , as visible in Fig. 5(b). At energy  $E \approx 1.0\mu\text{J}$  (Figs. 5(c)–(d)), just above RL threshold, the gain enhancement is  $G \approx 5$  with narrowing  $S_n \approx 0.62$ , i.e., FWHM dropping from  $24$  to  $9\text{nm}$ . Finally, at energy  $E = 1.53\mu\text{J}$  above  $E_k$  (Figs. 5(e)–(f)),  $G \approx 8$  with  $S_n \approx 0.55$ .

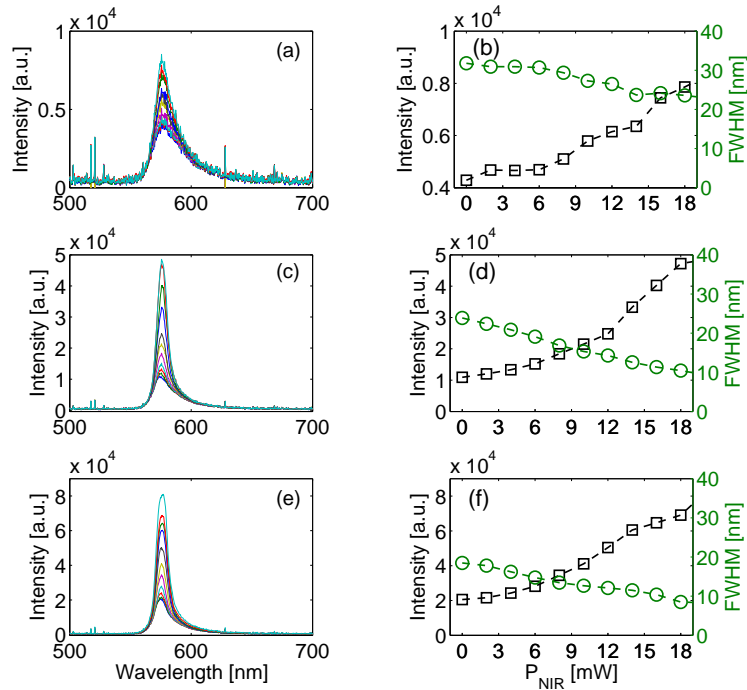


Fig. 5. Soliton assisted RL enhancement. (a) Emission spectra for nematicon powers from  $P_{NIR} = 0\text{mW}$  (broadest) to  $P_{NIR} = 18\text{mW}$  (narrowest) and (b) corresponding FWHM (circles) and peak emission intensity (squares) versus soliton power  $P_{NIR}$ , for a pump energy  $E = 0.66\mu\text{J}$  below threshold. (c-d) As in (a-b) but for  $E = 1\mu\text{J}$ , above threshold. (e-f) As in (a-b) or  $E = 1.53\mu\text{J}$ , above the kink in Fig. 4.

#### 4. Conclusions

We experimentally investigated the interaction between two nonlinear effects occurring in dye-doped nematic liquid crystals, namely random lasing in scattering media and beam self-confinement via a Kerr-like all-optical response. We demonstrated that an optical spatial soliton is able to modify the lasing properties of the strongly scattering random medium, altering the scattering paths and the resulting feedback available in the interaction volume. RL emission is assisted and enhanced by solitons through both light guiding and scattering modulation, resulting in gain enhancement, spectral narrowing and reduction in  $\beta$ -factor, mode selection and, eventually, kinks in the input/output characteristic. This report introduces a guest-host system where a passive nonlinear response (beam self-focusing and self-trapping) acts in synergy with an active mechanism (optical gain and laser action) to yield all-optical control of random lasing in the presence of strong disorder. Among the several advantages illustrated above with these preliminary data, we pinpoint light-controlled emission using beams of different wavelengths and intensities, an extended interaction volume with a large number of lasing modes, power-controlled gain enhancement as well as spectral narrowing. Such features are promising towards the implementation of nonlinearly adjusted light sources and processors.

**Funding**

Suomen Academy, Finland Distinguished Professor (282858); European Union (EU) COST action IC1208.

**Acknowledgments**

We thank S. Bolis for useful discussions and Dr. R. Barboza for precious suggestions and invaluable help with the experiments. S.P., A.P. and G.A. acknowledge the Academy of Finland for support through the FiDiPro grant no. 282858.

III

**BEAMING RANDOM LASERS WITH SOLITON CONTROL**

by

Sreekanth Perumbilavil, Armando Piccardi, Raouf Barboza, Oleksandr Buchnev, Martti Kauranen, Giuseppe Strangi and Gaetano Assanto, October 2018

Nature Communications vol. 9, no. 3863, pp. 1-6

© 2018 Nature Publishing Group

Reproduced with permission.





ARTICLE

DOI: 10.1038/s41467-018-06170-9

OPEN

# Beaming random lasers with soliton control

Sreekanth Perumbilavil<sup>1</sup>, Armando Piccardi<sup>2</sup>, Raouf Barboza<sup>1</sup>, Oleksandr Buchnev<sup>3</sup>, Martti Kauranen <sup>1</sup>, Giuseppe Strangi<sup>4,5</sup> & Gaetano Assanto <sup>1,2,6</sup>

Random lasers are resonator-less light sources where feedback stems from recurrent scattering at the expense of spatial profile and directionality. Suitably-doped nematic liquid crystals can random lase when optically pumped near resonance(s); moreover, through molecular reorientation within the transparency region, they support self-guided optical spatial solitons, i.e., light-induced waveguides. Here, we synergistically combine solitons and collinear pumping in weakly scattering dye-doped nematic liquid crystals, whereby random lasing and self-confinement concur to beaming the emission, with several improved features: all-optical switching driven by a low-power input, laser directionality and smooth output profile with high-conversion efficiency, externally controlled angular steering. Such effects make soliton-assisted random lasers an outstanding route towards application-oriented random lasers.

<sup>1</sup>Laboratory of Photonics, Tampere University of Technology, FI-33101 Tampere, Finland. <sup>2</sup>NooEL—Nonlinear Optics and OptoElectronics Lab, University “Roma Tre”, IT-00146 Rome, Italy. <sup>3</sup>Optoelectronics Research Centre, University of Southampton, SO17 1BJ Southampton, UK. <sup>4</sup>Department of Physics, Case Western Reserve University, Cleveland, OH 44106-7079, USA. <sup>5</sup>CNR-NANOTEC & University of Calabria, 87036 Rende, Italy. <sup>6</sup>CNR-ISC, IT-00185 Rome, Italy. Correspondence and requests for materials should be addressed to G.A. (email: [gaetano.assanto@uniroma3.it](mailto:gaetano.assanto@uniroma3.it))

Random lasers (RL) are cavityless light sources<sup>1</sup>, versatile in geometry, wavelength, and potential applications ranging from imaging to cancer diagnostics<sup>2–4</sup>, but such advantages are accompanied by poor spatial characteristics of the emitted light<sup>5</sup>. The quest for output directionality and improved profile<sup>6</sup> was previously addressed using, e.g., fibers<sup>7,8</sup>, microchannels<sup>9</sup>, tailored pump<sup>10</sup>, and nanostructures<sup>11</sup>.

Weakly scattering nematic liquid crystals (NLC) with organic dopants were used earlier for RL in thin cells, capillaries and free-standing films, exploiting thermal and electro-optic responses to adjust the emission wavelength and the efficiency<sup>12–21</sup>. NLC consist of elongated molecules with orientational order along the molecular director (optic-axis)  $\mathbf{n}$ . Its thermal dynamics, through fluctuations in the local dielectric tensor, cause anisotropic light scattering<sup>22</sup>, which can yield weak light-localization and feedback for lasing in the presence of optical amplification. Common NLC also exhibit birefringence and a large reorientational optical nonlinearity<sup>23</sup>, which supports self-guided beams—nematicons—of linearly polarized light at mW-powers and over mm-propagation distances<sup>24</sup>. Owing to the nonlocal response of such soft-matter, nematicons are stable three-dimensional optical solitons<sup>25</sup>; in uniaxial NLC they are extraordinary waves—which walk-off with the Poynting vector at a few degrees with the wave-vector (Methods)<sup>26</sup>—and operate as light-induced graded-index channels for co-polarized signals of arbitrary wavelengths<sup>24</sup>.

Hereby, we demonstrate that in dye-doped liquid crystals a suitable combination of passive nonlinear optics—namely near-infrared nematicons through self-focusing- and light-matter interaction—namely lasing in random media with optical pumping—can resolve a few crucial issues of RL. The investigated soliton-enhanced random laser is highly efficient and exhibits a smooth and directional emission, with output angle controlled by external stimuli such as voltage; it can also be turned off/on by a

low-power near-infrared input. These novel features can potentially boost the impact of soft-matter RL on photonics as well as other areas where cavityless/tunable lasers are potentially relevant, including cancer therapy, sensing, and speckle-free imaging.

## Results

**Nematicon-assisted random laser in liquid crystals.** We used the NLC host E7 with 0.3 wt% pyromethene 597 (guest dye) in planar cells to obtain random lasing in the initial (input) region of a near-infrared nematicon. Figure 1a, b shows the sample geometry and experimental setup. To generate a soliton in a 100  $\mu\text{m}$ -thick 2 mm-long planar cell containing the dye-doped NLC, a continuous-wave (cw) beam at 1.064  $\mu\text{m}$  was launched along  $z$  with electric field linearly polarized in the principal plane  $yz$ ;  $\mathbf{n}$  was aligned in the same plane at 45° with respect to  $z$  as to maximize the optical nonlinearity (i.e., reduce the power supporting the formation of nematicons)<sup>24,27</sup>. To pump the guest–host medium, an ordinary wave (with electric field  $\parallel x$ ) 6 ns-pulse beam at wavelength 532 nm was co-injected along  $z$ . In this configuration with molecular orientation defined by boundary conditions at the interfaces (see Methods), a pump beam with linear polarization orthogonal to  $\mathbf{n}$  yielded the highest conversion rate to fluorescence and forward RL emission<sup>28</sup>. Pump pulse-duration, repetition-rate (20 Hz) and energy prevented significant reorientational and/or thermal nonlinear effects. Green and NIR beams were focused in the same position with comparable waists of 3  $\mu\text{m}$ , i.e., a power density of 35.4  $\mu\text{W}/\mu\text{m}^2$  per 1 mW cw NIR input and a power density of 5.9  $\text{W}/\mu\text{m}^2$  per 1  $\mu\text{J}$  green input pulse. The resulting fluorescence and stimulated emission in the visible spectrum (around 580 nm) were co-polarized with—and therefore confined by—the nematicon. Owing to birefringent walk-off, the nematicon propagated in  $yz$  at an angle of about 7° off  $z$ , see Fig. 1f. The soliton was not only able to collect and guide

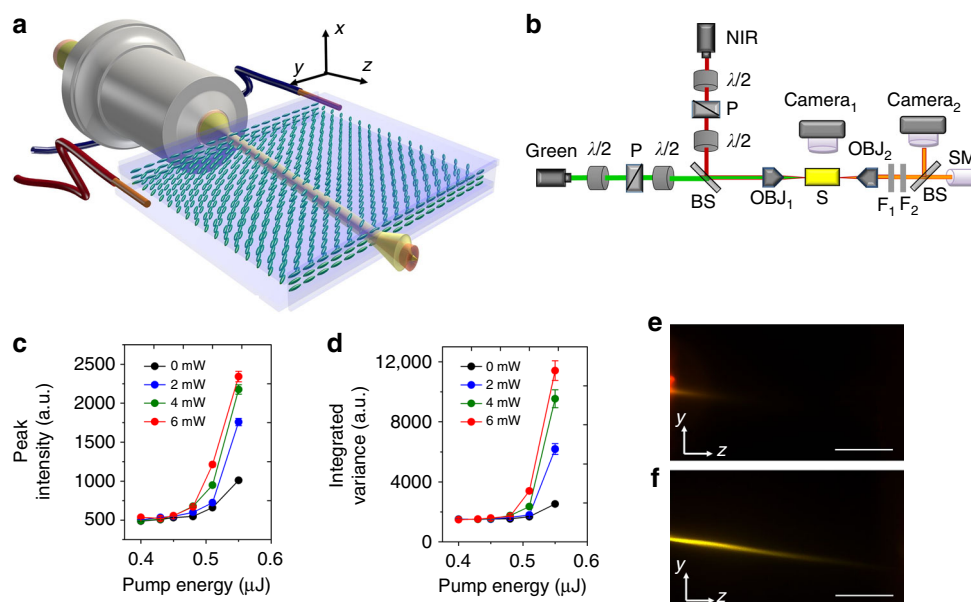


**Fig. 1** Configuration and basic features of nematicon-assisted random laser. **a** Planar cell configuration and orientation. Here, the two wires allude to the application of a bias voltage across the cell thickness (see Methods). The molecular director distribution  $\mathbf{n}$  (optic-axis) is represented by blue ellipses. **b** Sketch of the basic experimental setup, with green pulsed pump and continuous-wave near-infrared (NIR) lasers, microscope objectives (OBJ) to inject and collect light, beam splitters (BS), polarisers (P), waveplates ( $\lambda/2$ ), notch filters ( $F_1$  and  $F_2$ ), spectrometer (SM). **c** Typical input–output random laser characteristics for various soliton powers and an ordinary-wave pump, from the mean peak intensity. The legend indicates the input power of the near-infrared nematicon. **d** As in **c** but from the integrated variance  $\sigma_I^2$  of the averaged spectra (see Eq. (9) in the Methods) over 200 gated acquisitions (in 100 ms windows), carrying out the analysis detailed in the Methods. The error bars in **c** and **d** correspond to standard deviation over 200 acquisitions. **e** Photograph of emitted random laser light in the  $yz$  plane for a pump energy  $E = 0.55 \mu\text{J}$ , without nematicon. **f** As in **e** but in the presence of a 6 mW nematicon (the near-infrared was filtered out). The scale bars indicate a length of 500  $\mu\text{m}$

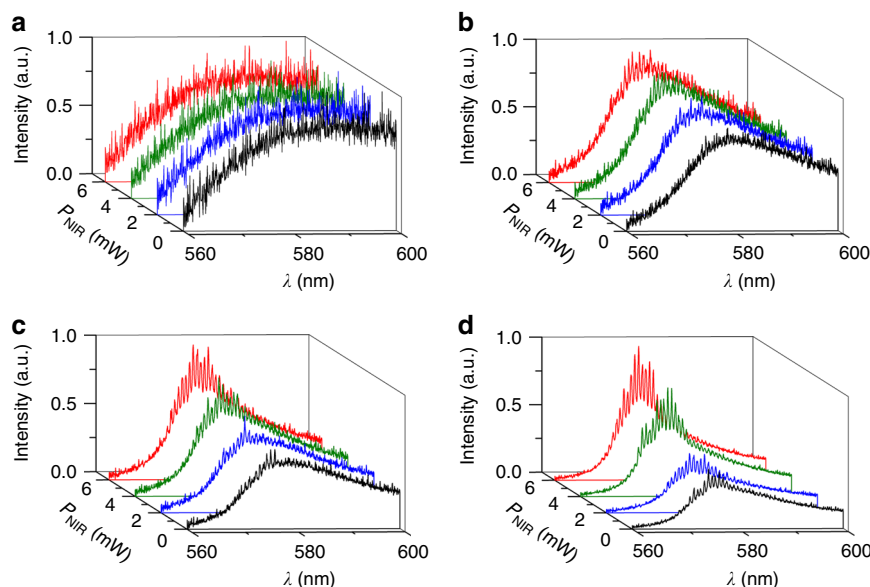


**Fig. 2** Emission spectra in the presence of nematicon. Spectral emission normalized to unity for nematicons of various powers (colors) co-launched with the ordinary-wave pump, averaged over 200 gated acquisitions. **a** Pump pulse energy  $E = 0.40 \mu\text{J}$ . **b**  $E = 0.48 \mu\text{J}$ . **c**  $E = 0.51 \mu\text{J}$ . **d**  $E = 0.55 \mu\text{J}$

fluorescence and stimulated emission due to pumping within the guest–host absorption spectrum, but also to affect the evolution of lasing modes in the longitudinally extended volume<sup>5</sup>, enhancing both RL directionality and profile. While some preliminary results on RL slope efficiency and spectral narrowing were reported earlier<sup>28,29</sup>, some salient basic features of soliton-aided RL are presented in Fig. 1c–f with reference to samples investigated hereby.

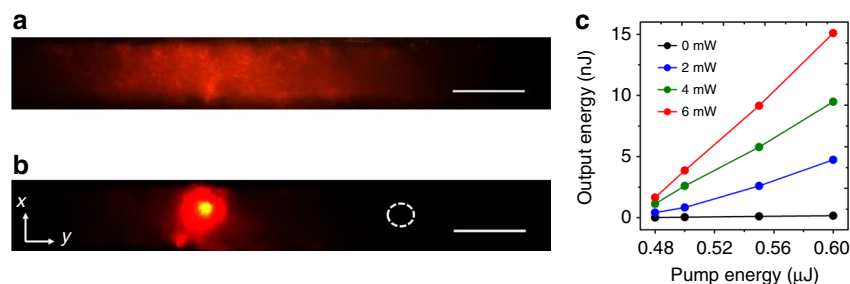
Due to randomness of the system and the substantial pedestal provided by fluorescence and amplified spontaneous emission (ASE), the lasing peaks emerged from the latter background, as typical of RLs. We first extracted the maximum intensity counts from each acquired emission spectrum, Fig. 1c, with lasing threshold at energies around  $0.48 \mu\text{J}$  and slope efficiency clearly improved by nematicons. Such threshold could not be retrieved when calculating the average intensity ( $\bar{I}$ , Methods) integrated versus wavelength over several gated spectral acquisitions (Supplementary Figure 3). Hence, we resorted to the statistical analysis of the intensity variance  $\sigma_I^2$  (sensitive to fluctuations), as summarized in the Methods. This approach yielded the in-out curves Fig. 1d, where a threshold can be readily appreciated and matches the one in Fig. 1c.

Figure 2 displays the emitted spectra averaged over several gated acquisitions and collected at the output (after propagation along  $z$ ) with/without nematicons of various powers co-launched with the pump below/above RL threshold. This illustrates the transition from fluorescence to ASE to random lasing: the effect of the nematicon is negligible at low energies, as the waveguide simply increases the collected fluorescence or ASE<sup>30</sup>; its role, however, becomes pronounced at higher pump energies, contributing to narrower multihump spectra and more intense lasing peaks. The transition (vs. energy) from the ASE stochastic spikes to the RL lasing peaks is boosted by the all-optical waveguide, which affects multiple scattering and shrinks the overall spectra in the pumped region near the sample input. As observed in ref.<sup>5</sup> and further reported in ref.<sup>21</sup>, the lasing peaks emerging from various realizations presented random amplitudes, but remained regularly spaced vs. wavelength when averaging over large numbers of pump shots (up to 200 gated measurements in 100 ms windows). Their separation suggests an equivalent cavity  $\approx 130 \mu\text{m}$  long, comparable to the extent of the

conical region where the pump is absorbed, as observed (via out-of-plane light diffusion) from above the cell (Fig. 1e). This appears consistent with weak scattering close to the regime of under-coupling (i.e., a cavity much shorter than the nematicon)<sup>5</sup>, although it was not experimentally ascertained as higher pump energies (needed to lengthen the cavity) induced bleaching and saturation<sup>29</sup>, to be further investigated. The negligible change in frequency spacing versus soliton power pinpoints the role of absorption in limiting the extent of the effective resonator<sup>5</sup>, enabling stimulated emission only in the initial fraction of the pumped volume.

**Spatial profile and efficiency of random laser.** The transversely localized RL spikes within the NIR nematicon tend to evolve along the waveguide, resulting in smoother profiles than the hot-spots commonly observed in thin samples<sup>12,16,17</sup>. Figure 3 shows typical RL output profiles, without/with a co-propagating nematicon. In the first case, RL light yields a diffuse pattern with low intensity; in the second case, instead, the emitted radiation remains essentially confined within the NIR-induced light channel. In essence, the (nonorthogonal) RL modes evolve and walk-off along the extraordinary wave soliton (Fig. 1f), interacting within the all-optical waveguide and roughly resulting in a bell-shape<sup>31</sup>. Conversely, in backward-emission experiments with light collected as it back-propagated out of the bulk toward the input, typical RL profiles were qualitatively different and exhibited several hot-spots (Supplementary Figure 5). Exploiting the achieved beaming of this random laser, in Fig. 3c we present the measured output energy vs. pump input energy above threshold, for various NIR nematicon powers. The measured values, averaged over 200 shots and corrected for Fresnel losses of the pump at the input interface ( $\approx 4\%$ ), Fresnel losses of the emitted light at the output interface ( $\approx 4\%$ ), and at the optical elements ( $\approx 17.6\%$ ) before the detector ( $F_1$ ,  $F_2$ ,  $\text{OBJ}_2$  in Fig. 1b), yield input/output conversion efficiencies as high as 2.62% when pumping at  $0.6 \mu\text{J}$ /pulse and co-launching NIR solitons at 6 mW, a substantial figure when considering the propagation losses over the 2 mm-long sample. Assuming scattering and absorption losses close to  $6.95 \text{ cm}^{-1}$  at visible wavelengths in the host NLC<sup>32</sup>, in the limit of a random laser with soliton propagation within the actively





**Fig. 3** Directional random lasing. Random lasing observed at the output facet of the sample, in the plane  $xy$ , for pump pulses above threshold,  $E = 0.55 \mu\text{J}$ . **a** Emitted light without a co-launched nematicon; **b** emitted light in the presence of 6 mW nematicon (the near-infrared was filtered out). The white dashed circle indicates the position of the input beam, launched with wave-vector parallel to  $z$ . The lateral displacement of the random laser spot is due to soliton walk-off in the plane  $yz$ . The scale bars refer to a length of  $100 \mu\text{m}$ . **c** Output random laser energy versus pump energy/pulse above threshold for various near-infrared nematicon powers. The measured values are averaged over 200 samples and corrected for Fresnel reflection losses due to filters, lens, and cell output facet

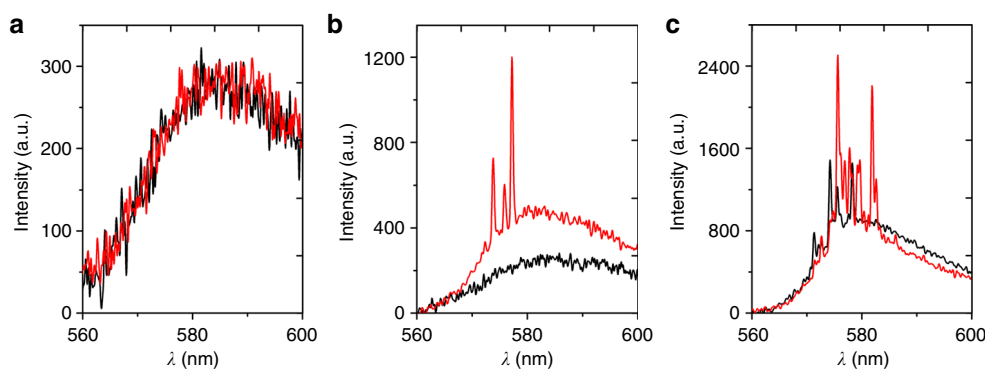


**Fig. 4** Soliton switching of random laser. Emission spectra gated over 100 ms, obtained without (black lines) and with a co-launched 6 mW nematicon (red lines) when the pump energy per pulse (in the absence of near-infrared input) is **a** below threshold ( $E = 0.45 \mu\text{J}$ ), **b** almost at ( $E = 0.48 \mu\text{J}$ ), **c** above threshold ( $E = 0.55 \mu\text{J}$ )

pumped region of  $\approx 130 \mu\text{m}$  (see above), then the extrapolated conversion efficiency reaches a remarkable 9.62%. Such a high figure in organic soft-matter compares well with those measured in Sulforhodamine B with  $\text{TiO}_2$ <sup>33</sup>.

#### Transistor-like operation of nematicon random laser.

Remarkably, in nematicon-assisted RL we could all-optically increase photon collection as well as pump-matter interaction and bring the system above threshold, turning-on the laser with continuous-wave NIR. Figure 4 shows 100 ms-gated emission spectra collected for pump energies well-below, almost at and above threshold in the presence of (red lines) or without (black lines) a 6 mW NIR nematicon, respectively. When injecting the latter in the system below threshold, no appreciable changes could be observed in the spontaneous emission (Fig. 4a); above threshold (Fig. 4c) the nematicon induced spectral shift and narrowing, with the appearance of more numerous and intense lasing peaks; almost at threshold (Fig. 4b) the soliton switched-on the RL, demonstrating a remarkable means to modulate the RL operation by a low-power nonresonant input and so realize a random transistor-laser (see also Supplementary Figure 4). Noteworthy, this all-optical switching does not rely on absorption and photothermal response<sup>19</sup>, but only on the linearly polarized NIR beam able to launch reorientational solitons.

**Angular steering of the random laser emission.** Nematicons are light-induced waveguides whose trajectories can be deviated by

external stimuli acting on the director distribution<sup>24</sup>. This allows steering the directional RL emission at will and beaming it to various output destinations. To demonstrate this in a simple case, we used thin film electrodes to apply a voltage across the cell thickness  $x$  in order to alter the principal plane  $yz$  of soliton propagation and its observable walk-off<sup>26</sup>. Figure 5a, b compares the RL emitted streaks along the observation plane  $yz$  for  $V = 0 \text{ V}$  (Fig. 5a) and  $V = 2 \text{ V}$  (Fig. 5b), respectively, when pumping above threshold. As  $V$  increases, the director realigns toward  $x$  and the nematicon changes direction and moves toward an ordinary-wave configuration with Poynting vector  $\mathbf{S}/k//z$ , with a vanishing walk-off (Supplementary Figure 2). Although the vector  $\mathbf{S}$  evolves on the surface of a cone (with axis in  $yz$  and apex angle defined by the initial walk-off, see Methods and Supplementary Figure 2), the RL streak gets steered from  $7^\circ$  to nearly  $0^\circ$ , as graphed in Fig. 5f, with an overall  $y$ -displacement of about  $245 \mu\text{m}$  at the output. The photographs in Fig. 5c, d show the RL output profile for  $V = 0$  (Fig. 5c) and  $V = 2 \text{ V}$  (Fig. 5d), respectively. The RL light diffusing out of the soliton at high voltage is attributed to the interplay of electro-optic reorientation and scattering at the cell entrance where boundaries play a stronger role; moreover, as the fixed-power nematicon evolves versus voltage towards an ordinary-wave configuration ( $\mathbf{S}/k$ ), it becomes progressively less confined/confining as the associated waveguide has a lower index contrast. Correspondingly, the emitted RL spectra exhibit lower peak intensities, as apparent in Fig. 5e. Despite the fact that the angular steering was not optimized for in-plane re-addressing, these results demonstrate a directional RL emission, with pointing

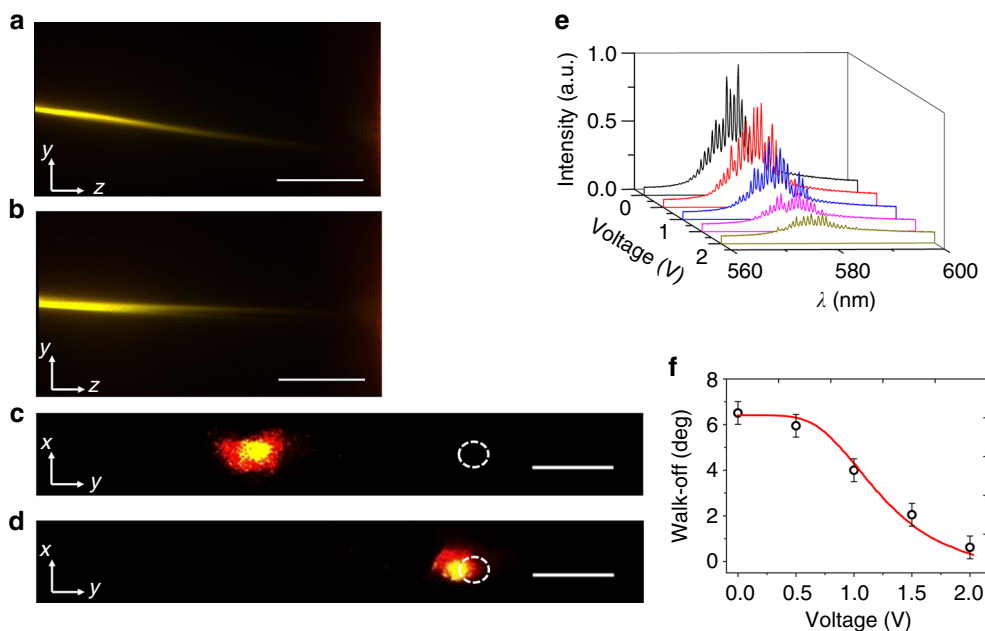


**Fig. 5** Controlled steering of soliton-assisted random laser emission. **a** Random lasing within a 5 mW near-infrared soliton, with walk-off at  $7^\circ$  in the plane  $yz$  in the absence of voltage bias. **b** Random lasing within a 5 mW near-infrared soliton, with vanishing walk-off at a bias  $V = 2$  V. The scale bars in **a** and **b** indicate a length of 500  $\mu\text{m}$ . **c** Output random laser spot in  $xy$  for  $V = 0$  V, corresponding to **a**. **d** Output random laser spot in  $xy$  for  $V = 2$  V, corresponding to **b**; the white dashed circles in **c** and **d** indicate the direction of the input wave-vector, the scale bars correspond to 100  $\mu\text{m}$ . **e** Random laser emission spectra acquired at the 5 mW nematociton output for various applied voltages. **f** Measured (symbols with error bars, s.d.) and calculated (solid line) walk-off versus applied voltage (see Eq. (5) in the Methods). The error bars (in s.d. units) are computed over 25 acquisitions and the pump energy per pulse is well above threshold

control adjusted by external stimuli such as voltage. Effective RL beaming can also be achieved by adopting alternative strategies to modify the nematociton trajectory within the principal plane  $yz$  of propagation. These include inter-digitated electrodes on the planar interfaces<sup>34</sup>, external light beams altering the director distribution<sup>24</sup>, magnetic fields<sup>35</sup>. The latter approach, in particular, allows doubling the overall angular swing by rotating the magnetic field in  $yz$  around  $x$ .

## Discussion

We have designed, investigated, and reported a random laser in light-sculpted dye-doped NLC, whereby the synergy of the non-resonant reorientational nonlinear response with optical gain and weak scattering enables cavityless soliton-enhanced laser emission. Besides the high-conversion efficiency and spectral narrowing, this soft-matter laser system entails all-optical low-power switching, emission directionality with smooth profile and pointing control by external stimuli, thereby introducing soliton-adjustable NIR-controlled RL.

These results demonstrate the benefits of suitably combining diverse nonlinear optical responses; they also solve some RL vexing issues, specifically poor directionality and profile. We foresee this synergistic route to impact on practical resonator-less lasers in disordered weakly scattering soft-media.

## Methods

**Samples.** Planar glass cells, 100  $\mu\text{m}$  thick ( $x$ ) 30 mm wide ( $y$ ) and 2 mm long ( $z$ ), were prepared with Borosilicate glass slides equipped with Indium Tin Oxide (ITO) thin film electrodes; the slides were subsequently spin-coated with polyimide and mechanically rubbed to ensure planar anchoring of the molecular director in the plane  $yz$  at  $45^\circ$  with respect to  $z$ , with a slight pretilt  $\leq 2^\circ$  to prevent the insurgence of the Freedericksz transition threshold and its angular degeneracy<sup>36</sup> vs. applied voltage. Spacers were inserted to define the thickness. Glass microscope cover slides 160  $\mu\text{m}$  thick were glued orthogonally to  $z$  in order to seal the cell and so define input and output facets. These extra interfaces prevented the formation of NLC

menisci and uncontrolled light depolarization; they were also coated with polyimide and rubbed along  $y$  to optimize the coupling of  $y$ -polarized electric fields to extraordinary waves in the NLC<sup>37</sup>. A mixture of commercial E7 (Merck) and 0.3 wt % Pyromethene 597 dye (Exciton) was introduced to fill the cell by capillary action. For the host medium at 1.064  $\mu\text{m}$  the elastic constants for splay and twist deformations are  $K_1 = 11.7$  pN and  $K_3 = 19.5$  pN, respectively; the refractive indices along the principal axes are  $n_{\parallel} = 1.71$  and  $n_{\perp} = 1.52$ .

**Experimental setup.** A frequency-doubled Nd:YAG laser operating in Q-switch at 20 Hz, 532 nm, and 6 ns pulses was the pump source; a NIR continuous-wave laser at 1.064  $\mu\text{m}$  was the spatial optical soliton source. Waveplates, polarisers and a microscope objective were employed to focus and co-launch the orthogonally polarized (green and NIR) beams in the midplane ( $x = 50$   $\mu\text{m}$ ) of the cell, avoiding reflections from upper and lower interfaces. Fluorescence and laser emission, as well as the NIR beam were imaged by NLC light scattering out of the observation plane  $yz$  and also in the transverse plane  $xy$  at the cell output, using optical microscopes and high-resolution CMOS cameras. A fiber-equipped spectrometer (Ocean Optics) was used to collect and spectrally resolve the emitted light, with a resolution of 0.15 nm; a Si-detector allowed measuring the random laser emission. Additional filtering elements were introduced whenever appropriate to eliminate pump and NIR light (see also Fig. 1b). A voltage bias from a 1 kHz generator could be applied across the cell thickness through the ITO electrodes. The AC voltage supply prevented undesired NLC convection and static charge effects.

**Model.** In the reference system  $xyz$  indicated in Fig. 1, the propagation of extraordinary polarized light beams in an anisotropic nonlinear material obeys a nonlinear Schrödinger-like equation:

$$2in_e(\theta_0)k_0 \left[ \frac{\partial A}{\partial z} + \tan \delta(\theta_0) \frac{\partial A}{\partial y} \right] + D_y \frac{\partial^2 A}{\partial y^2} + k_0^2 \Delta n_e^2(\theta_0, \phi) A = 0 \quad (1)$$

where  $A$  is the magnetic field envelope in the slowly varying amplitude approximation,  $k_0$  the vacuum wave number,  $\delta(\theta_0) = \arctan \left[ \frac{\epsilon_a \sin(2\theta_0)}{\epsilon_a + 2\epsilon_{\perp} + \epsilon_a \cos(2\theta_0)} \right]$  the walk-off angle ( $\epsilon_a = n_{\parallel}^2 - n_{\perp}^2$  is the optical anisotropy) at the orientation  $\theta_0$  between  $\mathbf{k}$  and  $\mathbf{n}$  at rest,  $D_y$  the diffraction coefficient along the  $y$  direction (sample width), and  $\Delta n_e(\theta_0, \phi)$  the extraordinary wave refractive index potential well due to the nonlinear reorientation  $\phi$ . The latter reorientation can be evaluated from the Euler-Lagrange equation<sup>23,24,38</sup> modeling the competing contributions of the driving field (light beam in our case) and the restoring elastic forces in the NLC,

resulting in the reorientation equation:

$$\nabla^2 \theta + \frac{\epsilon_0 \epsilon_a Z_0^2}{4K n_e^2(\theta_0) \cos^2 \delta} \sin[2(\theta - \delta)] |A|^2 = 0 \quad (2)$$

where  $\theta = \theta_0 + \phi$ ,  $K$  is the elastic Frank constant in the single elastic constant approximation ( $K \approx K_1 \approx K_3 \approx 12$  pN),  $\epsilon_0$  the vacuum dielectric constant,  $Z_0$  the vacuum impedance. Thus, starting from  $\theta_0$  and the forcing field, Eq. (2) determines the director orientation and the refractive index distribution to be considered in Eq. (1).

Equations (1) and (2) do not have—in general—exact soliton solutions<sup>27,39</sup>, but when integrated numerically with proper boundary conditions, they support reorientational spatial solitons in NLC—nematics—with a nondiffracting transverse profile corresponding to the normal mode of the nonlocal graded-index waveguide described by  $\Delta n_e(\theta_0, \phi)$ <sup>24,40</sup>. An example of the calculated evolution and profile of a near-infrared nematicon with the corresponding graded-index waveguide is provided in Supplementary Figure 1.

The Euler–Lagrange equation for the molecular director<sup>38</sup>, combined with the divergence-free condition for the electric displacement field, allows one to evaluate the voltage-driven elevation angle  $\eta$  of the optic axis  $\mathbf{n}$  from the plane  $yz$  of the cell:

$$\left[ (\epsilon_{\perp}^{\text{LF}} + \Delta\epsilon_{\text{LF}}) \sin^2(\eta) + \epsilon_{\perp}^{\text{LF}} \cos^2(\eta) \right] \frac{d^2 V}{dx^2} + \Delta\epsilon_{\text{LF}} \sin(2\eta) \frac{d\eta}{dx} \frac{dV}{dx} = 0 \quad (3)$$

$$\frac{d^2 \eta}{dx^2} + \frac{\epsilon_0 \Delta\epsilon_{\text{LF}}}{2K} \left( \frac{dV}{dx} \right)^2 \sin(2\eta) = 0 \quad (4)$$

with  $V$  the applied low-frequency (LF) bias,  $\epsilon_{\perp}^{\text{LF}}$  and  $\Delta\epsilon_{\text{LF}}$  the dielectric constant (for electric field perpendicular to the optic-axis) and the dielectric anisotropy, respectively. In this case the integration is performed along the direction  $x$  of the applied electric field and the resulting angular distribution of the molecular director  $\mathbf{n}$  provides the refractive index landscape in which the beam propagates<sup>24,26</sup>.

As the voltage is uniformly applied between the planar parallel (ITO) electrodes, the molecular director  $\mathbf{n}$  is pulled out of the alignment plane  $yz$  toward the vertical axis  $x$ , resulting in a rotation of the principal plane. Note that the injected nematicon remains an extraordinary wave as it adiabatically evolves in polarization through the transition region close to the input interface<sup>41</sup>.

For a given  $\eta(V)$ , the corresponding angle between  $\mathbf{k}$  and  $\mathbf{n}(V)$  becomes  $\psi = \arccos(\cos \eta \cos \theta_0)$ , with the consequent angular steering of the Poynting vector  $\mathbf{S}$  of the NIR soliton (yellow arrow in Supplementary Figure 2) and of the guided random laser emission, as seen in Fig. 5. It is straightforward to derive the projection of the voltage-dependent Poynting vector on the observation plane  $yz$  and compute the solid curve of the observed walk-off:

$$\alpha = \arctan \left( \frac{\tan \delta \cos \eta}{\sqrt{1 + \sin^2 \eta \cot^2 \theta_0}} \right) \quad (5)$$

as plotted in Fig. 5f.

**Statistical analysis of the emission spectra.** Random lasing emission in an extended system exhibits characteristic fluctuations. Specifically, the lasing modes emerge from the fluorescence/ASE background as spectral peaks at certain wavelengths (see, e.g., Fig. 2, Fig. 4, Supplementary Figure 4), where the intensity varies from shot to shot. The onset of lasing is therefore associated to deviations of the intensity from its average at a given wavelength and can be quantified by the corresponding variance<sup>42</sup>.

To analyze the emission properties of the NLC random laser, we calculate the average intensity and the variance over  $N$  output spectra, defined as

$$\bar{I}(\lambda) = \frac{1}{N} \sum_{k=1}^N I_k(\lambda), \quad (6)$$

$$\sigma_I^2(\lambda) = \frac{1}{N-1} \sum_{k=1}^N (I_k(\lambda) - \bar{I}(\lambda))^2, \quad (7)$$

respectively, at a specific wavelength  $\lambda$ . It is important to note that  $\sigma_I^2(\lambda) = 0$  only for a constant spectrum over its recorded values. Sample data of the quantities (6) and (7) above are shown in Supplementary Figure 4 vs. wavelength for various pump energies and nematicon powers.

Furthermore, in order to gain insight on the global operation of the random laser, the average intensity and the variance can be integrated over the spectrometer response window. This approach allows one to study the system behavior over the whole spectral window  $\Delta\lambda = \lambda_{\text{max}} - \lambda_{\text{min}}$ , measuring the integrated average

intensity and integrated variance, respectively, defined as:

$$\bar{I} = \frac{1}{\Delta\lambda} \int_{\lambda_{\text{min}}}^{\lambda_{\text{max}}} \bar{I}(\lambda) d\lambda, \quad (8)$$

$$\sigma_I^2 = \frac{1}{\Delta\lambda} \int_{\lambda_{\text{min}}}^{\lambda_{\text{max}}} \sigma_I^2(\lambda) d\lambda. \quad (9)$$

Since well-defined spikes above the fluorescence/ASE pedestal characterize the transition to lasing threshold, another useful parameter is the mean intensity maximum computed as:

$$\bar{I}_{\text{max}} = \frac{1}{N} \sum_{k=1}^N \max_{\lambda} I_k(\lambda). \quad (10)$$

As random lasing cannot be completely separated from ASE and fluorescence contributions, the integrated average intensity  $\bar{I}$  (plotted in Supplementary Figure 3) does not exhibit a clear threshold even after the laser onset<sup>42</sup>, despite the presence of spikes above a certain pump level (see Fig. 2). The integrated variance Eq. (9), however, is remarkably sensitive to the emergence of spectral features, including fluctuations in the lasing peaks. Hence, it manifests a threshold as it appears in the mean peak intensity  $\bar{I}_{\text{max}}$  (see Fig. 1c, d).

## Data availability

The datasets generated and analyzed during the current study are presented in this published article (and its Supplementary Information) in aggregated form as figures/graphs and are available from the corresponding author upon reasonable request.

Received: 26 April 2018 Accepted: 6 August 2018

Published online: 21 September 2018

## References

- Cao, H. Lasing in random media. *Waves Random Media* **13**, R1–R39 (2003).
- Wiersma, D. S. The physics and applications of random lasers. *Nat. Phys.* **4**, 359–367 (2008).
- Redding, B., Choma, M. A. & Cao, H. Speckle-free laser imaging using random laser illumination. *Nat. Photon.* **6**, 355–359 (2012).
- Polson, R. C. & Varden, Z. V. Random lasing in human tissues. *Appl. Phys. Lett.* **85**, 1289–1291 (2004).
- Wu, X. et al. Random lasing in weakly scattering systems. *Phys. Rev. A* **74**, 053812 (2006).
- Wiersma, D. S. Clear directions for random lasers. *Nature* **539**, 360–361 (2016).
- de Matos, C. J. S. et al. Random fiber laser. *Phys. Rev. Lett.* **99**, 153903 (2007).
- Abaie, B. et al. Random lasing in an Anderson localizing optical fiber. *Light Sci. Appl.* **6**, e17041 (2017).
- Jorge, K. C. et al. Directional random laser source consisting of a HC-ARROW reservoir connected to channels for spectroscopic analysis in microfluidic devices. *Appl. Opt.* **55**, 5393–5398 (2016).
- Leonetti, M., Conti, C. & Lopez, C. Random laser tailored by directional stimulated emission. *Phys. Rev. A* **85**, 043841 (2012).
- Schönhuber, S. et al. Random lasers for broadband directional emission. *Optica* **3**, 1035–1038 (2016).
- Strangi, G. et al. Random lasing and weak localization of light in dye-doped nematic liquid crystals. *Opt. Express* **14**, 7737–7744 (2006).
- Ford, A. D., Morris, S. N. & Coles, R. J. Photonics and lasing in liquid crystals. *Mat. Today* **9**, 36–42 (2006).
- Lin, J.-H. et al. Manipulation of random lasing action from dye-doped liquid crystals infilling two-dimensional confinement single core capillary. *IEEE Photon. J.* **7**, 1501809 (2015).
- Wiersma, D. S. & Cavaliere, S. Light emission: a temperature-tunable random laser. *Nature* **414**, 708–709 (2001).
- Ferjani, S. et al. Thermal behavior of random lasing in dye-doped nematic liquid crystals. *Appl. Phys. Lett.* **89**, 121109 (2006).
- Ferjani, S., Barna, V., De Luca, A., Versace, C. & Strangi, G. Random lasing in freely suspended dye-doped nematic liquid crystals. *Opt. Lett.* **33**, 557–559 (2008).
- Sznitko, L., Kaliciak, K., Adamow, A. & Mysliwiec, J. A random laser made of nematic liquid crystal doped with a laser dye. *Opt. Mater. B* **56**, 121–128 (2016).
- Bian, H. et al. Optically controlled random lasing based on photothermal effect in dye-doped nematic liquid crystals. *Liq. Cryst.* **41**, 1436–1441 (2014).

20. Lee, C.-R. et al. Electrically controllable liquid crystal random lasers below the Freedericksz transition threshold. *Opt. Express* **19**, 2391–2400 (2011).
21. Ye, L. et al. Tailoring of random lasing characteristics in dye-doped nematic liquid crystals. *Appl. Phys. B* **115**, 303–309 (2014).
22. De Gennes, P. G. & Prost, J. *The Physics of Liquid Crystals* (Oxford University Press, New York, USA, 1993).
23. Khoo, I. C. Nonlinear optics of liquid crystalline materials. *Phys. Rep.* **471**, 221–267 (2009).
24. Peccianti, M. & Assanto, G. Nematicons. *Phys. Rep.* **516**, 147–208 (2012).
25. Stegeman, G. I. & Segev, M. Optical spatial solitons and their interactions: universality and diversity. *Science* **286**, 1518–1523 (1999).
26. Peccianti, M., Conti, C., Assanto, G., De Luca, A. & Umetsu, C. Routing of highly anisotropic spatial solitons and modulational instability in liquid crystals. *Nature* **432**, 733–737 (2004).
27. Alberucci, A., Piccardi, A., Peccianti, M., Kaczmarek, M. & Assanto, G. Propagation of spatial optical solitons in a dielectric with adjustable nonlinearity. *Phys. Rev. A* **82**, 023806 (2010).
28. Perumbilavil, S. et al. Soliton-assisted random lasing in optically pumped liquid crystals. *Appl. Phys. Lett.* **109**, 161105 (2016).
29. Perumbilavil, S. et al. All-optical guided-wave random laser in nematic liquid crystals. *Opt. Express* **25**, 4672–4679 (2017).
30. Bolis, S., Virgili, T., Rajendran, S., Beekman, J. & Kockaert, P. Nematicon-driven injection of amplified spontaneous emission into an optical fiber. *Opt. Lett.* **41**, 2245–2248 (2016).
31. Florentin, R. et al. Shaping the light amplified in a multimode fiber. *Light Sci. Appl.* **6**, e16208 (2017).
32. Wu, S.-T. & Lim, K.-C. Absorption and scattering measurements of nematic liquid crystals. *Appl. Opt.* **26**, 1722–1727 (1987).
33. Van Soest, G. & Lagendijk, A.  $\beta$  factor in a random laser. *Phys. Rev. E* **65**, 47601 (2002).
34. Barboza, R., Alberucci, A. & Assanto, G. Large electro-optic beam steering with nematicons. *Opt. Lett.* **36**, 2611–2613 (2011).
35. Izdebskaya, Y., Shvedov, V., Assanto, G. & Krolkowski, W. Magnetic routing of light-induced waveguides. *Nat. Commun.* **8**, 14452 (2017).
36. Alberucci, A., Piccardi, A., Kravets, N., Buchnev, O. & Assanto, G. Soliton enhancement of spontaneous symmetry breaking. *Optica* **2**, 783–789 (2015).
37. Ye, L. et al. Study on the polarisation of random lasers from dye-doped nematic liquid crystals. *Nanoscale Res. Lett.* **12**, 27–34 (2017).
38. Simoni, F. *Nonlinear Optical Properties of Liquid Crystals* (World Scientific, Singapore, 1997).
39. MacNeil, J. M. L., Smyth, N. F. & Assanto, G. Exact and approximate solutions for optical solitary waves in nematic liquid crystals. *Physica D* **284**, 1–15 (2014).
40. Conti, C., Peccianti, M. & Assanto, G. Route to nonlocality and observation of accessible solitons. *Phys. Rev. Lett.* **91**, 073901 (2003).
41. Alberucci, A. et al. Self-healing generation of spatial solitons in liquid crystals. *Opt. Lett.* **30**, 1381–1383 (2005).
42. Ghofraniha, N. et al. Experimental evidence of replica symmetry breaking in random lasers. *Nat. Commun.* **6**, 6058 (2015).

## Acknowledgments

This work was funded by the Academy of Finland through the Finland Distinguished Professor grant no. 282858.

## Author contributions

G.A. conceived/directed the study and assembled the team, S.P., A.P. and R.B. conducted the measurements, O.B. and G.S. prepared the samples, G.A. and G.S. discussed and designed the random laser material and setup, R.B. carried out the statistical analysis, M.K. and G.A. supervised the activity. All the authors contributed to the manuscript preparation.

## Additional information

**Supplementary Information** accompanies this paper at <https://doi.org/10.1038/s41467-018-06170-9>.

**Competing interests:** The authors declare no competing interests.

**Reprints and permission** information is available online at <http://npg.nature.com/reprintsandpermissions/>

**Publisher's note:** Springer Nature remains neutral with regard to jurisdictional claims in published maps and institutional affiliations.



**Open Access** This article is licensed under a Creative Commons Attribution 4.0 International License, which permits use, sharing, adaptation, distribution and reproduction in any medium or format, as long as you give appropriate credit to the original author(s) and the source, provide a link to the Creative Commons license, and indicate if changes were made. The images or other third party material in this article are included in the article's Creative Commons license, unless indicated otherwise in a credit line to the material. If material is not included in the article's Creative Commons license and your intended use is not permitted by statutory regulation or exceeds the permitted use, you will need to obtain permission directly from the copyright holder. To view a copy of this license, visit <http://creativecommons.org/licenses/by/4.0/>.

© The Author(s) 2018

## Supplementary information

### Beaming Random Lasers with Soliton Control

Sreekanth Perumbilavil, Armando Piccardi, Raouf Barboza, Oleksandr Buchnev, Martti Kauranen, Giuseppe Strangi and Gaetano Assanto\*

\* E-mail: [gaetano.assanto@uniroma3.it](mailto:gaetano.assanto@uniroma3.it)

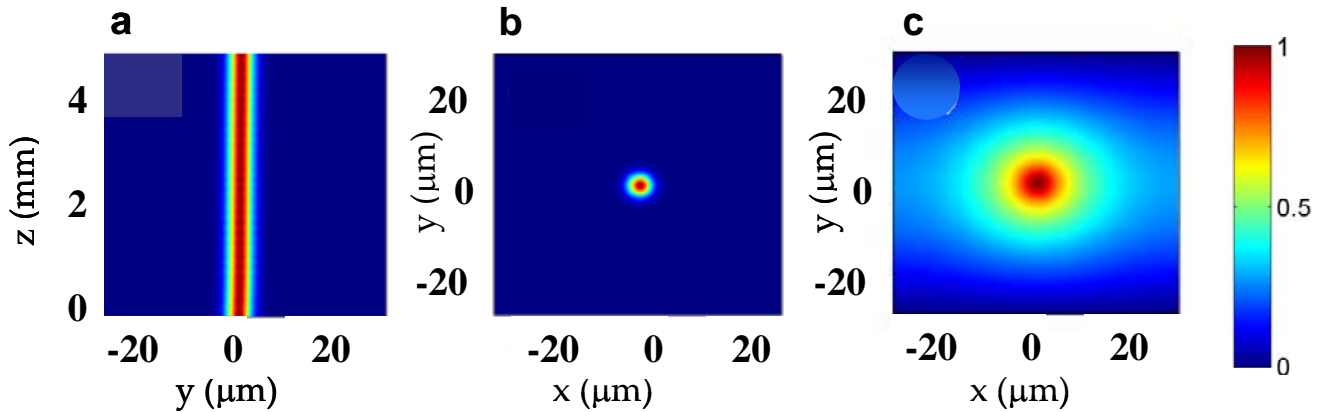


**Figure 1. Simulations of a near-infrared nematicon in standard nematic crystals**

**a** 4 mW soliton intensity evolution in the observation plane  $yz$ , for typical launch conditions of a Gaussian beam of  $3.6 \mu\text{m}$  waist with input wave-vector along  $z$  in a lossless nematic liquid crystal (E7) with molecular director  $\mathbf{n} = n(0, \pi/3, \pi/6)$  at rest and thickness  $60 \mu\text{m}$ . **b** Self-confined beam profile in the output transverse plane after propagation for 5 mm; **c** corresponding graded refractive index distribution in  $xy$ . For simplicity, linear birefringent walk-off was factored out from the model equations, hence it is not visible in these plots. The colour bar is in normalized (intensity or index) units.

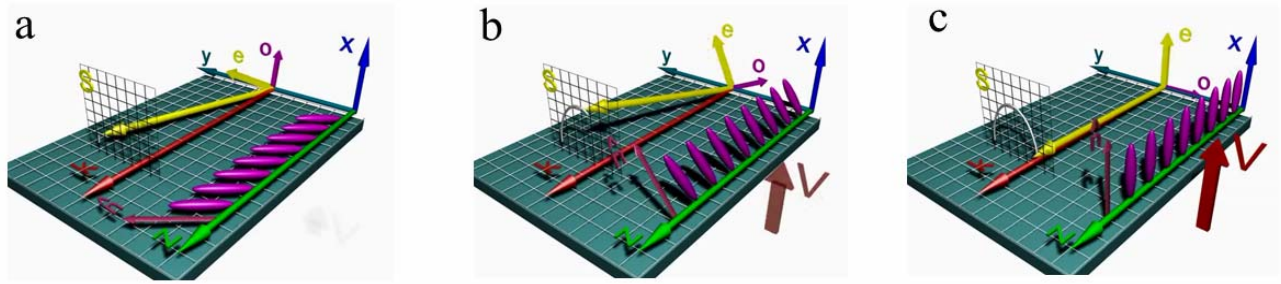


**Figure 2. Voltage-controlled steering**

Artist's sketch of the angular steering produced on a nematicon beam/waveguide by the application of a voltage  $V$  along  $x$ , as the latter increases from **a**  $V=0$  V to **b**  $V=1.2$  V and to **c**  $V > 2.5$  V in a standard nematic liquid crystal cell with director  $\mathbf{n}$  (violet arrow and ellipses) initially at  $45^\circ$  in the  $yz$  plane. The labels  $o$  and  $e$  stand for extraordinary and ordinary eigen-polarisations in the uniaxial medium. The walk-off, i. e. the angle between the Poynting vector  $\mathbf{S}$  (yellow arrow) and the wave-vector  $\mathbf{k}$  (red arrow), progressively reduces as  $V$  increases until  $\mathbf{S}$  and  $\mathbf{k}$  become collinear in **c**. The measurable angular steering stems from the projection of  $\mathbf{S}$  in the observation plane  $yz$ .

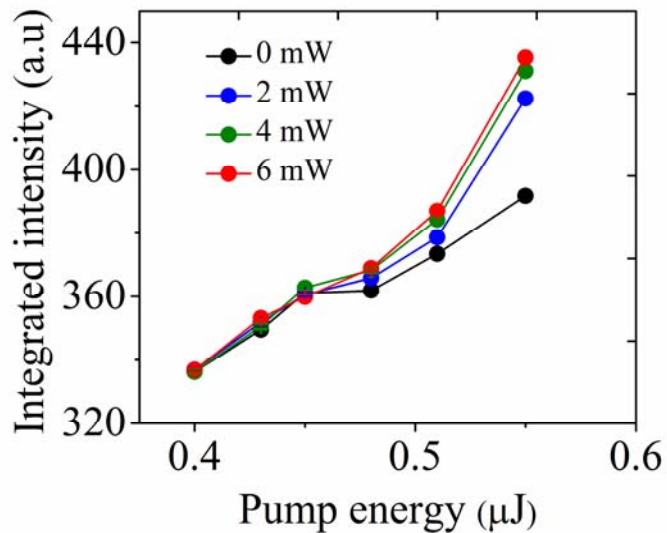


**Figure 3. Integrated average intensity  $\bar{I}$  versus pump energy for various nematicon powers**

The intensity spectra of the emitted light are averaged over 200 single-shot realizations (pump pulses) and integrated versus wavelength, according to Eq. (8) in the Methods. The legend indicates the power of the launched near-infrared nematicon. No threshold can be appreciated versus pump energy (at variance with Fig. 1c-d in the main text).

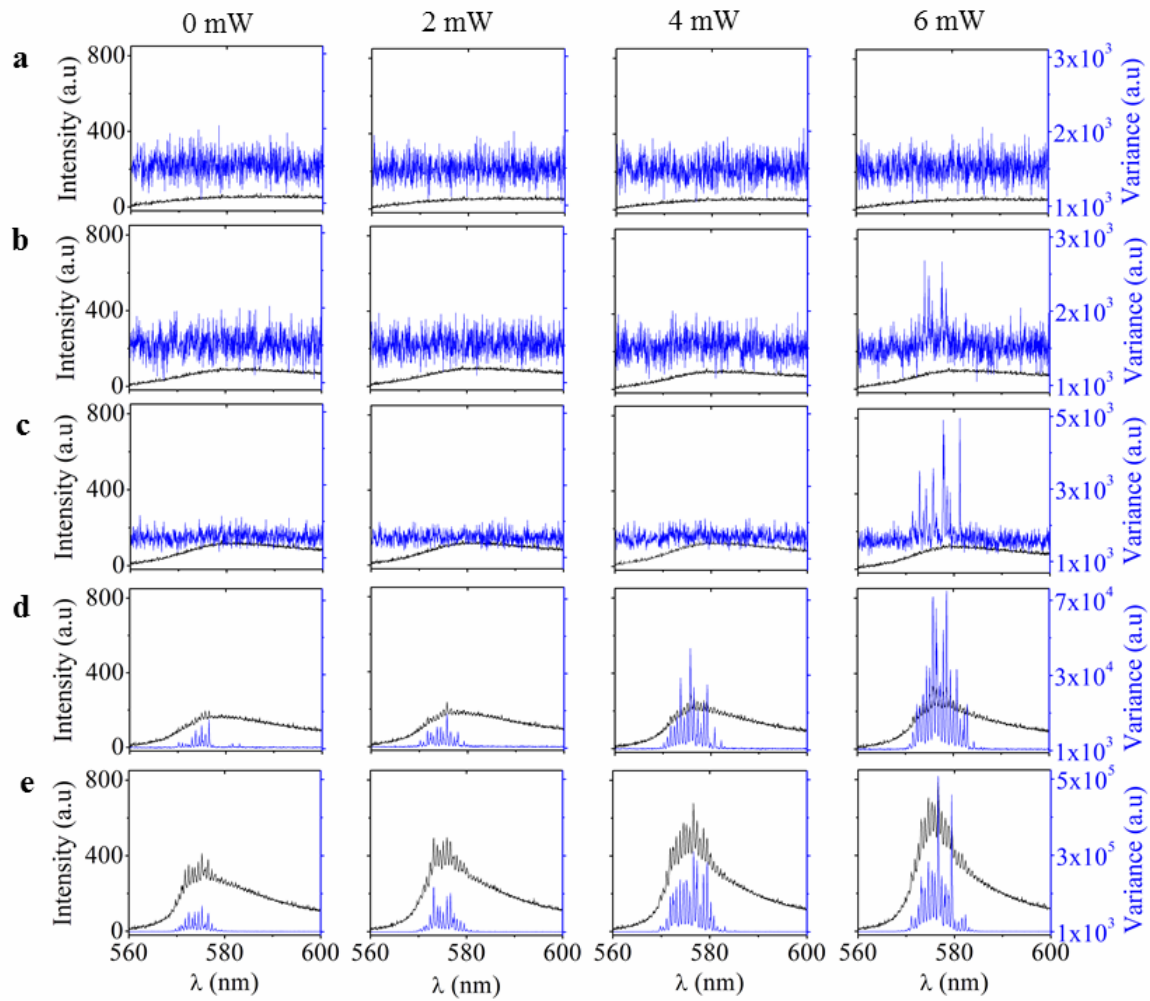


**Figure 4. Average intensity and variance of the emission spectra over 200 realizations**

Emission average intensity and variance are plotted versus wavelength and arranged in rows of equal pump energy and columns of equal near-infrared nematicon power. **a** Pump energy  $E = 0.43$   $\mu\text{J}$ ; **b**  $E = 0.45$   $\mu\text{J}$ ; **c**  $E = 0.48$   $\mu\text{J}$ ; **d**  $E = 0.51$   $\mu\text{J}$ ; **e**  $E = 0.61$   $\mu\text{J}$ .

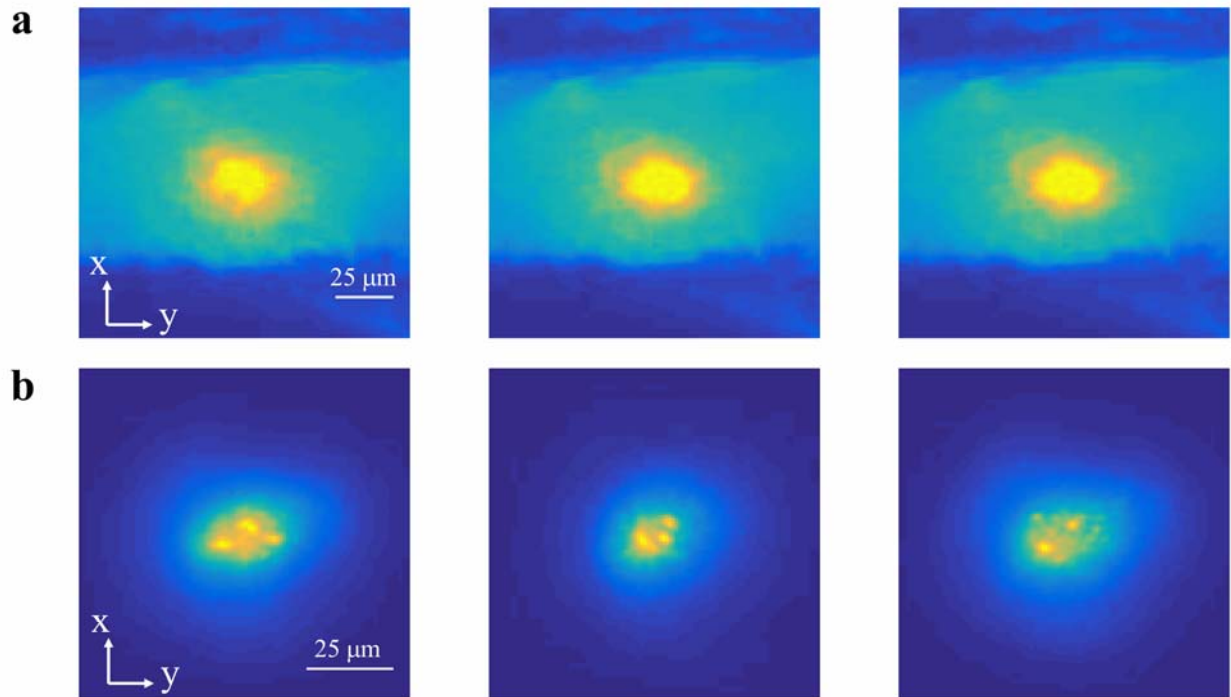


**Figure 5. Forward and backward random laser emission profiles**

**a** Single shot realizations of forward random laser emission profile after propagation in the nematic liquid crystal cell in the presence of a near-infrared soliton. The illuminated slab corresponds to the nematic liquid crystal sample, 100  $\mu\text{m}$  thick. **b** Single-shot realizations of backward random laser emission profile. The pump energy was  $E = 0.8 \mu\text{J}$  and the input nematic power  $P = 6 \text{ mW}$ .





# IV

## **MAGNETIC STEERING OF BEAM-CONFINED RANDOM LASER IN LIQUID CRYSTALS**

by

Sreekanth Perumbilavil, Martti Kauranen and Gaetano Assanto, October 2018

Applied Physics Letters vol. 113, p. 121107

© 2018 American Institute of Physics

Reproduced with permission.



# Magnetic steering of beam-confined random laser in liquid crystals

 Sreekanth Perumbilavil,<sup>1</sup> Martti Kauranen,<sup>1</sup> and Gaetano Assanto<sup>1,2,a)</sup>
<sup>1</sup>Laboratory of Photonics, Tampere University of Technology, FI-33101 Tampere, Finland

<sup>2</sup>NooEL-Nonlinear Optics and OptoElectronics Lab, University "Roma Tre," IT-00146 Rome, Italy

(Received 15 August 2018; accepted 30 August 2018; published online 19 September 2018)

Using an external magnetic field, we demonstrate in-plane angular steering of a green pumped random laser in dye-doped nematic liquid crystals, where a near-infrared reorientational spatial soliton provides a smooth output profile with emission in a well-defined direction. By varying the orientation of the applied magnetic field, the soliton-guided random laser beam can be steered over an angle as large as  $14^\circ$ , corresponding to a transverse displacement of 0.49 mm at the output facet of a 2 mm-long sample. *Published by AIP Publishing.* <https://doi.org/10.1063/1.5052272>

Random lasing occurs in disordered media with optical amplification when recurrent multiple scattering enables positive feedback.<sup>1,2</sup> Since its prediction<sup>3</sup> and first demonstration,<sup>4</sup> several efforts were devoted to obtaining random lasers (RLs) in various media<sup>5,6</sup> with a broad range of emission wavelengths.<sup>7,8</sup> Common RLs, however, emit light in a poorly controlled fashion in terms of directionality and output beam quality, hampering their applicability.<sup>9</sup> In this scenario, several approaches were undertaken to obtain directional RLs in various systems, including, for example, hollow-core optical waveguides,<sup>10</sup> engineered pump beams,<sup>11,12</sup> and optical fibers and nanostructures.<sup>13–15</sup>

Liquid crystals are mesophases with intermolecular links which favor self-assembly. In the nematic phase, positionally disordered rod-like molecules have their long axes aligned, on the average, along the molecular director  $\mathbf{n}$  or optic axis. The spontaneous dynamics of the molecular director leads to fluctuations in the local dielectric tensor, which in turn gives rise to anisotropic light scattering.<sup>16</sup> When excited by intense light beams, nematic liquid crystals (NLCs) can also support stable spatial solitons (nematocons) through re-orientational self-focusing.<sup>17,18</sup> NLCs behave as uniaxial crystals, and nematocons are extraordinary-wave beams self-confined by a graded index waveguide; such solitons can guide co-polarized signals of arbitrary wavelength. Nematocons propagate in the principal plane  $\mathbf{kn}$  at a walk-off angle  $\delta$  with respect to the wave-vector  $\mathbf{k}$ , being  $\tan \delta(\theta) = \frac{(n_{\parallel}^2 - n_{\perp}^2) \sin \theta \cos \theta}{n_{\perp}^2 + (n_{\parallel}^2 - n_{\perp}^2) \cos^2 \theta}$  where  $n_{\parallel}$  and  $n_{\perp}$  are the refractive indices for electric fields parallel and orthogonal to the molecular director, respectively, and  $\theta$  is the angle between  $\mathbf{k}$  and  $\mathbf{n}$ .<sup>19</sup> The trajectory of a nematocon can therefore be modified by external stimuli acting on the director distribution,<sup>20–22</sup> as long as it deviates from the initial arrangement.<sup>23,24</sup> Even an external magnetic field can reorient the director and effectively control the soliton trajectory.<sup>25</sup>

When suitably doped with dye molecules and optically pumped within the absorption region, NLCs have been reported to random lase with good conversion efficiency.<sup>26–28</sup> In this context, nematocons have been used to collect the generated fluorescence and the amplified spontaneous emission.<sup>29</sup>

Recently, we reported a nematocon random laser with collinearly launched pump and soliton, with enhancement of lasing efficiency, directionality, and spectral emission.<sup>30,31</sup> In this letter, we present the first example of a magnetically routed random laser in dye-doped nematic liquid crystals, whereby the active medium itself is altered to yield an angular deviation of the Poynting vector.

Our sample was a planar glass cell, 3 cm wide,  $100 \mu\text{m}$  thick, and 2 mm long, filled with the standard E7 (Merck) mixture doped with 0.3 wt. % Pyrromethene (PM597). The interfaces were mechanically treated to produce homogeneous alignment of the molecular director in the  $yz$  plane at  $45^\circ$  with respect to the input normal and the input beam wave-vector  $\mathbf{k}$  (Fig. 1).<sup>20</sup> The experimental setup included two laser sources, a pulsed one operating at a rep-rate of 20 Hz as the pump, with 6 ns pulses at the wavelength of 532 nm, and a continuous-wave one exciting the nematocon at the near-infrared (NIR) wavelength of  $1.064 \mu\text{m}$ . Both beams were gently focused using a microscope objective to comparable waists of about  $3 \mu\text{m}$  at the cell entrance. The light evolution in the observation plane  $yz$  was imaged through scattering using a microscope, whereas a

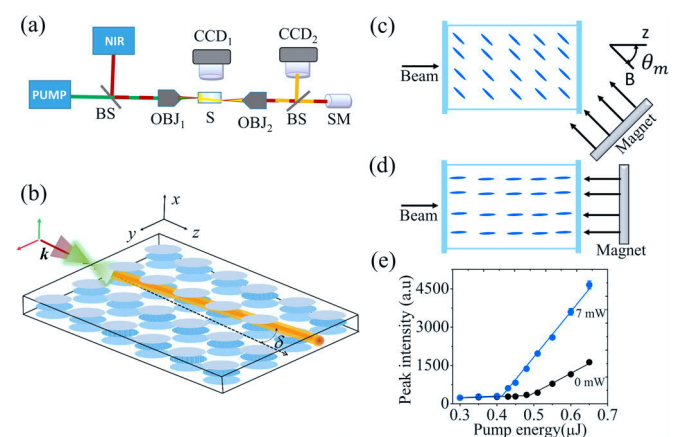


FIG. 1. (a) Sketch of the experimental setup (BS: beam splitter, OBJ: objective lens, S: sample, and SM: spectrometer) and (b) NLC planar sample (not in scale) with pump and NIR beams, nematocon, and emitted light. (c) and (d) Relative orientation of the magnetic field and cell (top view) for two limiting cases  $\theta_m = -50^\circ$  and  $\theta_m = 0^\circ$ , respectively. (e) Input-output random laser characteristics (single-shot peak values averaged over 200 pulses) without (black line and dots) and with a NIR nematocon (blue line and dots).

<sup>a)</sup>E-mail: gaetano.assanto@uniroma3.it

spectrometer ( $\Delta\lambda = 0.15$  nm) and a CCD camera resolved the emission spectrum and transverse profile at the output facet ( $xy$  plane) of the cell, respectively.

We launched orthogonally polarized NIR and green pump beams co-injected at the cell entrance. The NIR generated a stable spatial soliton, while the pump produced RL emission around 580 nm,<sup>31</sup> confined by the nematic into a smooth transverse profile and directed to the output along the inherent walk-off  $\delta$ . The experimental setup, the NLC sample and its optical configuration, the input output characteristics of this random laser without/with a nematic, and two examples of the magnet-cell orientation are illustrated in Fig. 1. When pumping the guest-host material, the emitted light was polarized as an extraordinary wave; above the lasing threshold [see Fig. 1(e)] and in the presence of a NIR nematic, the RL emission was therefore confined within the spatial soliton and *beamed* along the walk-off angle  $\delta \cong 7^\circ$ , corresponding to the calculated value with  $n_{\parallel} = 1.71$  and  $n_{\perp} = 1.52$ .<sup>30,31</sup>

Taking advantage of the magnetic response of NLCs,<sup>32,33</sup> the initial (homogeneous) orientation ( $\theta = 45^\circ$ ) of the molecular director with respect to  $k/z$  could be modified by the application of an external magnetic field coplanar with  $k$  and  $n$ . To this extent, we placed a cylindrical permanent magnet (diameter 25 mm) mounted on a rotation stage (rotation around  $x$ ) with  $yz$  translation close to the output facet of the sample [see Figs. 1(c) and 1(d)]. The magnetic field strength at about 2 mm from the cell was  $\approx 0.23$  T, large enough to reorient the NLC in the whole volume of interest despite its spatial distribution and the cell size. The angle  $\theta_m$  between the magnetic field vector and  $z$  determined the walk-off  $\delta = \delta(\theta)$  with  $\theta = \theta_m$ .

In order to steer the soliton-guided RL beam, we applied the magnetic field and varied its angular direction with respect to  $z$  in the  $yz$  plane. As the magnetic field forces the molecular director to reorient at an angle  $\theta = \theta_m$  in the bulk of the NLC sample (away from the planar boundaries), the input NIR beam remains an extraordinary wave and the resulting walk-off experienced by both the NIR soliton and the RL emission gets modified. By varying  $\theta_m$  from  $-50^\circ$  to  $+50^\circ$ , the walk-off in the used guest-host with E7 was expected to vary from  $-7^\circ$  to  $+7^\circ$  for near-infrared light. Typical experimental results for the RL beam evolution when pumping above threshold ( $>0.48$   $\mu\text{J}$ ) are illustrated in Fig. 2 for various  $\theta_m$ , where the NIR and pump components have been filtered out. The photographs show the RL emission produced by a pump at  $0.6$   $\mu\text{J}/\text{pulse}$  and guided by a  $7$  mW nematic waveguide along the walk-off associated with magnetic field orientation. The measured propagation angles within the plane  $yz$  are in perfect agreement with the calculated values, as apparent from the graph in Fig. 3. It is noteworthy that as the walk-off approaches zero for  $\theta_m \rightarrow 0$ , the nonlinearity tends to vanish as well, resulting in an all-optical waveguide with progressively lower index contrast.<sup>34</sup>

We also acquired photographs of the magnetically routed RL beam at the output of the NLC cell, with the exception of the case  $\theta_m = 0$  when the magnet eclipsed the beam. Sample results are displayed in Fig. 4 for  $\theta_m = \pm 50^\circ$ . It is apparent that soliton confinement provides beam-like features to the random laser emission,<sup>35</sup> whereby its output spot is much smoother than in previously reported RLs. As

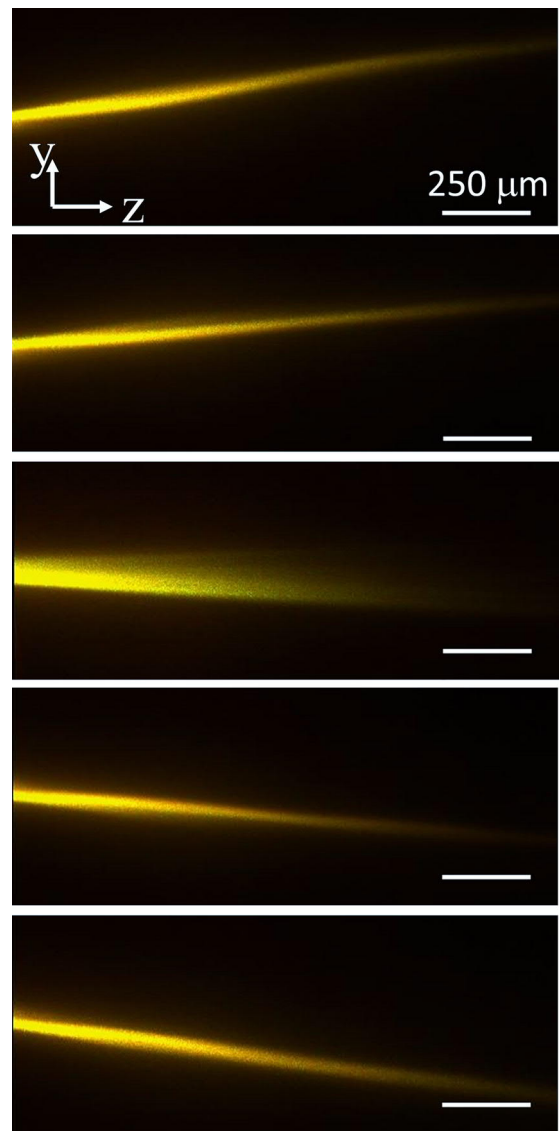


FIG. 2. Photographs of the RL emission along a 7 mW nematicon in the  $yz$  plane for various magnetic orientations  $\theta_m$  from top to bottom  $\theta_m = -50^\circ$ ,  $-30^\circ$ ,  $0^\circ$ ,  $+30^\circ$ , and  $+50^\circ$ , respectively. NIR light and pump light were filtered out.

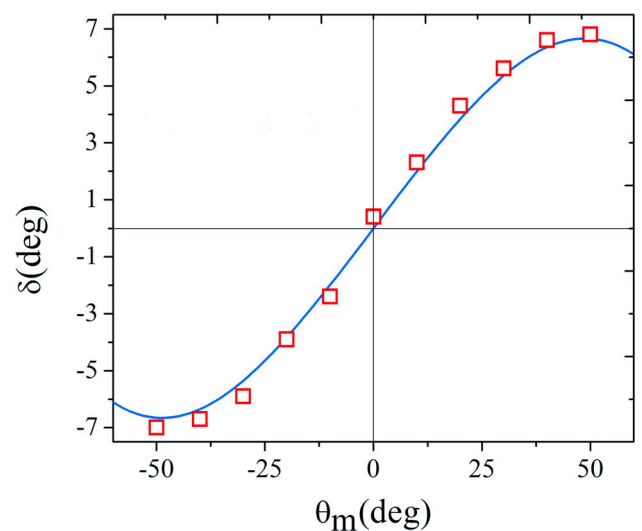


FIG. 3. Measured (squares) and calculated (solid line) RL walk-off angles  $\delta$  for various  $\theta_m$  values.

the nematic is magnetically steered, the RL output profile remains essentially the same as it moves in-plane with an overall transverse displacement of about  $490\ \mu\text{m}$  across  $y$  and without shifts in the orthogonal transverse direction  $x$ , at variance with electro-optic steering with a voltage applied across the sample thickness.<sup>20,35</sup>

Since at rest (in the absence of an external magnetic field) the optic axis  $\mathbf{n}$  of the NLC is pre-aligned according to the boundary conditions at the treated glass plates forming the cell, we measured both the response time of the RL beam towards the magnetic vector and the relaxation time back to the original configuration. In the absence of the magnetic field ( $\theta = 45^\circ$ ), the RL beam propagated at  $\delta \sim +7^\circ$ ; applying a magnetic field at  $\theta_m = -50^\circ$ , the measured time needed for the RL beam to reach  $\delta \sim -7^\circ$  was about 60 s. Conversely, a time interval close to 200 s was required for the RL beam to relax to its original trajectory (i.e., from  $\delta = -7^\circ$  to  $\delta = +7^\circ$ ) after the magnet was removed. This slow time response can be ascribed to the large thickness of the anchored NLC and to the modest amplitude of the magnetic field.

Finally, we acquired the output RL emission spectra for various magnetic field orientations. Figure 5 illustrates the results after averaging over 200 single-shot pump realizations, for symmetrically chosen  $\theta_m$  values. The averaged emission spectra corresponding to symmetric orientations of the magnetic field values are essentially the same despite the random nature of the emission. This confirms that complete reorientation of the NLC director was accomplished despite the initial anchoring at the boundaries. For  $\theta = \theta_m$  close to zero, the observed small reductions in RL emission are associated with the soliton waveguide being less confining and therefore<sup>34</sup> less effective in collecting RL emitted light. In all cases, however, the averaged spectra exhibit regularly spaced RL peaks, suggesting the role of an effective cavity about  $130\ \mu\text{m}$  long, related to the pump absorption length.<sup>6</sup> The spectral influence of transverse geometric resonances within the light-induced waveguide remains to be ascertained.

In conclusion, by combining a NIR soliton with collinear pumping in dye-doped NLCs, we demonstrated in-plane magneto-optic steering and beaming of a random laser in a planar cell. We managed to steer the random laser emission over  $14^\circ$  while maintaining the RL beam in the observation plane  $yz$ . The spectral features indicate that the magnetic field was effective in reorienting the NLC director in the bulk of the sample without hampering the key properties of the random laser.

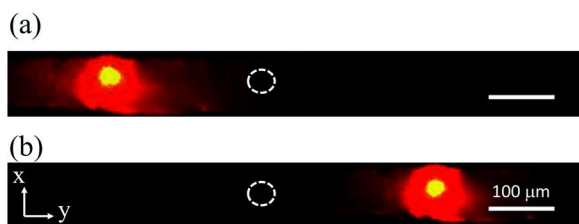


FIG. 4. Single shot photographs of the RL emission at the cell output in the plane  $xy$  for (a)  $\theta_m = +50^\circ$  and (b)  $\theta_m = -50^\circ$ . The white dashed circle indicates the direction of the input wave vector  $\mathbf{k}/\|\mathbf{z}$ .

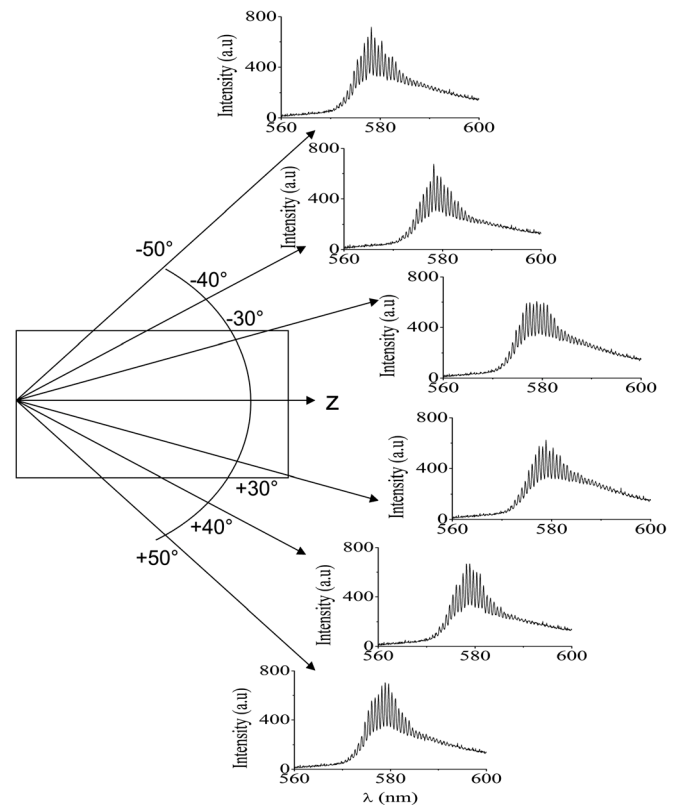


FIG. 5. RL emission spectra averaged over 200 single-shot realizations for various  $\theta_m$  values, as indicated.

This work was supported by the Academy of Finland, Finland Distinguished Professor Grant No. 282858. We thank R. Barboza, O. Buchnev, and G. Strangi for their help with sample and setup.

- <sup>1</sup>H. Cao, *Waves Random Media* **13**, R1 (2003).
- <sup>2</sup>D. S. Wiersma, *Nat. Phys.* **4**, 359 (2008).
- <sup>3</sup>V. S. Letokhov, *Sov. Phys. JETP* **26**(4), 835 (1968).
- <sup>4</sup>N. M. Lawandy, R. M. Balachandran, A. S. L. Gomes, and E. Sauvain, *Nature* **368**, 436 (1994).
- <sup>5</sup>R. Polson, A. Chipouline, and Z. V. Vardeny, *Adv. Mater.* **13**, 760 (2001).
- <sup>6</sup>X. Wu, W. Fang, A. Yamilov, A. A. Chabanov, A. A. Asatryan, L. C. Botten, and H. Cao, *Phys. Rev. A* **74**, 053812 (2006).
- <sup>7</sup>Y. Zeng, G. Liang, K. H. Liang, S. Mansha, B. Meng, T. Liu, X. Hu, J. Tao, L. Li, and A. G. Davies, *ACS Photonics* **3**, 2453 (2016).
- <sup>8</sup>H. Cao, Y. Zhao, S. Ho, E. Seelig, Q. Wang, and R. Chang, *Phys. Rev. Lett.* **82**, 2278 (1999).
- <sup>9</sup>D. S. Wiersma, *Nature* **414**, 708 (2001).
- <sup>10</sup>K. C. Jorge, M. A. Alvarado, E. G. Melo, M. N. P. Careno, M. I. Alayo, and N. U. Wetter, *Appl. Opt.* **55**, 5393 (2016).
- <sup>11</sup>N. Bachelard, J. Andreasen, S. Gigan, and P. Sebbah, *Phys. Rev. Lett.* **109**, 033903 (2012).
- <sup>12</sup>M. Leonetti, C. Conti, and C. Lopez, *Phys. Rev. A* **85**, 043841 (2012).
- <sup>13</sup>C. J. S. de Matos, L. D. Menezes, A. M. Brito-Silva, M. A. Martinez Gámez, A. S. L. Gomes, and C. B. de Araújo, *Phys. Rev. Lett.* **99**, 153903 (2007).
- <sup>14</sup>B. Abaie, E. Mobini, S. Karbasi, T. Hawkins, J. Ballato, and A. Mafi, *Light Sci. Appl.* **6**, e17041 (2017).
- <sup>15</sup>S. Schönhuber, M. Brandstetter, T. Hisch, C. Deutsch, M. Krall, H. Detz, A. M. Andrews, and G. Strasser, *Optica* **3**, 1035 (2016).
- <sup>16</sup>H. Stark and T. C. Lubensky, *Phys. Rev. Lett.* **72**, 2229 (1996).
- <sup>17</sup>I. C. Khoo, *Phys. Rep.* **471**, 221 (2009).
- <sup>18</sup>M. Peccianti and G. Assanto, *Phys. Rep.* **516**, 147 (2012).
- <sup>19</sup>M. Peccianti, A. Fratolocchi, and G. Assanto, *Opt. Express* **12**, 6524 (2004).
- <sup>20</sup>M. Peccianti, C. Conti, G. Assanto, A. De Luca, and C. Umeton, *Nature* **432**, 733 (2004).

- <sup>21</sup>A. Piccardi, M. Peccianti, G. Assanto, A. Dyadyusha, and M. Kaczmarek, *Appl. Phys. Lett.* **94**, 091106 (2009).
- <sup>22</sup>R. Barboza, A. Alberucci, and G. Assanto, *Opt. Lett.* **36**, 2611 (2011).
- <sup>23</sup>F. Sala, N. F. Smyth, U. Laudyn, M. Karpierz, A. A. Minzoni, and G. Assanto, *J. Opt. Soc. Am. B* **34**, 2459 (2017).
- <sup>24</sup>U. Laudyn, M. Kwasny, F. Sala, M. Karpierz, N. F. Smyth, and G. Assanto, *Sci. Rep.* **7**, 12385 (2017).
- <sup>25</sup>Y. Izdebskaya, V. Shvedov, G. Assanto, and W. Krolikowski, *Nat. Commun.* **8**, 14452 (2017).
- <sup>26</sup>G. Strangi, S. Ferjani, V. Barna, A. De Luca, C. Versace, N. Scaramuzza, and R. Bartolino, *Opt. Express* **14**, 7737 (2006).
- <sup>27</sup>A. D. Ford, S. N. Morris, and R. J. Coles, *Mater. Today* **9**, 36 (2006).
- <sup>28</sup>S. Ferjani, V. Barna, A. De Luca, C. Versace, and G. Strangi, *Opt. Lett.* **33**, 557 (2008).
- <sup>29</sup>S. Bolis, T. Virgili, S. Rajendran, J. Beeckman, and P. Kockaert, *Opt. Lett.* **41**, 2245 (2016).
- <sup>30</sup>S. Perumbilavil, A. Piccardi, O. Buchnev, M. Kauranen, G. Strangi, and G. Assanto, *Appl. Phys. Lett.* **109**, 161105 (2016).
- <sup>31</sup>S. Perumbilavil, A. Piccardi, O. Buchnev, M. Kauranen, G. Strangi, and G. Assanto, *Opt. Express* **25**, 4672 (2017).
- <sup>32</sup>L. M. Blinov, *Electro-Optical and Magneto-Optical Properties of Liquid Crystals* (Wiley, New York, 1984).
- <sup>33</sup>L. Ye, C. Zhao, Y. Wang, Y. Cui, and Y. Lu, *J. Appl. Phys.* **116**, 053103 (2014).
- <sup>34</sup>A. Alberucci, A. Piccardi, M. Peccianti, M. Kaczmarek, and G. Assanto, *Phys. Rev. A* **82**, 023806 (2010).
- <sup>35</sup>S. Perumbilavil, A. Piccardi, R. Barboza, O. Buchnev, M. Kauranen, G. Strangi, and G. Assanto, "Beaming random lasers with soliton control," *Nat. Commun.* (in press).

Tampereen teknillinen yliopisto  
PL 527  
33101 Tampere

Tampere University of Technology  
P.O.B. 527  
FI-33101 Tampere, Finland

ISBN 978-952-15-4268-8

ISSN 1459-2045